Scale-free activity as a basis for spatial learning and memory in the brain

by

Predrag Živadinović

December, 2025

A thesis submitted to the
Graduate School
of the
Institute of Science and Technology Austria
in partial fulfillment of the requirements
for the degree of
Doctor of Philosophy

Committee in charge:

Paul Schanda, Chair
Jozsef Csicsvari
Maximilian Jösch
Alessandro Treves

The thesis of Predrag Živadinović, titled *Scale-free activity as a basis for spatial learning and memory in the brain*, is approved by:

Supervisor: Jozsef Csicsvari, ISTA, Klosterneuburg, Austria

Signature: _____

Committee Member: Maximilian Jösch, ISTA, Klosterneuburg, Austria

Signature: _____

Committee Member: Alessandro Treves, SISSA, Trieste, Italy

Signature: _____

Defense Chair: Paul Schanda, ISTA, Klosterneuburg, Austria

Signature: _____

Signed page is on file

ISTA Thesis, ISSN: 2663-337X

I hereby declare that this thesis is my own work and that it does not contain other people's work without this being so stated; this thesis does not contain my previous work without this being stated, and the bibliography contains all the literature that I used in writing the dissertation.

I accept full responsibility for the content and factual accuracy of this work, including the data and their analysis and presentation, and the text and citation of other work.

I declare that this is a true copy of my thesis, including any final revisions, as approved by my thesis committee, and that this thesis has not been submitted for a higher degree to any other university or institution.

I certify that any republication of materials presented in this thesis has been approved by the relevant publishers and co-authors.

Signature: _____

Predrag Živadinović
December, 2025

Signed page is on file

Abstract

A major challenge in neuroscience is deciphering how the brain orchestrates behavior in response to changes in environmental conditions. This process is characterized by several processing stages, from perception to the storage of important information. Information storage is performed by a memory system implemented through complex networks of highly interconnected neurons. The collective operational principles of neuronal networks that support formation and storage are the main topics of this thesis.

To investigate the collective dynamics of the hippocampus from the perspective of the brain criticality hypothesis, I started by analyzing cascades of neural activity ¯ neuronal avalanches ¯ that have been characterized by the absence of a typical spatial or temporal scale. Measures derived from neuronal avalanches suggested that during wakefulness the hippocampus operated further away from criticality than during sleep/rest. In addition, neural activity propagated differently in these two brain states, as indicated by different collapses of the avalanche shapes. Next, the Phenomenological Renormalization Group approach also indicated conceptually similar differences, through the scaling exponent of activity variance α, which was higher during sleep/rest than during awake. These results confirmed that the activity of the hippocampus exhibits signatures of criticality and that these signatures change with the state of the brain.

Next, I found that memory retention was predicted by the scaling exponent of activity variance α. The exponent α measured during the sleep/rest session that followed learning correlated with memory retention during the subsequent unrewarded testing session. Moreover, α predicted performance even when controlled for reactivation that occurs in parallel. Second, α measured in the sleep/rest phase that preceded learning was correlated with the learning speed. I analyzed distributions of the cells' characteristic timescale and burstiness. The day-to-day variability of these distributions, during sleep/rest that followed learning, correlated with the scaling exponent of activity variance α, as well as with memory retention. These findings confirmed that variance scaling and functional heterogeneity provide behaviorally meaningful perspectives on hippocampal activity, as they are directly related to memory consolidation.

I further investigated the process of memory acquisition and consolidation between the hippocampus CA1 and the mEC. During learning, CA1 cells shifted their firing field towards the goals, while mEC cells remained mostly stable, shifting their firing fields towards the goals during sleep/rest that followed learning. This shift during sleep/rest was supported by the reactivation process, which occurred in two ways, synchronously with CA1 (during SWRs) and independently of the hippocampal SWRs. Both types of reactivation predicted subsequent memory retention, as well as the amount of goal-related remapping. Again, the day-to-day variability of the distribution of the cell timescales correlated with the goal-related remapping, in CA1 during the learning session and in mEC during sleep/rest. These results suggest that in spatial navigation tasks, the functional responsibilities of CA1 and mEC change between learning and sleep/rest and that their function benefits from increased functional heterogeneity among cells.

Acknowledgements

I would like to thank Professor Jozsef Csicsvari for supervising my work and giving me the opportunity to pursue my PhD in his group, even though I had no prior experience in neuroscience or in experimental lab work. I also thank Professor Maximilian Jösch for actively participating as a committee member and regularly providing me with advice during the project, from the qualifying exam until the production of this thesis. In addition, I am grateful that Professor Alessandro Treves has been an enthusiastic member of my PhD committee.

Close collaboration with Fabrizio Lombardi had an enormous impact on my motivation and end results of my PhD project. As I lack formal training in physics, Fabrizio introduced me to the topic of brain criticality, helped me learn fundamental concepts, and refine my thinking about the brain from the perspective of collective phenomena. I would like to express my gratitude to him, since this project and the results presented in this thesis would not be achievable without his guidance.

Additionally, I want to thank Charlotte Boccara and Gašper Tkačik for devoting their time to support me and provide me invaluable research advice. Their contributions helped shape some of the most important results presented in this thesis, which would look substantially different without their input.

I also want to thank other members of the Csicsvari group, with whom I have worked in the previous five years. I especially want to highlight Heloisa Chiossi and Juan Villegas who helped me learn the basic techniques necessary for conducting experimental neuroscience, therefore kick-starting my career in neuroscience. I also want to mention Lars Bollman, Michele Nardin, Uladzislau Barayeu, Sofia Taveira, and Andrea Cumpelik, with whom I had many pleasant and insightful conversations over the years.

It has been my pleasure to work at ISTA and I want to thank all people, not explicitly mentioned here, who helped me conduct research that led to this PhD thesis. I am grateful to the professors at the University of Niš and senior colleagues from previous work, under whose influences I developed a love for science and research.

I want to express my gratitude to my family and friends for providing unconditional support over the last few years. Maintaining close relations with them helped me adjust to the new country and achieve the educational and scientific goals I had set for myself. Finally, I am grateful to have a wonderful partner, Marija Krstić, whose listening, patience, and positive attitude helped me overcome difficult times and make the right decisions.

My work has been funded through the project "Functional Advantages of Critical Brain Dynamics" of the ISTA interdisciplinary fund and through the FWF.

About the Author

Predrag Živadinović completed a BSc in Computer Science at the Faculty of Sciences and Mathematics, University of Niš in 2015. At the same university, in 2018, he completed his MSc in Machine Learning, with a thesis on adversarial attacks in deep reinforcement learning. For a few years, he worked in the industrial $R\&D$ sector, where he participated in the research and development of machine learning algorithms for real-time video processing. Predrag started his PhD at ISTA in the fall of 2019 and joined the lab of Jozsef Csicsvari in 2020. In the lab, he investigated the computational mechanisms that underlie spatial learning and memory consolidation. He participated in all phases of research, from experiment design, through rat surgeries and *in vivo* electrophysiology recordings, to data analysis and modeling. During his PhD studies, Predrag presented posters and gave talks about results of his research at multiple conferences and workshops. His main research interests include fundamental principles of information processing in complex systems and exploring potentials for practical application of those principles.

List of Collaborators and Publications

List of collaborators:

- Fabrizio Lombardi
  Advice regarding data analysis in Chapter 2 and Chapter 3
- Charlotte Boccara
  Recording and pre-processing of data for Chapter 3 and Chapter 4, published in Boccara et al. 2019, illustrations on Figure 1.1 A and Figure 3.6 A
- Juan Felipe Ramirez Villegas
  Recording and pre-processing of data for Chapter 3
- Peter Baracskay
  Recording and pre-processing of data for Chapter 2, published in Bollmann et al. 2025
- David Dupret
  Recording and pre-processing of data for Chapter 3, published in Dupret et al. 2010
- Gašper Tkačik
  Advice regarding data analysis for Chapter 2 and Chapter 3
- Jozsef Cscicsvari
  Advice regarding experimental work, data analysis, data presentation and writing

Conference talks:

- "Critical scaling exponents of hippocampal activity predict spatial memory performance"
  Talk at ANA meeting, ISTA, September 2025
- "Critical scaling exponents of hippocampal activity predict spatial memory performance"
  Talk at Collective Dynamics and Information Processing in Neural Systems, Satellite meeting of StatPhys29, Venice, July 2025
- "Measures of critical dynamics in the hippocampus of freely moving rats"
  Talk at ACAIN, September 2024

Conference posters:

- "Signatures of critical dynamics in the rat hippocampus"

  Poster at FENS forum, Vienna, June 2024, containing project updates

- "Signatures of critical dynamics in the rat hippocampus"
  Poster at FENS forum, Berlin, September 2023

Table of Contents

Abstract vii

Acknowledgements viii

About the Author ix

List of Collaborators and Publications x

Table of Contents xi

List of Figures xiii

List of Tables xiv

List of Abbreviations xiv

1 Introduction 1
- 1.1 Hippocampus and medial entorhinal cortex . . . 2
- 1.2 Collective dynamics and brain criticality . . . 9
- 1.3 Aims of the Thesis . . . 12

Methods 13
- Experimental Methods . . . 13
- Data analysis . . . 15

2 Criticality in the hippocampus 25
- 2.1 Neural avalanches and distance to criticality . . . 26
- 2.2 Phenomenological Renormalization Group . . . 31
- 2.3 Discussion . . . 38

3 Functional role of scaling in the hippocampal activity 43
- 3.1 Scaling of activity variance predicts retention of spatial memory . . . 44
- 3.2 Scaling of activity variance predicts spatial memory retention together with reactivation . . . 48
- 3.3 The scaling of activity variance predicts the speed of learning . . . 51
- 3.4 Scaling of activity variance during sleep/rest and functional heterogeneity of hippocampal cells . . . 54
- 3.5 Discussion . . . 56

4 Functional heterogeneity and CA1-mEC encoding dynamics 59
4.1 Differential functional heterogeneity during learning and sleep/rest 60
4.2 Online goal-oriented remapping in CA1, offline goal-oriented remapping in mEC 62
4.3 Offline reactivation in mEC supports spatial memory consolidation 64
4.4 Distribution of characteristic timescale correlates with goal-related remapping 67
4.5 Discussion 68

5 Conclusion and outlook 71
5.1 Summary of results 71
5.2 Open questions 73
5.3 Broad research themes 75

S Supplementary materials 77
S.1 Supplementary figures related to Chapter 2 77
S.2 Supplementary figures related to Chapter 3 79
S.3 Supplementary figures related to Chapter 4 83

Bibliography 87

List of Figures

1.1 *CA1 and mEC*. . . . 3
1.2 *Spatial representation in CA1 and mEC*. . . . 5
1.3 *Theta and SWR oscillations*. . . . 8
1.4 *Criticality*. . . . 10

2.1 *Neuronal avalanches*. . . . 27
2.2 *Distributions and scaling of neuronal avalanches*. . . . 28
2.3 *Temporal profiles of neuronal avalanches - avalanche shapes*. . . . 29
2.4 *Criticality in wakefulness and sleep/rest*. . . . 30
2.5 *Phenomenological Renormalization Group*. . . . 32
2.6 *Distribution of non-zero, coarse-grained activity*. . . . 33
2.7 *Scaling of free energy under coarse-graining*. . . . 34
2.8 *Scaling of activity variance under coarse-graining*. . . . 34
2.9 *Scaling and collapsing of the covariance matrix spectrum of clustered activity*. 35
2.10 *Scaling and collapsing of the autocorrelation function*. . . . 36
2.11 *Scaling exponents of PRG during wakefulness and sleep/rest*. . . . 37
2.12 *Relation between scaling exponents of PRG and avalanches*. . . . 38

3.1 *Behavioral paradigm*. . . . 45
3.2 *Performance on the cheeseboard task*. . . . 45
3.3 *Scaling of activity variance during Post-Sleep predicts memory retention*. . . . 47
3.4 *Relations between PRG scaling exponents*. . . . 48
3.5 *Excluding SWRs and HSEs does not influence behavioral predictions of PRG scaling exponents*. . . . 49
3.6 *Goal-related reactivation in CA1*. . . . 50
3.7 *Scaling of activity variance and goal-related reactivation*. . . . 51
3.8 *Scaling of activity variance during learning predicts memory retention*. . . . 52
3.9 *Scaling of activity variance predicts the speed of learning*. . . . 52
3.10 *Scaling of activity variance reflects functional variability of hippocampal cells*. . 55

4.1 *Distribution of characteristic timescales during learning and Post-Sleep*. . . . 61
4.2 *Goal-related remapping in the CA1 and mEC*. . . . 63
4.3 *Reactivation during SWRs in CA1 and mEC*. . . . 65
4.4 *Goal-related remapping in the CA1 and mEC*. . . . 66
4.5 *Distribution of characteristic timescales and goal-related remapping*. . . . 68

S.1 *PRG exponents for different duration of temporal bins*. . . . 78
S.2 *Memory retention performance*. . . . 80
S.3 *PRG scaling exponents*. . . . 81
S.4 *Scaling of activity variance and network activity measures*. . . . 81
S.5 *Scaling of activity variance does not correlate with reactivation quality*. . . . 82

S.6 *Scaling of activity variance vs median burstiness* 83
S.7 *Goal-related remapping* 84
S.8 *Reactivation and functional heterogeneity in CA1 and mEC* 85

List of Tables

1.1 Animals used in this thesis 13

List of Abbreviations

BIC Bayesian information criterion
CA1 Cornu Ammonis 1
CA2 Cornu Ammonis 2
CA3 Cornu Ammonis 3
CDF Cumulative distribution function
DG Dentate gyrus
DCC Distance to criticality coefficient
EC Entorhinal cortex
HD Head direction
HSE High synchrony event
ISI Inter spike interval
lEC Lateral entorhinal cortex
mEC Medial entorhinal cortex
MUA Multi-unit activity
PRG Phenomenological Renormalization Group
PV Population vector
QCD Quartile coefficient of dispersion
REM Rapid eye movement
RG Renormalization Group
SEM Standard error of the sample mean
SWS Slow wave sleep
SWR Sharp wave-ripple

CHAPTER 1

Introduction

In the animal kingdom, a critical skill for survival is identifying effective strategies to forage for resources and avoid danger. These two behaviors require sophisticated navigation through various environments and the ability to adapt to evolving external conditions. The brain orchestrates these behaviors by encoding and recalling significant landmarks and events, as well as acquiring new information, which is then integrated with pre-existing memories. According to traditional views (Kandel, Dudai, and Mayford 2014) the memory system in the brain supports two types of long-term memory, procedural (implicit) and declarative (explicit). The former allows animals to perform a set of skills, often subconsciously, while the latter allows animals to remember events (episodes), objects, and experiences and assign them semantic meanings. The support for declarative memory in the brain is crucial for steering animals away from adverse experiences while guiding them towards favorable ones, and it is indispensable in social interactions that enhance survival across a multitude of species. Furthermore, declarative memory serves as a vital tool for handling recurrent challenges, allowing animals to utilize strategies formulated from past experiences. The process of memory is supported by a continuous, lifelong learning mechanism that expands the animal's repository of experiences, incorporating data about novel alterations in their environment. These cognitive processes involve multiple stages and several brain regions, ranging from the primary sensory cortices to the deep-seated thalamic structures, to the hippocampus and the cerebral cortex. To effectively execute these functions, brain networks perform local processing while simultaneously maintaining long-range communication with other neural networks. Thus, the brain coordinates these dual functions, ensuring that neither is compromised while they are executed concurrently.

The domain of spatial information processing refers specifically to the encoding positions of various objects and landmarks, which, in turn, play a crucial role in facilitating spatial navigation. Within the brain, two regions are intimately involved in spatial information processing: the medial entorhinal cortex (mEC) and the hippocampus. The mEC and the hippocampus are positioned at the top of the hierarchy for spatial information processing and serve as the primary centers for spatial memory formation and consolidation.

Learning and memory have long been the subjects of scientific investigation because of their essential functions in animal behavior. This thesis aims to further explore and expand the existing body of knowledge on these topics, with a particular emphasis on the mechanisms underlying memory consolidation. I approach this topic from an unconventional standpoint as I examine the "brain criticality hypothesis" and try to connect the concept of "criticality" to the

processes of learning and memory consolidation within the hippocampus. By doing so, I hope to provide novel insights into computational principles that guide spatial learning and memory.

1.1 Hippocampus and medial entorhinal cortex

Contemporary understanding of the role of these brain areas in memory functions traces back to the seminal finding of the $1950s$. The patient known as HM underwent a bilateral medial temporal lobectomy, a surgical procedure aimed at mitigating his severe epileptic seizures (Scoville and Milner 1957). This surgical intervention involved the removal of significant portions of his hippocampal structures, which consequently prevented the patient from forming new episodic and semantic memories. However, the intervention did not alter the intellectual abilities of the patient or the ability to acquire procedural skills. The clinical case of HM provided the first empirical indication that declarative memory is a specialized cognitive function tied to a specific anatomical region within the brain (Eichenbaum 2013). Following this report, in subsequent decades extensive research efforts have been dedicated to the hippocampus and enthorinal cortex, their anatomy, physiology, and function.

Before the entorhinal cortex and the hippocampus can act, the process of handling information from a dynamic environment involves several stages. First, the sensory organs capture the information and transmit it to the thalamic nuclei, which then convey it to the cortex (Adams et al. 2002; Sherman 2006; Mitchell et al. 2014). The sensory cortices then process specific modalities through several stages before relaying the information to higher cortical areas. Here, information from various sources is integrated and processed to perform higher-order cognitive functions. The pathway I described here appears straightforward, but it is far from simple, as it involves multiple feedback loops and interactions, but ultimately brings us to the top of the cortical hierarchy and the main topic of this thesis: the entorhinal cortex and the hippocampus.

The entorhinal cortex (EC) serves as a major hub for memory and navigation, receiving diverse inputs from various subcortical and cortical regions (Canto, Wouterlood, and Menno P. Witter 2008). It is connected to numerous thalamic and hypothalamic nuclei and midbrain areas and also receives input from the amygdala and basal ganglia. Importantly, the medial septum, which plays a role in theta oscillations, projects onto to the EC.

The cortical inputs to the entorhinal cortex (EC) are diverse, with direct contributions from various sensory and association cortices (Canto, Wouterlood, and Menno P. Witter 2008). The perirhinal and postrhinal cortices provide essential input to the EC for object recognition, spatial navigation, and memory. The olfactory cortex directly projects and conveys information regarding smell and general olfactory cues. In addition, EC also receives projections from various associative regions, while the subiculum and hippocampus provide spatial-related information to the EC (Figure 1.1 B).

All this input means that EC processes and integrates various information modalities using about $600,000-700,000$ neurons in rats (Rapp et al. 2002), arranged in a six-layer architecture. Layers I and IV function as plexiform layers, primarily containing axons and dendrites with a negligible proportion of somas, while layers II, III, V and VI serve as cell layers. Across all layers of the entorhinal cortex, there are numerous cell types distributed, such as abundant pyramidal cells, bipolar cells, and interneurons (Figure 1.1 D) (Canto, Wouterlood, and Menno P. Witter 2008).

In addition to anatomical stratification, the researchers further divide the entorhinal cortex (EC) into medial (mEC) and lateral (LEC) subdivisions, each region exhibiting unique characteristics.

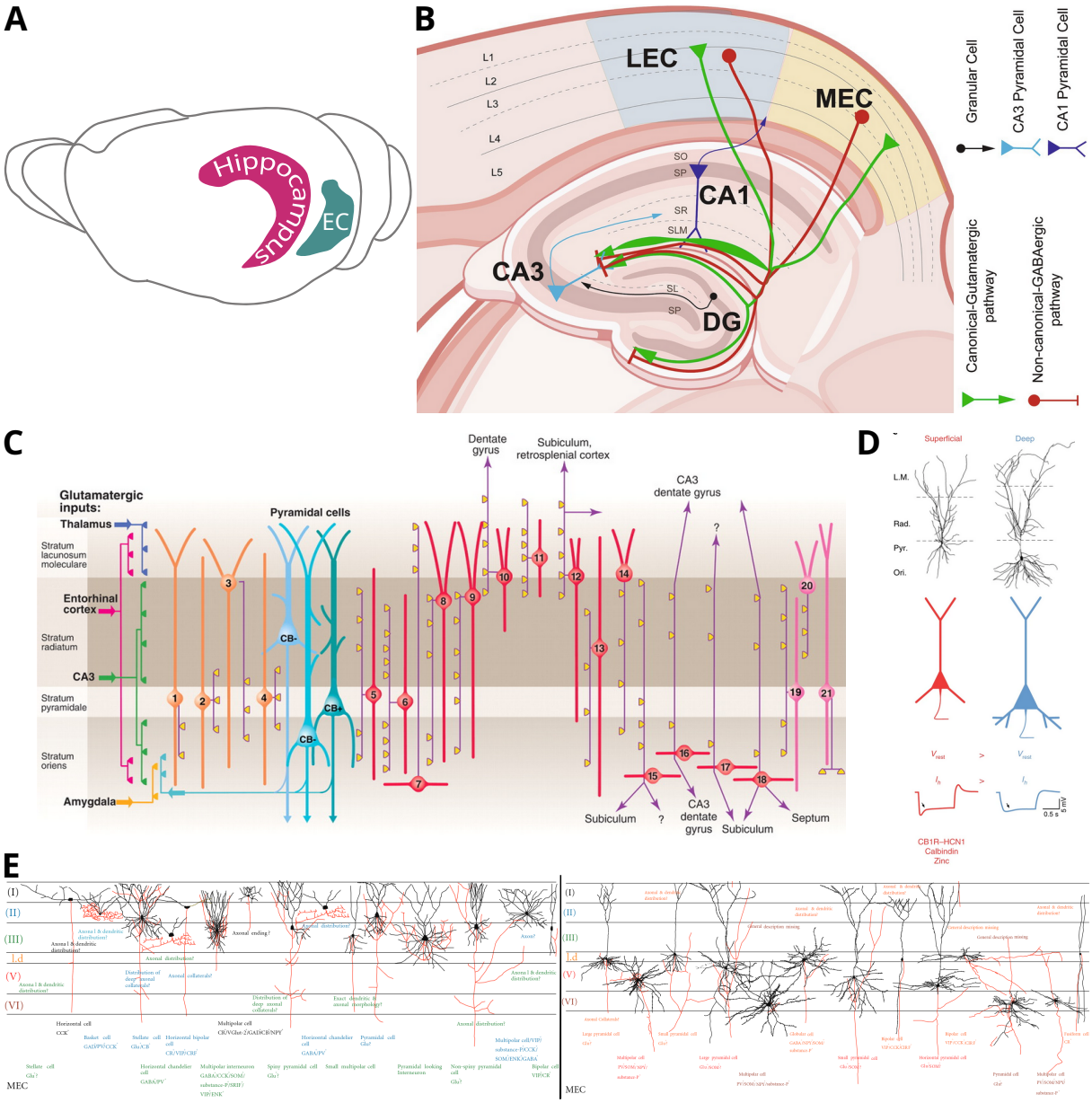

Figure 1.1: *CA1 and mEC.*

A - illustration of hippocampus and entorhinal cortex in the rat brain, **B** - schematic representation of the EC-hippocampus connectivity (adapted from Hernández-Frausto and Vivar 2024), **C** - schematic representation of diverse cell types in the hippocampus (3 subtypes of pyramidal and 21 subtypes of interneurons) (adapted from Klausberger and Somogyi 2008), **D** - different morphological (soma and dendrites, top and middle) and physiological (resting potential and somatic current) properties between superficial and deep pyramidal cells in CA1 (adapted from Soltesz and Losonczy 2018), **E** - diagram of cell types within mEC (left: superficial layers I-III, right: deep layers IV-VI, adapted from Canto, Wouterlood, and Menno P. Witter 2008).

The lateral entorhinal cortex is primarily involved in the processing of object-related information and displays minimal spatial tuning capabilities. In contrast, the medial entorhinal cortex is notable for its abundance of spatially tuned cells (Hargreaves et al. 2005; Van Cauter et al. 2013). Based on their spatial tuning characteristic, cells in mEC can be put into three main groups: grid cells, border cells, and head-direction cells.

Grid cells represent the most famous subset of cells within the medial entorhinal cortex. They exhibit periodic hexagonal firing patterns that tessellate the whole environment (Hafting et al. 2005). Grid cells form distinct functional modules along the dorso-ventral axis of the MEC. Each module maintains a uniform grid spacing and orientation relative to external landmarks. Grid cells in the same module display varying spatial phases, with their firing fields randomly offset from each other. The grid cells in a module collectively cover all spatial points, providing a robust population-level code for location. Moreover, grid fields remain stable and anchor to external cues, maintaining their stability even after removing these cues. Due to these characteristics, the medial entorhinal cortex (mEC) has been proposed as an area that provides a reliable metric of space in the brain (Edvard I. Moser and M.-B. Moser 2008). Furthermore, grid cells have been suggested to play a vital role in the path integration process. This is because they are capable of updating the internal representation of an organism's position using only self-generated motion cues, such as the running speed and direction. This capability allows maintaining positional awareness without the need for continuous sensory input from external landmarks (Bush, Barry, and Burgess 2014). However, the whole picture is more nuanced, as recent studies have indicated that there is a reorganization of grid cell maps towards the reward locations (Boccara et al. 2019; Butler, Hardcastle, and Giocomo 2019).

Border cells (Solstad, Boccara, et al. 2008; Savelli, Yoganarasimha, and Knierim 2008), also known as boundary vector cells, exhibit neural firing patterns relative to particular distances and orientations of the boundaries of an environment. This firing behavior is crucial for spatial navigation, as it enables the encoding of positional information in relation to environmental edges. Within the MEC, a significant percentage of border cells are observed to predominantly fire along a single wall of the environment. Their firing patterns are robust to other external conditions, suggesting that they fire in an allocentric (world centered) reference frame, anchored to the physical structure of the environment.

Similarly to the subiculum, mEC is also a home for head direction (HD) cells (Taube, R. U. Muller, and J. B. Ranck 1990; Taube, R. U. Muller, and J. B. Ranck 1990; Sargolini et al. 2006). An HD cell fires selectively and persistently when the animal's head is pointing in a specific allocentric direction, regardless of the animal's location. The population of HD cells, with their preferred directions uniformly distributed throughout the $360\check{r}$ of the horizontal plane, provides a continuous internal representation of the orientation of the animal, acting like a compass. In the MEC, the properties of HD cells are aligned along the dorsoventral axis, with a decrease in directional tuning from dorsal to ventral.

Besides these, mEC contains cells that do not fit into the specified categories yet still show spatial selectivity. The mEC population provides a spatial reference frame and internal navigation system, and, along with the LEC, significantly inputs to the hippocampus.(Figure 1.1 B), while also receiving direct CA1 output (Canto, Wouterlood, and Menno P. Witter 2008; Hernández-Frausto and Vivar 2024).

Cells in deep layers V and VI are targets for projections from the hippocampus and subiculum, whereas cells from the superficial layers II and III project onto the hippocampus (Hernández-Frausto and Vivar 2024). The connection between the entorhinal cortex (EC) and the hippocampus involves the trisynaptic and perforant pathways (Amaral and M. P. Witter

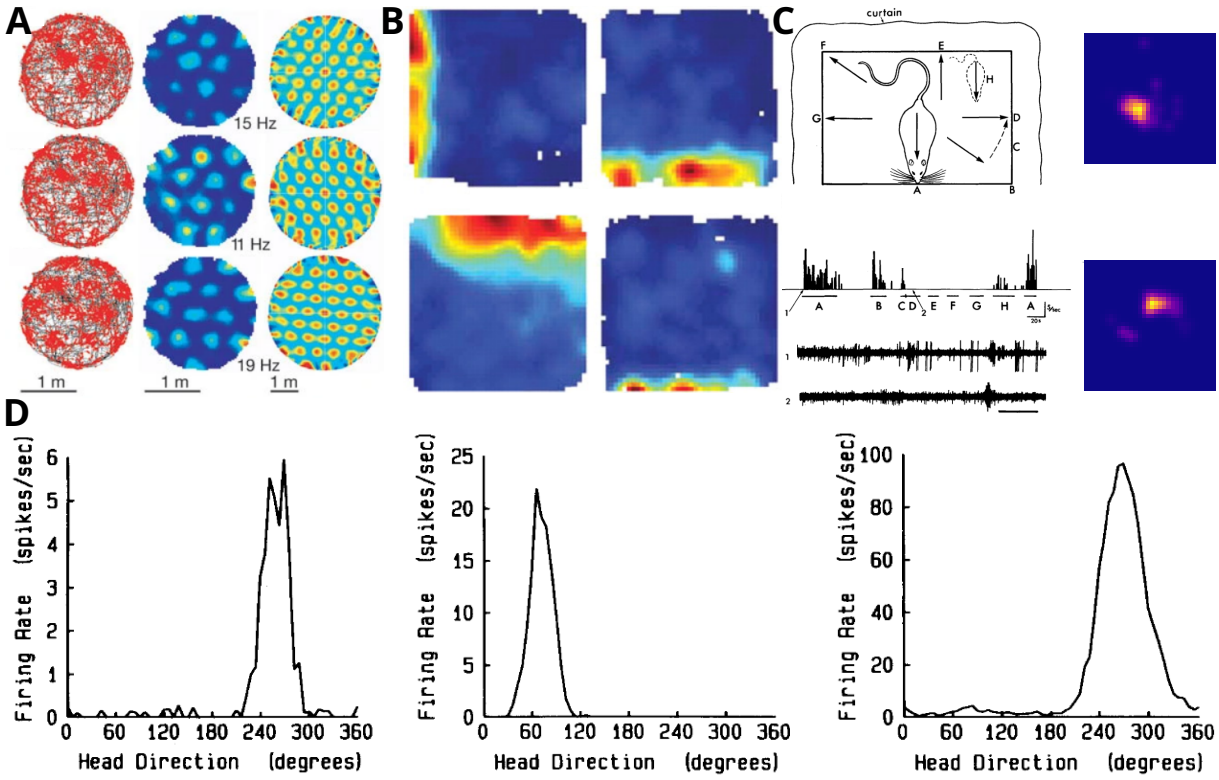

Figure 1.2: *Spatial representation in CA1 and mEC.*

A - grid cells in mEC, left: rat trajectory with superimposed spikes, middle: firing rate maps, right: spatial autocorrelation (adapted from Hafting et al. 2005), **B** - firing rate maps of border cells in mEC (adapted from Solstad, Boccara, et al. 2008), **C** - hippocampal place cells, left: first reported place cell, histogram at the bottom shows firing rate at different positions marked with letters (adapted from J. O'Keefe and Dostrovsky 1971), right: example firing rate maps of cells analyzed in this study, **D** - head direction cells in subiculum (adapted from Taube, R. U. Muller, and J. B. Ranck 1990).

1989; Menno P. Witter et al. 2000; Canto, Wouterlood, and Menno P. Witter 2008). The trisynaptic pathway refers to projections that are initiated from layer II of the mEC and extend to the dentate gyrus (DG), which subsequently relays signals to the CA3 region, which, in turn, transmits signals to CA1, completing the pathway. Initially, granule cells located in the dentate gyrus receive direct excitatory projections originating from layer II of the mEC and lEC. Subsequently, the dentate granule cells transmit the processed information through mossy fibers to the CA3 region. Here, the pyramidal cells of the CA3 area send their axons, known as Schaffer collaterals, and make synaptic connections with the pyramidal cells in the CA1 region. The perforant pathway refers to the direct transmission of signals from layer III cells of the mEC to the CA1 region, predominantly its deep pyramidal neurons. (Hernández-Frausto and Vivar 2024). In addition to excitatory glutamatergic projections, interneurons of mEC also make inhibitory GABAergic projections onto the hippocampus (Basu et al. 2016; Hernández-Frausto and Vivar 2024) using both the trisynaptic and perforant pathway. Finally, pyramidal cells located in the CA1 region, together with subiculum neurons, transmit processed information back to the deeper layers of the entorhinal cortex (EC) and other regions of the brain. This effectively closes the loop between the entorhinal cortex and the hippocampus, facilitating the continuous flow and processing of information within these regions of the brain.

The entorhinal cortex serves as the main source of input to the hippocampus; however, it is not the sole contributor. In addition, the hippocampus establishes connections with other regions,

including the amygdala and the medial septum. To process all these inputs, the hippocampus is divided into specific regions known as the dentate gyrus (DG), the hippocampus proper, which includes the *Cornu Ammonis* areas *CA1*, *CA2*, and *CA3*, as well as the subiculum. CA1 is divided according to the anatomical organization and packing of the cell bodies, axons, and dendrites. *Stratum lacunosum moleculare* is a dendritic layer where the EC projections reach CA1. Just above is the *stratum radiatum*, where the CA3 pyramidal cells project onto CA1. The cell bodies of the pyramidal cells constitute the *stratum pyramidale*. At the top of CA1 is the dendritic layer *stratum oriens*.

In the hippocampus, GABAergic interneurons constitute $10 - 15\%$ (Pelkey et al. 2017) of all cells, with diverse anatomical and functional properties (Pelkey et al. 2017; Topolnik and Tamboli 2022; Klausberger and Somogyi 2008) (Figure 1.1 C). The majority are pyramidal cells ($85 - 90\%$), which also exhibit great heterogeneity in both structure, physiology, and connectivity patterns (Soltesz and Losonczy 2018; Cembrowski and Spruston 2019) (Figure 1.1 D).

Primarily spatial inputs, which are processed by complex circuits within the hippocampus, lead to the generation of a spatial code in the CA1. This code is exemplified by the activity of place cells, which are neurons that activate when an organism is in particular locations within its environment, known as place fields (J. O'Keefe and Dostrovsky 1971). Collectively, these place fields cover the entire environment (R. Muller, J. Kubie, and J. Ranck 1987). This comprehensive coverage contributes to the formation of the cognitive map (John O'Keefe and Nadel 1978). Different environments have different hippocampal representations (Alme et al. 2014). When an animal changes environments, the hippocampus undergoes a process termed "remapping", where it shifts from one representation to another (R. U. Muller and J. L. Kubie 1987; Colgin, Edvard I. Moser, and M.-B. Moser 2008; John L. Kubie, Levy, and Fenton 2020). The emergence of hippocampal representations in novel environments has been extensively studied, showing the condition-dependent speed of the emergence of spatial representations (Hill 1978; Bostock, Robert U. Muller, and John L. Kubie 1991; Lever et al. 2002; Cacucci et al. 2007; Law, Bulkin, and Smith 2016). Since the majority of the input signals the hippocampus receives are from the entorhinal cortex, which is characterized by a multitude of specialized spatial neurons, including grid cells, border cells, and head direction cells (Zhang et al. 2013), it was proposed that the hippocampus place cells arise as a predictable transformation of this upstream activity (Solstad, Edvard I. Moser, and Einevoll 2006; Bruce L. McNaughton et al. 2006; Monaco and Abbott 2011). However, recent studies demonstrated a very straightforward way to generate place fields, based on thresholded gaussian processes (Mainali, Azeredo da Silveira, and Burak 2025), which reproduce the diversity among the shapes and sizes of place fields (Rich, Liaw, and Lee 2014; Fenton et al. 2008; Cohen and Drugowitsch n.d.). In addition, place firing depends on the radial position (Danielson et al. 2016) within CA1, and the hippocampal maps are modulated by rewards (Gauthier and Tank 2018; Boccara et al. 2019).

Despite the diversity in spatial tuning, the activity of hippocampal cells is not chaotic and independent, but often coordinated and rhythmic. The two primary categories of rhythms that have been extensively researched are theta ($6 - 10Hz$, Figure 1.3 A) and sharp wave–ripples ($150 - 250Hz$, Figure 1.3 B). These rhythms serve as a substrate for different functions in the hippocampus and cells are often coupled to different phases of each oscillation (Figure 1.3 C).

Theta oscillations occur during active locomotion and REM sleep, in all sub-regions of the hippocampus. The generation of the theta rhythm in the hippocampus is primarily influenced by the rhythmic neuronal activity within the septal regions. When the septal areas are damaged,

there is a notable disruption in the hippocampal theta activity (Green and Arduini 1954). In addition, intrinsic circuits within the hippocampus also play a crucial role in modulating this theta rhythm. In a simplified perspective, the primary contribution involves the rhythmic firing of the septal interneurons, which send GABAergic projections to the hippocampal interneurons. This process results in the disinhibition of hippocampal pyramidal cells in an oscillatory fashion. However, this mechanism is more intricate, as demonstrated by the varying theta modulation observed among different subtypes of hippocampal interneurons and pyramidal cells (Klausberger, Magill, et al. 2003; Klausberger and Somogyi 2008; Colgin 2016). In addition to the GABAergic input, the medial septum transmits cholinergic projections that significantly modulate the excitability of the hippocampus, further amplifying theta oscillations (Colgin 2016; Vandecasteele et al. 2014). Finally, the intrinsic properties of hippocampal cells, related to HCN channels (Colgin 2016 for review), contribute to theta rhythm generation, as evidenced by spontaneous emergence of theta rhythm *in vitro* (Goutagny, Jackson, and Williams 2009).

The coordinated synchronous activity observed in the theta rhythm has been identified as functionally significant. The association between the presence of theta waves and enhanced learning speed, as well as improved memory function, has been recognized in earlier research (Berry and Thompson 1978; Winson 1978) and has been reaffirmed in more contemporary studies (reviewed in Colgin 2016), leading to the theory that theta is essential for memory formation. Theta cycles exhibit a close relationship with the firing of place cells, as observed in theta phase precession (William E. Skaggs, Bruce L. McNaughton, M. A. Wilson, et al. 1996). This is a phenomenon where a neuron initially fires at a late phase within the theta cycle and progressively advances to earlier phases within the same cycle, as the animal repeatedly navigates through the neuron's place field. However, place fields can form even when theta is experimentally blocked (Brandon et al. 2014) or is naturally absent (in flying bats, Yartsev and Ulanovsky 2013, which implies that theta oscillations are not necessary for the formation of spatial representations. Yet, the formation of memory representations is a complex process that involves a large number of neurons. Theta rhythm has been proposed to play a crucial role in organizing these neural ensembles that serve to represent distinct individual memories. Nested in theta cycles, these ensembles are called theta sequences (William E. Skaggs, Bruce L. McNaughton, M. A. Wilson, et al. 1996; Foster and M. A. Wilson 2007) ¯ organized groups of place cells that activate in a specific order. Moreover, theta sequences represent behaviorally meaningful information; they segment the environment into smaller portions (Gupta et al. 2012), encode a trajectory towards an upcoming goal (Wikenheiser and Redish 2015; Tang et al. 2025), or "sweep" unvisited parts of the maze (Vollan et al. 2025). Theta rhythm is also related to locomotion and stepping, which in rats occurs with a similar frequency of $8Hz$, and is synchronized with spatial representation. The current position of the animal is represented when the forelimbs are on the ground, while sequences encoding possible future location occur within the interval between two steps (Joshi et al. 2023). In addition to locally important coding properties, the hippocampal theta rhythm is coupled with the activity of other cortical areas (Siapas, Lubenov, and M. A. Wilson 2005; Backus et al. 2016; Nardin et al. 2023) and thalamic nuclei (Ramirez-Villegas, Besserve, et al. 2021), thus being proposed as a substrate for long range communication between the hippocampus and other areas of the brain (Eichenbaum 2017). Finally, brain-wide theta rhythms are associated with sensory processes and may coordinate the integration of multi-modal sensory information and its higher-level processing (Colgin 2016).

Another important class of hippocampal oscillations are sharp wave ripples (SWR), transient oscillations in the frequency range of $150 - 250Hz$ (Buzsaki et al. 1992) that occur during

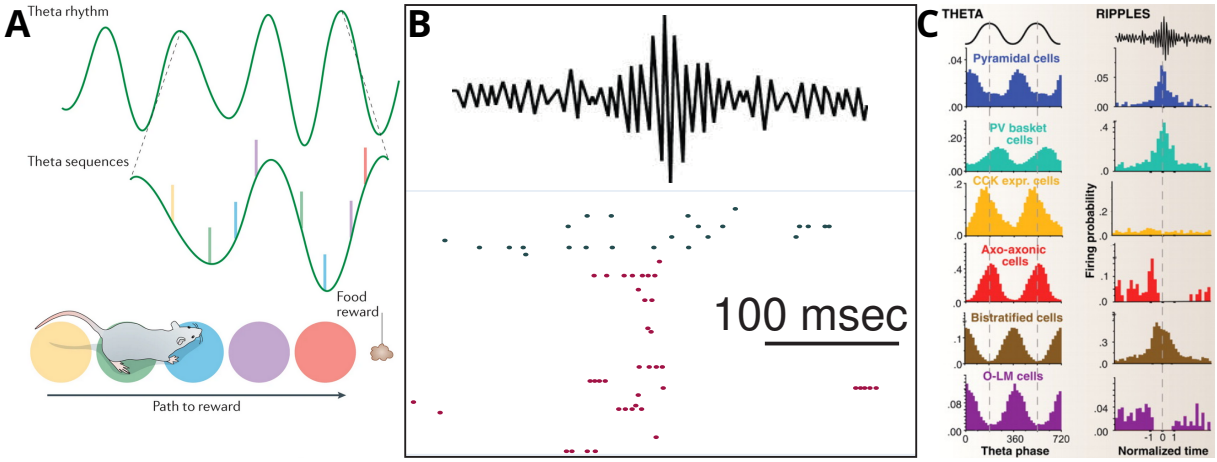

Figure 1.3: *Theta and SWR oscillations.*

A - illustration of theta oscillations and theta sequences (adapted from Colgin 2016), **B** - illustration of SWR (top), spike raster of mEC (green) and CA1 (crimson) activity during SWR, **C** - recruitment and phase locking of different classes of hippocampal cells during theta and SWRs, histograms of firing rates (adapted from Klausberger and Somogyi 2008).

slow wave sleep and quiet immobility. SWRs are generated within the hippocampus and consist of two distinct elements: a sharp wave component and superimposed ripple oscillations. Sharp waves are large amplitude excitatory events that originate in the CA3 region of the hippocampus and that are subsequently propagated to the CA1 area (György Buzsáki 1986), while ripples are generated by local CA1 interneurons (Klausberger, Magill, et al. 2003; Colgin 2016). The characteristics of SWRs vary across the hippocampus (t. Csicsvari et al. 1999; Taxidis et al. 2015; Ramirez-Villegas, Logothetis, and Besserve 2015; Sebastian et al. 2023), mainly due to differential input mechanisms and possibly due to different functional properties (Taxidis et al. 2015; Robinson et al. 2025; Castelli et al. 2025).

Sharp wave-ripples play a significant functional role during periods of active wakefulness, as their disruption has been shown to negatively impact task performance (Jadhav et al. 2012) and to destabilize place fields (Roux et al. 2017). As a consequence of these findings, it has been hypothesized that SWRs are integral to memory-driven planning processes related to task execution (Carr, Jadhav, and Loren M. Frank 2011; Roumis and Loren M Frank 2015). SWRs are widely recognized for their significant contribution to the process of memory consolidation (G. Buzsáki 1989; G. Buzsáki 1996; György Buzsáki 2015). The function of SWR in the consolidation of memory is observable through the processes of neuronal reactivation and replay (M. Wilson and B. McNaughton 1994; Louie and M. A. Wilson 2001; Lee and M. A. Wilson 2002; Joseph O'Neill et al. 2010). The process of memory reactivation plays an essential role in reinforcing and stabilization of memories over time. It is a process in which neural activity patterns that are initially exhibited during wakeful behavior are subsequently reactivated during periods of sleep or quiet wakefulness, particularly when SWRs occur. The causal role of reactivation in memory consolidation was demonstrated by disrupting SWR-related hippocampal reactivation during sleep, thereby impairing memory consolidation and recall (Girardeau, Benchenane, et al. 2009; Ego-Stengel and M. A. Wilson 2009). Moreover, disrupting only assemblies that encode a specific environment affects only memory associated with disrupted assemblies, leaving other memories intact (Gridchyn et al. 2020). On the other hand, prolonging existing SWRs improves memory (Fernández-Ruiz et al. 2019). It should be noted that CA1 representations are not necessarily affected by optogenetic disturbance of SWRs during sleep (Kovács et al. 2016). The disturbance may primarily affect assemblies that

have not been stabilized, whereas those that have already achieved a stable configuration may remain unaffected. (Ven et al. 2016). Finally, the functional importance of reactivation during SWRs for brain-wide memory processes is exemplified through the brain-wide coupling of oscillations during slow wave sleep, where SWRs are nested in the troughs of thalamic spindles ($12 - 15Hz$), themselves nested in the excitable up-state of the cortical slow oscillations ($< 1Hz$) (Klinzing, Niethard, and Born 2019).

The brain-wide integration and intrinsic computational characteristics allow the hippocampus and entorhinal cortex to be crucial components in the formation and use of declarative memories (Kandel, Dudai, and Mayford 2014). These memories refer to information about events (episodic memory) and associated meaning attached to different types of entities (semantic memory) and can be represented by the hippocampal-enthorinal circuit that enables the representation of spatial maps and spatial relations (György Buzsáki and Edvard I Moser 2013). Therefore, place cells in CA1 and grid cells in mEC, along with object representation in lEC (Tsao, M.-B. Moser, and Edvard I. Moser 2013), are believed to be the most important neural substrate of declarative long-term memory, its formation, and its conscious use (Kandel, Dudai, and Mayford 2014).

From a theoretical perspective, memory has undergone a comprehensive investigation within the framework of attractor network models (Hopfield 1982). This is a circuit with recurrent connectivity, where the weights between nodes reflect interactions between neurons. In attractor networks, the dynamic behavior typically evolves to form stable, self-perpetuating configurations known as attractors. These attractors are crucial, as they embody the representation of memories encoded within the network. Since its initial publication, attractor networks have become a key concept in computational neuroscience for modeling how the brain stores and retrieves memories using collective dynamics.

1.2 Collective dynamics and brain criticality

Attractor networks demonstrate how interactions among numerous simple neurons can lead to the emergence of computational capabilities. Emergence describes the phenomenon where complex high-level properties arise that cannot be easily explained by the system's basic components. This insight inspired a lot of subsequent research on collective dynamics in neuroscience and how it can lead to the emergence of brain functions. One such approach to investigating collective dynamics is known as brain criticality, the hypothesis that the brain operates near a border between order and chaos (Figure 1.4 A, Plenz et al. 2021; O'Byrne and Jerbi 2022; Tian et al. 2022).

This abstract view of brain activity is based on three important concepts: the subcritical regime, the supercritical regime, and the critical point. In the subcritical regime (Figure 1.4 B left), the system (population of neurons in our case) is very ordered, exhibiting large domains of uniform activity and negligible variability over space (cell population) and time. Within this regime, the activity of neural networks is attenuated and diminishes as time progresses. This particular regime hinders the effective processing of information, as it adversely affects local neural processing and the sensitivity to incoming signals. Furthermore, it also disrupts the communication between neurons over longer distances, thereby impeding the overall efficiency of neural information transmission.

At the other extreme of the spectrum is the supercritical regime (Figure 1.4 B right), characterized by disordered neural activity that resembles chaotic behavior. The activity propagates

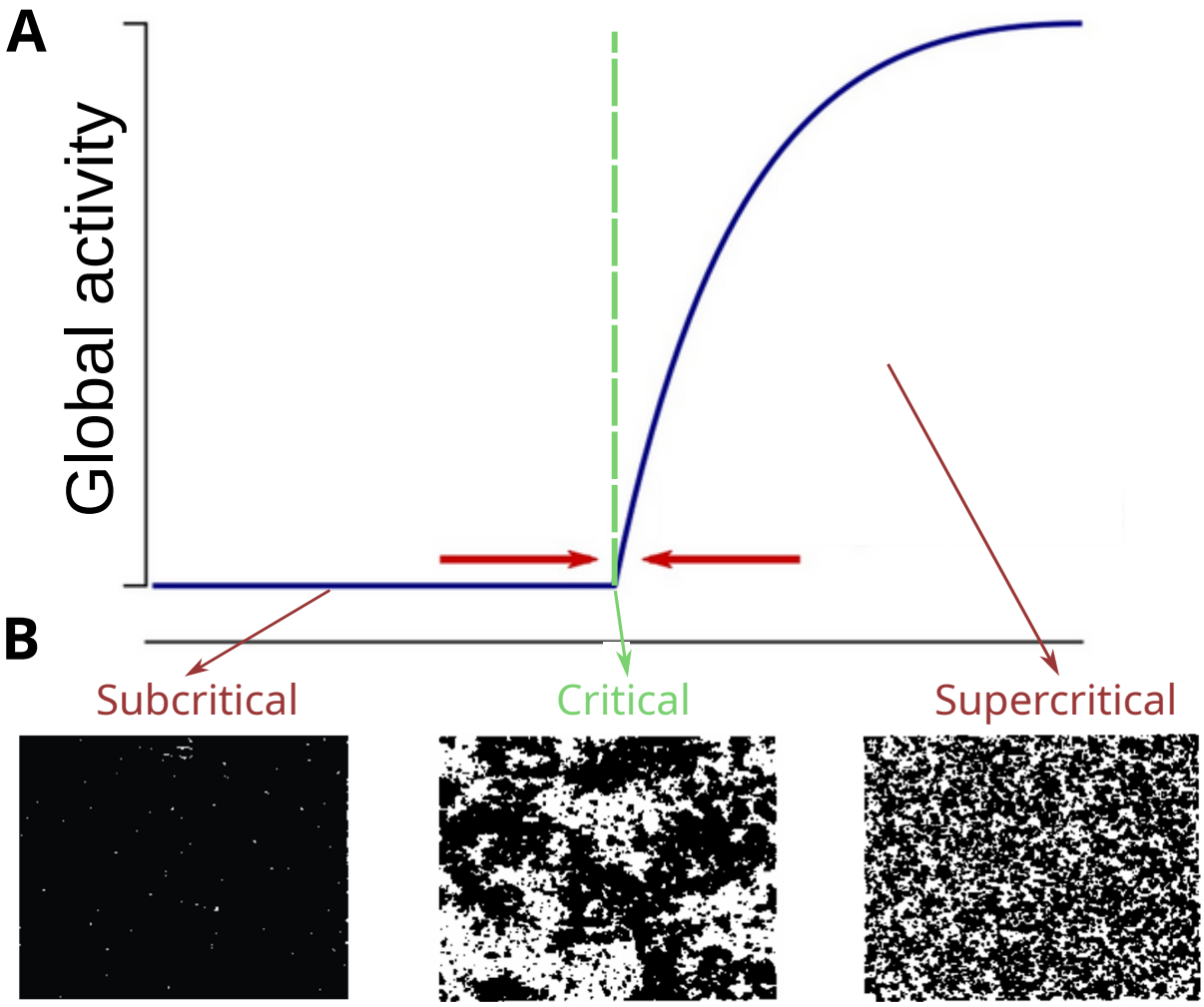

Figure 1.4: *Criticality.*
A - the critical point as a border between silence and chaos, (adapted from Wilting and Priesemann 2019), **B** - snapshots of Ising model during subcritical, critical and supercritical state (adapted from Chialvo 2010).

quickly, leading to sustained neural firing that does not show features of collective behavior. In this disordered system, there exists the potential for unchecked dissemination of activity across the network, which may culminate in hyper-synchronization, resembling the phenomena observed during an epileptic seizure (Lepeu et al. 2024; Liu, F. Li, and Wan 2023)). Once more, this regime is not computationally desirable due to its heightened sensitivity and the insufficient segregation of units, as it leads to numerous components responding in a similar manner to identical stimuli.

At the middle, in the sweet spot, resides the concept of criticality ¯ a condition wherein the system functions in proximity to the boundary, known as the critical point, separating two distinct phases. Compared to two other regimes, the system in this regime demonstrates markedly distinct characteristics, not only temporally but also spatially, across various neurons in the network. Neural activity is balanced, avoiding both uncontrolled proliferation into disordered states and degradation or decline. Neurons demonstrate long-distance correlations, and complex patterns of neural activity can arise solely from relatively weak interactions among cells. These activity patterns generally do not exhibit a distinct temporal or spatial scale (number of neurons), and their features obey the power law. This implies that events of

various magnitudes and lengths are possible, encompassing a wide range of sizes and durations. The scale-free nature of dynamics implies that dynamic operations are the same across varying scales, ranging from individual local circuits to extensive large-scale networks.

Finally, the brain criticality hypothesis is not based only on theoretical principles but also on experimentally observed signatures of brain criticality in neural recordings. The first signatures of criticality observed in the brain have been neuronal avalanches ("avalanche criticality", Beggs and Plenz 2003; Beggs and Plenz 2004). These are cascades of neural activity that propagate through the network, displaying a distinctive absence of a characteristic scale. As a result, the distributions of their sizes and durations adhere to a power law (Figure 2.1, Section 2.1). Neuronal avalanches have been documented in recordings spanning a range of scales, from slice cultures (Beggs and Plenz 2003; Mazzoni et al. 2007; Pasquale et al. 2008), over cortical populations *in vivo* (Petermann et al. 2009; Gireesh and Plenz 2008; Hahn, Petermann, et al. 2010; Yu et al. 2011; Xu et al. 2024), and to the level of the whole-brain (Adrián Ponce-Alvarez, Kringelbach, and Deco 2023; Freeman et al. 2003; Meisel et al. 2013; Solovey et al. 2012; Poil et al. 2012; Lombardi, Shriki, et al. 2021).

If brain activity is critical and marked by the appearance of scale-free characteristics, it is sensible to analyze it varying spatial and temporal scales. In other words, the underlying system can be more comprehensively understood by taking a broader perspective, or "zooming out," to examine if it retains properties that are anticipated to remain consistent regardless of the scale at which they are observed. Statistical physics offers a well developed theoretical framework known as the Renormalization Group (RG) (Kadanoff 1966; K. G. Wilson 1975; Sethna, Dahmen, and Myers 2001), which is utilized for this kind of methodological approach. Given the current lack of clarity regarding whether the brain satisfies the formal prerequisites necessary for the application of the traditional Renormalization Group, Meshulam et al. 2019 introduced the Phenomenological Renormalization Group (PRG) as a modification of the RG applicable to neural data (Figure 2.5, Section 2.2, Chapter 3). By employing this method, scale-free activity patterns, similar to those predicted in a critical state, have been detected throughout the rodent brain (Meshulam et al. 2019; Morales, Santo, and Muñoz 2023; Castro et al. 2024) and across different species (Castro et al. 2024).

However, in order to exhibit these characteristics, the brain is not required to function precisely at the critical point. Instead, it can operate in proximity to this point or within a region that is nearly critical, often referred to as a quasi-critical region (Williams-García et al. 2014; Tian et al. 2022). One way to achieve and maintain proximity to a (quasi-)critical state can be accomplished through the meticulous adjustment of control parameters, such as those influenced by neuromodulators Chialvo 2010. However, certain natural systems appear to have inherent mechanisms that enable them to self-organize to reach a critical point, a phenomenon known as self-organized criticality. It is hypothesized that the brain may be one of such systems, capable of self-organization (Hesse and Gross 2014; Plenz et al. 2021) and enjoys the benefits of criticality.

Maintaining operations at or near criticality provides a diverse range of functional benefits (Shew and Plenz 2013). In many modeling studies, it has been shown that operating at (quasi-)criticality facilitates long-range communication (Lombardi, Shriki, et al. 2021; Avramiea et al. 2022) and maximizes input sensitivity (Kinouchi and Copelli 2006). In the context of this thesis, the most relevant aspects are those that explain how operating close to criticality affects the storage of memory and the transfer of information in neural networks. The number of different configurations of cortical networks is maximized when they operate in a regime that exhibits signatures of criticality (Shew, Yang, Yu, et al. 2011), linking the concept of

criticality to the maximal information capacity of the network. Furthermore, the identical operational regime enhances the information transmission, which is quantitatively evaluated through the mutual information between the input and the output (Shew, Yang, Yu, et al. 2011).

1.3 Aims of the Thesis

Despite the computational advantages and the presence of well-documented signatures of criticality within the brain, it is still not well established whether the concept of criticality is behaviorally relevant. This is particularly evident in the case of the hippocampus, where there is a lack of direct understanding of how its dynamics, when examined through the lens of criticality, correlates with its roles in memory processes. However, memory is not an exclusive feature of the hippocampus, and the mechanism of memory consolidation involving the hippocampus and other cortical regions remains a significant subject of ongoing research. Thus, I sought to broaden the understanding of this complex process. Consequently, the objectives of this thesis can be outlined as follows:

1. Characterize hippocampal activity from the point of view of criticality using neuronal avalanches and the Phenomenological Renormalization Group and examine relationships between these two views
2. Investigate whether criticality-related measures of hippocampal activity are related to spatial memory consolidation
3. Investigate encoding dynamics and CA1-mEC communication in relation to spatial memory

While conducting the analysis related to the listed aims, I found relationships between the signatures of criticality and functional heterogeneity among cells. This led to two smaller goals:

1. Develop measures of the functional variability of neurons in CA1 and mEC
2. Investigate whether functional variability supports the functioning of CA1 and mEC

Methods

Experimental Methods

Animals

All animals used in this study were Long-Evans rats, 10-20 weeks old, weighing $300 - 400g$. In total, the analysis was performed on 16 animals. Parts of the dataset used were previously published. Details are in Table 1.1:

Experimenter	**Publication**	**Num. animals**	**Num. rec days**	**Chapter**
Peter Baracksay	Bollmann et al. 2025	3	8	2
Charlotte Boccara	Boccara et al. 2019	4	13	3, 4
David Dupret	Dupret et al. 2010	3	8	3
Juan Felipe Ramirez Villegas		2	2	3
Predrag Živadinović		3	5	3

Table 1.1: Animals used in this thesis

The three animals I recorded were used for optogenetic experiments (detail below). However, there was no light stimulation in the recording days used for this study.

All experimental procedures were carried out in accordance with the Austrian Federal Law for experiments with live animals and under a project license approved by the Austrian Federal Science Ministry.

Maze Aparatus

I used the same "cheeseboard" maze as previously described (Dupret et al. 2010; Boccara et al. 2019). The maze is made of a circular PVC board with a diameter of $1.2m$ and a thickness of $2cm$. The maze has 177 food wells drilled on the board in a regular grid with a spacing of $8cm$ between the centers of the wells. Alongside the maze was placed the start box of size $30x20cm$ with $50 - 60cm$ in height. The start box is not covered and has doors lower than the walls, allowing the animal to be tracked inside. A black curtain surrounded the entire apparatus.

Behavioral paradigm

The behavioral protocol used in this study has already been published (Dupret et al. 2010; Boccara et al. 2019). It was developed to assess spatial learning and memory in rats. On each

day of recording, rats were tasked with finding and remembering three new wells in which food pellets ($20mg$) were hidden. All days of recording followed the same protocol, starting with a "*Pre-Probe*" session during which the rats were free to explore the maze without any food rewards present in it, for 10-25 minutes. The rats were then put into a separate sleep box for the 30-90-minute "*Pre-Sleep*" session. Then came the "Learning" session, during which rats learned to locate and remember the locations of three rewarded wells. The "Learning" session typically consisted of 20-40 trials and was followed by the "Post-Sleep" session. Finally, rats' memory recall was tested in the second unrewarded "*Post-Probe*" session. To prevent rats from using odor-guided navigation to locate food pellets, the maze was covered with a food powder made from the same pellets that were given to rats.

Pre-training procedure

Similar protocols were used in all subsets of animals (Dupret et al. 2010; Boccara et al. 2019). At the beginning of every experiment, rats were pre-handled and habituated to both the experimenter and the recording environment. After the initial habituation period, implantation surgery was performed, followed by a recovery period of a week. Subsequently, rats were put on a food restriction protocol during which their weight was slowly reduced to the target value of $85 - 88\%$ of the starting weight. During this period, rats were exposed to the maze and trained to locate three food pellets ($20mg$) and, after consuming them, returned to the start box. At every trial start, the start box door would open, allowing rats to come out onto the maze, then the doors would close and remain so until rats located all three food pellets. Upon locating and eating all the pellets, the start box door would open, allowing the rats to return. To motivate them to return, food pellets were also placed in the start box. This procedure was repeated for 10-20 trials per training day, depending on the motivation of the rats'. The whole protocol was repeated for 4-6 days, until the rats performed the given task consistently and until they reached the target body weight.

Extracellular Recordings

The recordings were performed using microdrives consisting of 16 or 32 independently movable tetrodes. The tetrodes were made from four tungsten wires twisted and heated to bind together. The wire used was 10 or $12\mu m$ thick, while the tips were gold-plated to achieve a target impedance of $400 - 500k\Omega$. Each bundle of tetrodes consisted of 16 tetrodes implanted in the right hemisphere. Drives with 32 tetrodes had two bundles implanted bilaterally. On each recording day, tetrode positions were tuned to ensure that they remained within the dorsal CA1, using LFP features as visual guidance.

All data were recorded using Axona or Intan acquisition systems for electrophysiological recordings. Wideband ($0.4 - 9kHz$) recordings were made and amplified local field potentials were digitized at $20kHz$ or $24kHz$.

Isolating single-unit activity

In data recorded by Predrag Živadinović and Juan Villegas, individual spikes were detected as events whose amplitude crossed the threshold of five standard deviations over the mean amplitude of the signal. The spikes were assigned to the clusters using a combination of automatic clustering with Mountainsort (Chung et al. 2017) and manual curation with Phy (*Manual Clustering Practical Guide (by S. Lenzi and N. Steinmetz) - phy* 2025). Details about processing of previously published data can be found in the corresponding publications.

Position Recordings

On top of the microdrives were mounted LEDs that were used for position tracking. The position of the rat was recorded using a separate camera positioned above the maze. The camera was recording at 39.0625 frames per second and was synchronized with the acquisition system via a TTL pulse.

Drive implantation and recovery

Surgical implantation was performed as previously described (Dupret et al. 2010; J. O'Neill et al. 2017; Boccara et al. 2019). The rats were put under Isoflurane anesthesia ($1-2\%$) and treated with analgesics throughout the procedure. The craniotomies were open and drives were implanted so that the tetrode bundles are positioned over the dorsal CA1 (2-4mm ML, -2.5 -5mm AP). During implantation, the tips of the tetrodes were positioned superficially, 1 to $1.4mm$ from the surface of the brain. After surgery, rats were allowed at least a seven-day recovery period. After the recovery period, the tetrodes were slowly lowered towards the hippocampus, over the following few days.

Optogenetic stimulation

In some animals, an optogenetic excitation of hippocampal interneurons was performed. Channelrhodopsin ChR2 was expressed in cells containing the mDLx promoter using Adenovirus AAV1 as a vector (Dimidschstein et al. 2016). The virus was injected into six locations spread over dorsal CA1 ($200nl$ in each location) in a separate surgery performed three weeks before microdrive implantation. Stimulation was performed using pulses of blue light delivered through optical fibers attached to the microdrives. For the analysis in this study, I used only days during which no light stimulation was performed.

Data analysis

Unless stated otherwise, data analysis pipelines are implemented using Linux core utils, Python programming language (Van Rossum and Drake 2009), and packages from its vast data analysis ecosystem: numpy (Harris et al. 2020), scikit-learn (Pedregosa et al. n.d.), scipy (Virtanen et al. 2020), statsmodels (Seabold and Perktold 2010), pandas (McKinney 2010; The pandas development team 2020), matplotlib (Hunter 2007), plotly (Inc 2015), seaborn (Waskom et al. 2014), plotnine (The plotnine development team n.d.), joblib (Developers 2025).

The quantities in the text are expressed as $mean \pm standard\,error$, unless stated otherwise. In the text $N.S.$ denotes $p > 0.1$, $*$ denotes $p < 0.05$, $**$ denotes $p < 0.01$, $***$ denotes $p < 0.001$, $****$ denotes $p < 0.0001$.

Bayesian information criterion The Bayesian information criterion (BIC) is a quantity used for model selection. BIC measures the likelihood of the model while accounting for the complexity of the model (number of parameters). The model with the lowest BIC is preferred.

BIC is computed as:

$$BIC = k \cdot ln(n) - 2 \cdot ln(L)$$

where k is the number of parameters in the model, n is the sample size, L is the likelihood of the model.

Quartile coefficient of dispersion

The quartile coefficient of dispersion (QCD) is a measure of dispersion of a distribution. It is one of the robust measures of scales. It is calculated from the first and third quartiles (Q_1 and Q_3):

$$QCD = \frac{Q_3 - Q_1}{Q_3 + Q_1}$$

Sarle's bimodality coefficient

Sarle's bimodality coefficient b quantifies the "modality of the distribution". For a finite sample, it is calculated as follows:

$$b = \frac{g^2 + 1}{k + \frac{3(n-1)^2}{(n-2)(n-3)}}$$

where n is the number of elements in the sample, g is the sample skewness and k is the sample excess kurtosis. The value of b lies between 0 and 1, with the value of $5/9$ assumed by the uniform distribution. The value of 1 is assumed by a Bernoulli distribution with two values.

Neuronal avalanches

Temporal Binning

The duration of temporal bins used in the avalanche analysis was calculated as the average inter-spike interval of spikes from all available cells. This was done for each session individually. First, spikes from all available cells were collected into a single list and ordered by time. Then, the average difference between successive spike times was computed on this list and used as the duration of the temporal bins.

Detection, size, and duration of neuronal avalanche

Next, I binned the spikes in temporal bins and identified bins that did not contain spikes ("silent bins"). A neuronal avalanche is defined as a period of non-zero activity between two successive silent bins. The duration of the avalanche is defined as the total number of active bins (1 or more spikes), while the size of the avalanche is defined as the total number of spikes emitted during an avalanche.

Avalanche Size and Duration Power Laws

To find power laws associated with neuronal avalanches, I first computed histograms of avalanche duration and size. Then, I set the scaling range as $[1, 30]$ for the duration of the avalanches and $[1, 100]$ for the size of the avalanches. Using only values that fall within the given range, I found the maximum likelihood fit. I used the Python package "powerlaw" to perform the calculation. The power law exponent fitted to the avalanche duration distribution is labeled with α, while the exponent related to the avalanche size distribution is τ.

Scaling Relation

To compute the scaling relation between the duration and the size of avalanches ($\frac{1}{\sigma\nu z}$), I first collected all distinct durations of the avalanche and, for each duration, calculated the mean size of the avalanche. Then, I applied a log transformation to both distinct durations and mean sizes. I fitted a line to these data using the ordinary least squares method. The scaling relation is the slope of the fitted line.

DCC

The Distance to criticality coefficient is defined as the absolute difference between the scaling relation and the ratio between power law exponents for duration and size:

$$DCC = |\frac{1}{\sigma\nu z} - \frac{\alpha - 1}{\tau - 1}|$$

Temporal profiles (avalanche shapes)

To compute temporal profiles of avalanches (avalanche shapes), I first identified distinct avalanche durations. For every unique duration, I collected all avalanches. Then, for every avalanche duration, I calculated the temporal profile as the mean number of spikes per-bin, across all avalanches with the given duration.

For a given scaling parameter s, I obtained scaled temporal profiles by bringing all profiles to a uniform duration $t \in [0, 1]$ and multiplying the mean size per time point by t^s. In critical systems, rescaling the temporal profiles with parameter $s = \frac{1}{\sigma\nu z}$ collapses all durations onto a single line. To find the scaling exponent Σ that gives the best collapse, I used the method described in (Marshall et al. 2016). It performs a grid search to find a value of the parameter s that minimizes the variance of rescaled shapes. The code implementation is from NCC Toolbox (Marshall et al. 2016).

Phenomenological Renormalization Group

Brief outline

Consider a collection of N neurons, where the temporarily binned (details below) activity of the i-th neuron is denoted by $x(i)$. Neurons are grouped during each step K of the phenomenological renormalization group (PRG) process based on the criterion of the maximum pairwise Pearson correlation coefficient. Denote by $\overline{x}_i^k$ the activity of the coarse-grained unit i at step K of the PRG. Initially, the activities $\overline{x}_i^0$ coincide with the original cell activities. Each step begins by selecting the most correlated pair of cells (i, j), and merging their activities into a new coarse-grained variable:

$$\overline{x}(1)^k = \frac{\overline{x}(i)^{k-1} + \overline{x}(j)^{k-1}}{c}$$

where c is picked so that the mean non-zero activity is equal to one and preserves 0s. Subsequently, we merge the next most-correlated pair and continue until we form $N/2$ coarse-grained units, each comprising the aggregated activity of the 2 original cells. In the next iteration, the procedure produces the third PRG level ($K = 4$) with $N/4$ coarse-grained units, each consisting of four original cells. This procedure is repeated iteratively until only one unit remains.

Calculating temporal bin duration ($Geom.ISI$)

The duration of temporal bins used in the PRG analysis was calculated as the geometric mean of the inter-spike intervals of the spikes of all available cells. This was done for each session individually. First, spikes from all available cells were collected into a single list and ordered by time. Then, the differences between successive spike times were calculated, producing a list $[d_1 \dots d_n]$. The geometric mean of this list was calculated as follows:

$$GeomMean(d_1 d_2 \dots d_n) = \sqrt[n]{d_1 d_2 \dots d_n} = \frac{exp(ln(d_1) + ln(d_2) + \dots ln(d_n))}{n}$$

.

Pairwise Correlations

Pairwise Pearson correlations were computed between units at the given level of PRG. If $x(i)$ represents the activity of the ith unit, the Pearson correlation between units i and j was calculated as:

$$\rho(i,j) = \frac{(E[(x(i) - E[x(i)])(x(j) - E[x(j)])]}{\sigma_{x(i)}\sigma_{x(j)}}$$

Distribution of Non-Zero activity Q(x)

The distributions of non-zero activity $Q_K(x)$ are plotted as a histogram of non-zero activity at the given PRG level K.

Probability of Silence, free energy F, and scaling exponent β

I computed the probability of silence P_0 for each coarse-grained PRG unit at each PRG step K. For a given coarse-grained unit at the PRG level K, the probability of silence is the number of bins valued 0 divided by the total number of bins. The free energy F is computed as:

$$F = -ln(P_0)$$

After computing the free energy F for every unit in the PRG, I calculated the mean free energy $< F(K) >$ for each PRG level K. Then I plotted $< F(K) >$ as a function of K. Next, I calculated a logarithm of $< F(K) >$ and fitted a line. The scaling exponent β is the slope of the fitted line.

Activity Variance and the scaling exponent α

I computed the activity variance of each coarse-grained PRG unit at every PRG step K. For a given coarse-grained unit at PRG level K, I first traced the K cells that comprise the given unit. Then I concatenated the activity of the traced cells into a single array and calculated the variance of the concatenated array.

After computing the activity variance of every unit in PRG, I calculated the mean activity variance $< M2(K) >$ for each PRG level K. Then I plotted $< M2(K) >$ as a function of K. Next, I calculated a logarithm of $< M2(K) >$ and fitted a line. The scaling exponent α is the slope of the fitted line.

Covariance matrix spectrum and the scaling exponent μ

For a given PRG level K and a given coarse-grained unit u_K^i, the original cells $\{c^{i_1} \dots c^{i_K}\}$ that comprise it were isolated. Then, among the original cells $\{c^{i_1} \dots c^{i_K}\}$ a pairwise correlation

matrix c_K^i was calculated. Then the eigenvalues $\{\lambda^{i_1} \dots \lambda^{i_K}\}$ of the matrix c_K^i were computed. Each eigenvalue had an associated fractional rank. The fractional rank is computed as the eigenvalue rank divided by K:

$$FractionalRank(\lambda^i) = \frac{Rank(\lambda^i)}{K}$$

Next, all eigen values across all pairwise correlation matrices of all PRG levels were plotted as a function of their fractional rank. The scaling exponent μ was obtained by fitting the following function to the eigenvalue-fractional rank relation:

$$\lambda = B * FractionalRank(\lambda)^{-\mu}$$

Decay of autocorrelation time and the scaling exponent z

The decay of autocorrelation time was calculated for every PRG level and refers to the exponential decay constant of the population autocorrelation function.

The autocorrelation function has been estimated from binned activity time series (binned spike trains with bin duration $GIEI$ at $K = 1$, coarse-grained activity for $K > 1$). For each unit at a given PRG level K, the binned activity was first z-scored, then the average was computed across all units at the given level K. After this, normalized autocorrelation function was computed:

$$(X(t1), X(t2)) = \frac{cov(X(t_1), X(t_2))}{\sigma(t_1)\sigma(t_2)} = \frac{E(X(t_1) - \mu(t_1))(X(t_2) - \mu(t_2))}{\sigma(t_1)\sigma(t_2)}$$

The decay constant $tau(K)$ was obtained by fitting an exponentially decaying function of the form:

$$autocorrelation(X_t) = Ae^{-(t/\tau)} + B$$

Then I plotted $\tau(K)$ as a function of K. Next, I calculated a logarithm of $\tau(K)$ and fitted a line. The scaling exponent z is the slope of the fitted line.

Behavior

Occupancy Maps

Estimates of the probability of visiting each part of the maze are represented as occupancy maps. To compute them, I assign the recorded $x - y$ positions to the spatial bins and then smoothed the bin counts with a Gaussian kernel ($SD = 2$ or $SD = 1.5$). To determine bin limits, I divided the maze into a square grid with $5cm$ spacing along both axes.

Occupancy Subsampling

Across sessions: Since rats spend different amounts of time around goals in *Post-Probe* than in *Pre-Probe* (EoL than in BoL), I implemented a subsampling procedure that equalizes occupancy between *Pre-Probe* and *Post-Probe* (or BoL and EoL).

To equalize occupancy between sessions $S1$ and $S2$, I divided the maze into a grid with $30cm$ spatial bins. To each bin I associated a number of animal visits N_{vis} corresponding to

the minimum occupancy of the given bin in sessions $S1$ and $S2$. Then, for each session, I performed downsampling with replacement of N_{vis} events in each spatial bin. I repeated this procedure 200 times for each session, computing the change in FBV between sessions $S1$ and $S2$, for every random sample.

Within sessions: Since rats do not visit all parts of the maze equally, I implemented a subsampling procedure that makes occupancy during a given session more uniform.

For given session S I divided the maze into a grid with $30cm$ spatial bins. To each bin I associated a number of animal visits N_{vis} corresponding to the minimum occupancy across all bins during sessions S. Then, I performed downsampling with replacement of N_{vis} events in each spatial bin. I repeated this procedure 200 times, computing the change in FBV between *the* preprobe and *the* postprobe (BoL and EoL).

Learning curve, learning performance, and learning speed

The learning curve is produced by measuring the distance covered by the animals in each learning trial. The lower distance is interpreted as better than the longer distance. To account only for parts of the trial relevant to the task, I calculated the distance between the exit from the start box and the last visit to any of the three reward sites. This excluded the last part of each trial, returning to the start box, as it is not relevant to the task and may include additional noise.

In chapter 4, to quantify behavior during learning, I used "learning performance". It was defined as $1/learning\,curve$.

The speed of learning was defined as the number of trials necessary for an animal to achieve a distance equal to 20% of the distance of the first trial.

Memory Retention Performance

In chapter 4, memory retention performance was evaluated as the number of crossings of reward zones - circles centered on rewards with a radius of $10cm$. In chapter 3, memory retention performance was evaluated as normalized time spent in reward zones.

Both quantities were normalized relative to the baseline. I first calculated the time in the real reward zones $RZ_{time\,real}$ or the crossings of the real reward zones $RZ_{crossings\,real}$. Then I randomly sampled 1000 reward configurations outside of existing reward zones and calculated the time spent at the sampled rewards $RZ_{time\,sampled}$ or the number of crossings of the sampled reward zones $RZ_{crossings\,sampled}$. Finally, I calculated the following index:

$$RZ_{time\,normalized} = \frac{RZ_{time\,real} - AVG(RZ_{time\,sampled})}{RZ_{time\,real} + AVG(RZ_{time\,sampled})}$$

$$RZ_{crossings\,normalized} = \frac{RZ_{crossings\,real} - AVG(RZ_{crossings\,sampled})}{RZ_{crossings\,real} + AVG(RZ_{crossings\,sampled})}$$

where the AVG function calculates the average of given values.

Both normalized quantities assume values from $[-1, 1]$, and a value of 1 occurs if the animal visits only the reward zones, while a value equal to -1 occurs if the animal never visits any of the reward zones.

Single cell activity

All procedures described in this section have been computed on a single-cell basis for every cell analyzed in the recorded data.

Firing Rate Maps

Spatial firing rate maps were calculated for every cell separately. First, I divided the whole maze into $5x5cm$ spatial bins. Then, I counted the number of emitted spikes in every spatial bin and smoothed the bin counts with a Gaussian kernel of $SD = 1.5$. Then, I divided smoothed bin counts with the smoothed occupancy map to compute estimates of firing rates for every position bin. In most situations, unless otherwise stated, I used only periods of mobility, with $speed > 5cm/s$.

Spatial Information Content

I calculated the spatial information content of the principal cells in bits / spike as (William E. Skaggs, Bruce L. McNaughton, Katalin M. Gothard, et al. 1992; William E Skaggs, Bruce L McNaughton, and Katalin M Gothard 1993; Markus et al. 1994; Souza et al. 2017):

$information\,content = \sum_{x,y} P_{x,y} \frac{R_{x,y}}{R} log2(\frac{R_{x,y}}{R})$

Where $P_{x,y}$ is the occupancy of the bin (x, y), $R_{x,y}$ is the mean firing rate of the cell in the bin (x, y) and R is the overall mean firing rate of the cell.

Spatial Information Criteria

In the reactivation analysis in chapter 3 and in the whole of chapter 4 I used only cells with spatial tuning.

To determine if a cell had spatial tuning, I first created a per-cell shuffled distribution by 200 times randomly shifting the cell's firing rate map along the x and y axes. For every random shift, I calculated the spatial information content to obtain a shuffle distribution. A cell had spatial tuning if its information content was greater than both the $95th$ percentile of the shuffled distribution and greater than the threshold. For the analysis in chapter 4 I used a threshold of $2\,bits/spike$ for CA1 cells and $1.5bits/spike$ for mEC cells (and $95th$ percentile of per-cell shuffled distribution). For the reactivation analysis in chapter 3 I used a threshold of $1.5bits/spike$.

Goal-related Remapping Score (FBV)

The goal-related remapping score, or the firing-by-vicinity score (Boccara et al. 2019), is a weighted average firing rate around goal locations. It is computed on a cell-by-cell basis by multiplying a cell's normalized firing rate map with a kernel and then summing the multiplied values. The kernel is designed by generating three two-dimensional Gaussian kernels with $\sigma = 10cm$ and centering them on reward locations. This procedure, when calculating the average firing rate, assigns higher importance to locations closer to the goals and lower importance to locations further away from the goals.

I calculated FBV in the first three minutes of *Pre-Probe* and *Post-Probe* sessions, and in blocks of five trials over learning.

Characteristic Timescale

Characteristic timescale of a cell is defined as the exponential decay constant of the cell's autocorrelation function.

The autocorrelation function has been estimated from binned spike trains (bin duration Geom. ISI in chapter 3 and $51.2ms$ in chapter 4). After binning, I first z-scored spike trains and then computed normalized autocorrelation function, essentially computing time-lagged Pearson correlation coefficient:

$$(X(t1), X(t2)) = \frac{cov(X(t1), X(t2))}{\sigma(t1)\sigma(t2)} = \frac{E(X(t1) - \mu(t1))(X(t2) - \mu(t2))}{\sigma(t1)\sigma(t2)}$$

I then fitted an exponentially decaying function of the form:

$$autocorrelation(X_t) = Ae^{-(t/\tau)} + B$$

The characteristic time scale is the value of the fitted parameter τ.

Burstiness

Cell burstiness was calculated on a single-cell basis. It is defined as the proportion of inter-spike intervals shorter than $6ms$.

Predicting Goal-Related Remapping from Reactivation

To predict goal-related remapping during *Post-Sleep* in mEC, I fitted a linear model that predicts single-cell firing-by-vicinity score based on activity during reactivation periods. For each mEC cell, the input features are its increase in its firing rate during SWRs and independent HSEs, relative to the cell's firing rate outside of reactivation events ($FR_{reac}/FR_{outside\_reac}$). The target value was the cell's goal-related remapping value (firing-by-vicinity) score. For a population of N mEC cells, the input to the model was a data matrix $X \in \mathbb{R}^{N\times 2}$, while the output was a matrix $Y \in \mathbb{R}^{N\times 1}$. I fitted two models, one on the beginning of *Post-Sleep* and one on the end of *Post-Sleep*. Both models were evaluated using Pearson's correlation coefficient between predictions and ground truth. All evaluation metrics obtained using five-fold cross validation. Shuffled distributions were generated by randomly shuffling labels (cells' goal remapping score).

Population activity

Population Vectors

For every position bin, a list of firing rates of all cells in that position bin is a population vector. To calculate population vectors, I first stacked firing rate maps of analyzed cells along the z-axis. Then I took the firing rates along all the spatial coordinates $x - y$.

Detecting High Synchrony Events (HSE)

I detected HSEs using a method very similar to that used in (Davidson, Kloosterman, and M. A. Wilson 2009; J. O'Neill et al. 2017). I selected HSEs based on multi unit activity (MUA) derived from the activity of the principal cells. First, MUA was binned into $1.5ms$ bins and smoothed with a Gaussian kernel with $SD = 15ms$. Next, I z-scored the smoothed MUA and marked all continuous bin blocks with z-score > 3 as HSEs. I determined the beginning of HSE by extending left from the peak while the z-scored MUA was greater than 1. I determined the end of HSE by extending right from the peak while the z-scored MUA was greater than 1. All subsequent HSEs that occur within $50ms$ were merged. I kept only HSEs with a duration between $50ms$ and $1000ms$. I kept only HSEs with at least 5 emitted spikes. I kept only HSEs

with a number of active cells larger than 4 or 10% of the total number of cells. For chapter 4, I detected HSEs in CA1 and mEC separately. For mEC, I used only HSEs that did not overlap in time with SWRs.

Reactivation

Reactivation analysis was computed during the sleep session SS (*Pre-Sleep* or *Post-Sleep*) and based on awake activity recorded during the first three minutes of *Post-Probe* or *Pre-Probe* session. First, population vectors (**PVs**) were calculated based on the first three minutes of *Post-Probe* or *Pre-Probe* session. For each of the three goals, a list of **PVs** was compiled from the $10cm$ reward zone and only PVs from these lists were used for the reactivation analysis. The activity corresponding to SWR (or independent HSE in mEC) events was then isolated during *Post-Sleep*. Each candidate event had an associated activity vector with cell firing rates. Activity during all candidate events was compared with **PVs** of all three goals, allowing a detailed look at per-goal reactivation. For a given goal G_i and a given candidate event e, the Pearson correlation coefficient was calculated between the activity vector of the event and all **PVs** related to the goal G_i. The maximum correlation coefficient ρ_{max} was selected. If the corresponding correlation was significant ($p < 0.05$), ρ_{max} was compared with the shuffle distribution. If ρ_{max} exceeded the $95th$ percentile of the shuffle distribution, the candidate event e was marked as an event that reactivated the goal G_i. This procedure was repeated for the two remaining goals, allowing each candidate event to reactivate more than one goal at a time.

To investigate the relationship between reactivation and memory retention, for each goal, a fraction of events reactivating the given goal was calculated. This was correlated with the normalized number of crossings (Chapter 4) or the normalized time spent around the goal (Chapter 3). All correlations were bootstrapped 5000 times.

To generate the shuffle distribution, the **PVs** were calculated by randomly shifting the awake firing rate maps of each cell independently, along both axes. Values that shifted beyond the last position are re-introduced at the first. This procedure maintains single-cell place selectivity but breaks spatial correlations among cells. Random shuffling was performed 200 times and for each random draw the maximum correlation ρ_{max} between the shuffled **PVs** and SWR/HSE activity was kept. This ensured a fair comparison as ρ_{max} calculated from the data was compared with the distribution of random ρ_{max}-es.

Reactivation maps were calculated for each event separately. Each **PV**, from the whole map and not only the reward zones, was correlated with the activity vector of the event. The reactivation map is a **2D** array of Pearson correlation coefficients between **PVs** and the event's activity vector.

LFP Analysis

SWR detection

As in (J. Csicsvari et al. 1999) to detect SWRs I analyzed the local field potentials of tetrodes located in CA1. For each tetrode, I first performed a band-pass filter to 150-250Hz and calculated the instantaneous power of the signal. Then, I summed the power from the signal of all CA1 tetrodes and z-scored it. The SWR peaks were then identified as moments in which the z-scored power was higher than 6. To determine the beginning and end, I extended from the peak until the z-scored power was larger than 1.2. Finally, I kept only SWRs that overlapped with hippocampal HSEs.

CHAPTER 2

Criticality in the hippocampus

Abstract

The brain criticality hypothesis offers a perspective into the activity of the brain that has the potential to explain the emergence of computational properties from the collective activity of individual cells. Signatures of brain activity that indicate criticality have been observed in different brain regions; however, criticality in the hippocampus under different behavioral conditions has not been studied extensively. In addition, brain criticality can be analyzed using multiple different approaches, whose results are typically not related to each other. To bridge some of these gaps, in this Chapter, I analyzed the activity of the hippocampus during sleep/rest and active wakefulness using two different approaches rooted in the brain criticality hypothesis. I first analyzed cascades of neural activity, neuronal avalanches, that have been characterized by the absence of a typical spatial or temporal scale. The absence of a typical scale is indicated by power law distribution of duration and sizes, as well as scaling relation between duration and size. Inferring exponents of neuronal avalanches from data allows us to estimate the distance from the system to the critical point DCC . The estimated DCC was larger during wakefulness than during sleep/rest, suggesting that during wakefulness the hippocampus operated farther away from criticality than during sleep/rest. Next, I used the Phenomenological Renormalization Group (PRG) to perform iterative simplification of the system ("coarse-graining") and observe scaling of the select properties of neural activity. Most PRG-derived scaling exponents did not differ between sleep/rest and wakefulness, except the scaling exponent of activity variance α. This exponent was higher during sleep/rest than during awake, indicating conceptually similar differences to those observed using neuronal avalanches. Together, the results presented in this Chapter confirmed that the activity of the hippocampus exhibits signatures of criticality and that these signatures change with the state of the brain.

Introduction

This study aims to examine how criticality influences the functioning of the hippocampus. Prior to this analysis, it is essential to verify the presence of "signatures of criticality" in hippocampal activity. These signatures are often observed as power laws in avalanche distributions and scale-invariant population activity (Beggs and Plenz 2003; Beggs and Plenz 2004; Friedman et al. 2012; Meshulam et al. 2019; Morales, Santo, and Muñoz 2023; Munn et al. 2024).

Signatures of criticality have been documented in slice cultures (Beggs and Plenz 2003; Mazzoni et al. 2007; Pasquale et al. 2008), the cortex *in vivo* (Petermann et al. 2009; Gireesh and Plenz 2008; Hahn, Petermann, et al. 2010; Yu et al. 2011; Xu et al. 2024), and at the level of the whole-brain (Adrián Ponce-Alvarez, Kringelbach, and Deco 2023; Freeman et al. 2003; Meisel et al. 2013; Solovey et al. 2012; Poil et al. 2012; Lombardi, Shriki, et al. 2021), but there is less extensive research in the context of the sleeping or resting hippocampus (Morales, Santo, and Muñoz 2023; Ribeiro et al. 2010).

The presence of criticality signatures suggests that the hippocampus functions at or near the border between completely ordered and disordered states (Larremore et al. 2012; Tian et al. 2022). Concurrent theoretical research indicates that criticality enhances both information processing (Beggs and Plenz 2003; Shew, Yang, Yu, et al. 2011) and storage capacities in neural networks (Haldeman and Beggs 2005). Given its role in learning and memory consolidation, operating in this regime may be advantageous to the hippocampus, making it an interesting region for further study of critical phenomena.

To achieve this, I analyzed extracellular recording data from the dorsal CA1 area of freely moving rats. Rats were trained to locate three food rewards in a cheeseboard maze (refer to Methods for specifics), while neural activity was captured during wakefulness and approximately 20 hours of post-learning sleep (Bollmann et al. 2025), from the previously published data set. The analysis in this chapter includes data from eight sessions recorded from three animals.

2.1 Neural avalanches and distance to criticality

To assess criticality in the hippocampus through what is called "avalanche criticality", I first isolated neuronal avalanches (Beggs and Plenz 2003; Beggs and Plenz 2004) —cascades of uninterrupted activity separated by quiescence periods (Figure 2.1). In my analysis, I define neuronal avalanches based on spikes emitted by the entire CA1 population. I binned spikes in temporal bins whose duration was calculated separately for every session as the average inter-spike interval of all emitted spikes (Beggs and Plenz 2003; Ribeiro et al. 2010; Fontenele et al. 2019) ($2.1 \pm 0.25ms$ during wakefulness, $3.1 \pm 0.30ms$ during sleep/rest, $mean \pm sem$). This procedure ensures the existence of silent bins (and, by extension, avalanches) by accounting for different numbers of recorded cells and the variation of firing rates between sleep and wakefulness. Importantly, as the number of recorded cells grows, this binning strategy produces shorter temporal bins. Therefore, for a very large number of recorded cells one can expect sub-millisecond temporal bins, on a timescale faster than spikes. It is not clear what the avalanche statistics would look like in this case, however, with $100 - 200$ recorded cells, the data used in this work were far from this limit, as evidenced by the reported average inter-spike intervals.

To assess neuronal avalanches, I quantified their duration in number of temporal bins and size in number of spikes. In systems operating at the critical point, avalanche duration $P(T)$ and size $P(S)$ follow power law distributions:

$$P(T) \sim T^{\alpha}$$

and

$$P(S) \sim T^{\tau}$$

with exponents $\alpha = -2$ and $\tau = -1.5$, respectively (*The Theory of Branching Processes* 2025; Zapperi, Lauritsen, and Stanley 1995; Eurich, J. Michael Herrmann, and Ernst 2002;

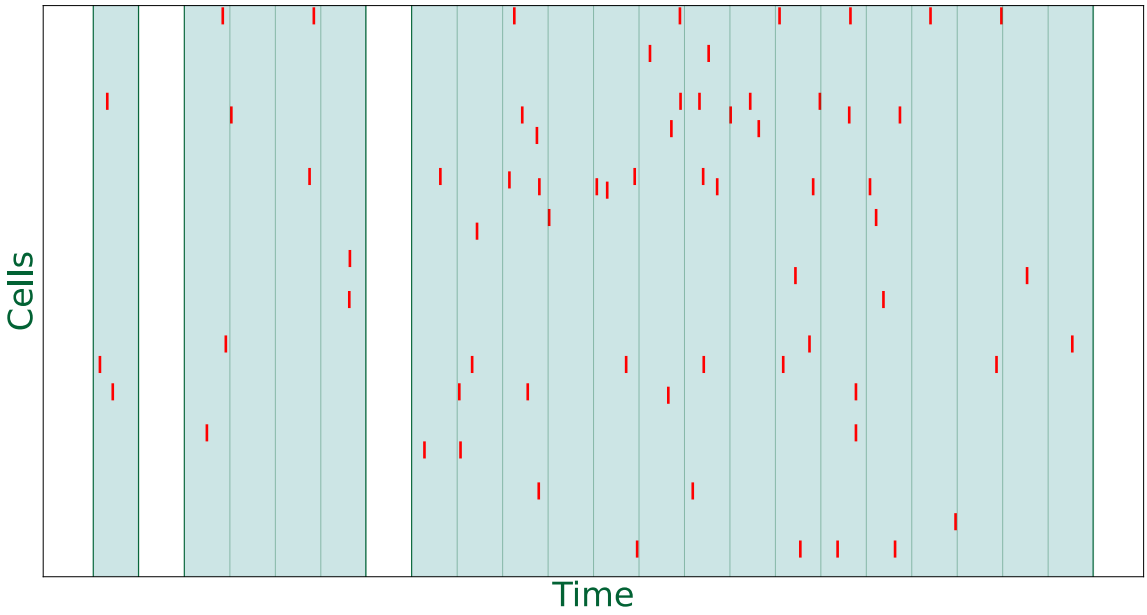

Figure 2.1: *Neuronal avalanches.*
Spike raster of CA1 activity, individual cells are arranged along the y-axis, temporal bins along the x-axis. Red ticks denote individual spikes, vertical lines indicate temporal bins, and green shaded areas mark avalanches. Silent bins are in white.

Paczuski, Maslov, and Bak 1996). The histograms of the duration and size of the avalanches are shown in Figure 2.2. The power law fitting yielded an exponent $\alpha = -1.701 \pm 0.011$ for duration during wakefulness and $\alpha = -1.754 \pm 0.008$ during sleep/rest. For size, the exponents were $\tau = -1.508 \pm 0.009$ in wakefulness and $\tau = -1.566 \pm 0.006$ in sleep/rest. Although different from the theoretical values expected in critical systems ($\alpha = 2, \tau = 1.5$), these results align with values from similar *in vivo* spike avalanche studies (Fontenele et al. 2019; Viola Priesemann, Wibral, et al. 2014; Bédard, Kröger, and A. Destexhe 2006; Ma et al. 2019; Hahn, Adrian Ponce-Alvarez, et al. 2017).

Next, I characterized the relation between avalanche duration and size by calculating the average avalanche size for every available avalanche duration (Figure 2.2 C and F). Avalanche size increases exponentially with duration, adhering to the "scaling relationship" $\frac{1}{\sigma\nu z}$ (Friedman et al. 2012; Sethna, Dahmen, and Myers 2001). In my study, I measured a value of $\frac{1}{\sigma\nu z} = 1.340 \pm 0.004$ during awake periods and $\frac{1}{\sigma\nu z} = 1.345 \pm 0.004$ during sleep/rest periods, again similar to previous reports (1.3 in Friedman et al. 2012, 1.32 ± 0.12 under different conditions in Fontenele et al. 2019, 1.16 in Ma et al. 2019, $1.23 - 1.5$ in Mariani et al. 2021, depending on the analysis).

Neuronal avalanches are cascades of activity throughout the population, so I analyzed the propagation of activity by evaluating the internal temporal structure of these cascades — avalanche shapes (Marshall et al. 2016; Friedman et al. 2012; Sethna, Dahmen, and Myers 2001, Figure 2.3 A and B). For a specific duration, an avalanche shape is calculated by averaging the spike count in each temporal bin across all avalanches of that duration. In critical systems, temporal profiles exhibit a parabolic shape and collapse onto a single line when rescaled using the scaling relation exponent $\frac{1}{\sigma\nu z}$ (Friedman et al. 2012). In my analysis, the avalanches collapsed near, but not exactly, the same line, particularly during awake periods

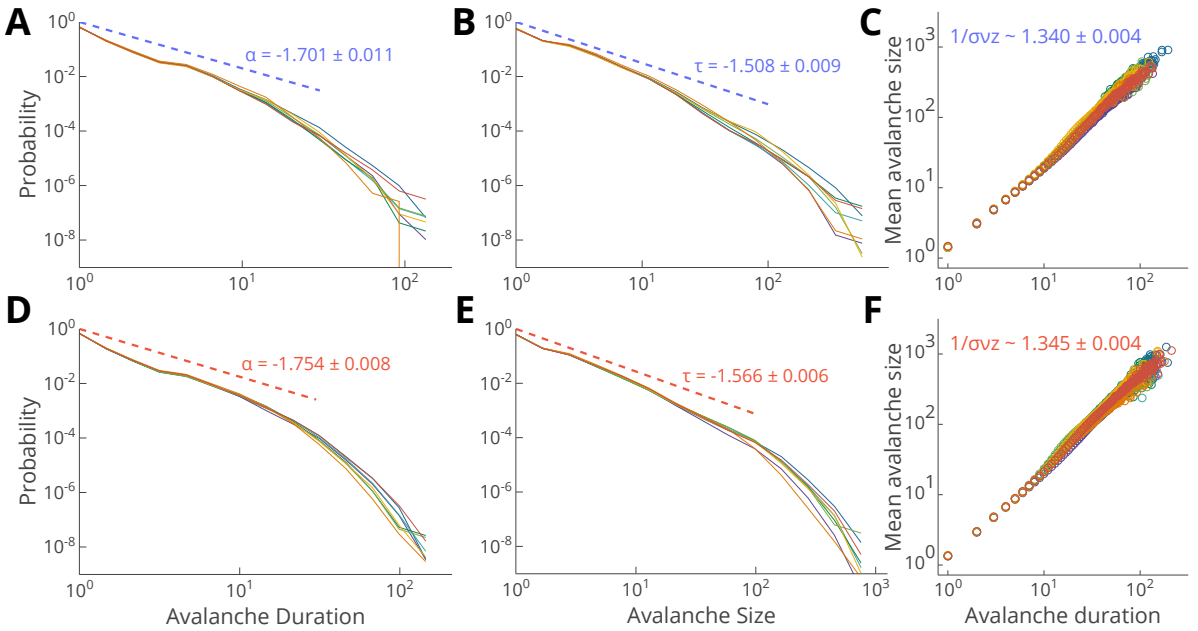

Figure 2.2: *Distributions and scaling of neuronal avalanches.*

A - distribution of avalanche durations during wakefulness (number of bins), **B** - distribution of avalanche sizes during wakefulness (number of spikes), **C** - scaling relation during wakefulness, **D** - distribution of avalanche durations during sleep/rest (number of bins), **E** - distribution of avalanche sizes during sleep/rest (number of spikes), **F** - scaling relation during sleep/rest. Line colors on panels **A**,**B**,**D** and **E**, alongside circle colors on panels **C** and **F**, correspond to different recording days. Exponent and scaling relation values are reported as the mean across recording days ± standard error.

(2.3 B and E). I sought the exponent value that optimally collapses observed avalanches as close as possible to a single line. One way to calculate this value is to find an exponent Σ that minimizes variance across scaled shapes (Marshall et al. 2016) (see Methods). The observed value of Σ was different from the scaling relation $\frac{1}{\sigma\nu z}$ during awake periods ($p = 0.008$, Wilcoxon Signed-Rank test), but not during sleep/rest ($p = 0.08$, Wilcoxon Signed-Rank test). The differences between the optimal scaling exponent Σ and scaling relation $\frac{1}{\sigma\nu z}$ were evident in the distinct collapse of avalanche shapes with these two values (2.3 B to F).

Next, I applied the described avalanche properties to estimate the state of the CA1 network relative to the critical point. In critical systems, the scaling relation $\frac{1}{\sigma\nu z}$ is equal to the ratio of power law exponents for duration and size $\frac{\alpha-1}{\tau-1}$ (Friedman et al. 2012). As described in previous research (Ma et al. 2019), I calculated the "distance to criticality coefficient" to quantify the discrepancy between these two values:

$$DCC = |\frac{1}{\sigma\nu z} - \frac{\alpha - 1}{\tau - 1}|$$

For strictly critical systems $DCC = 0$, while in my study DCC I observed $DCC = 0.038 \pm 0.0044$ in wakefulness and $DCC = 0.014 \pm 0.003$ in sleep/rest.

Lastly, I compared the distance from the critical point in the CA1 network during wakefulness and sleep using DCC (Figure 2.4 A). This revealed that DCC was greater in the awake state than in sleep/rest ($p = 0.039$, Wilcoxon Signed-Rank test). This suggests that the network approaches a critical state during sleep and moves away from it when awake. These results align with previous analyses of neocortex data in freely moving rats (Xu et al. 2024)

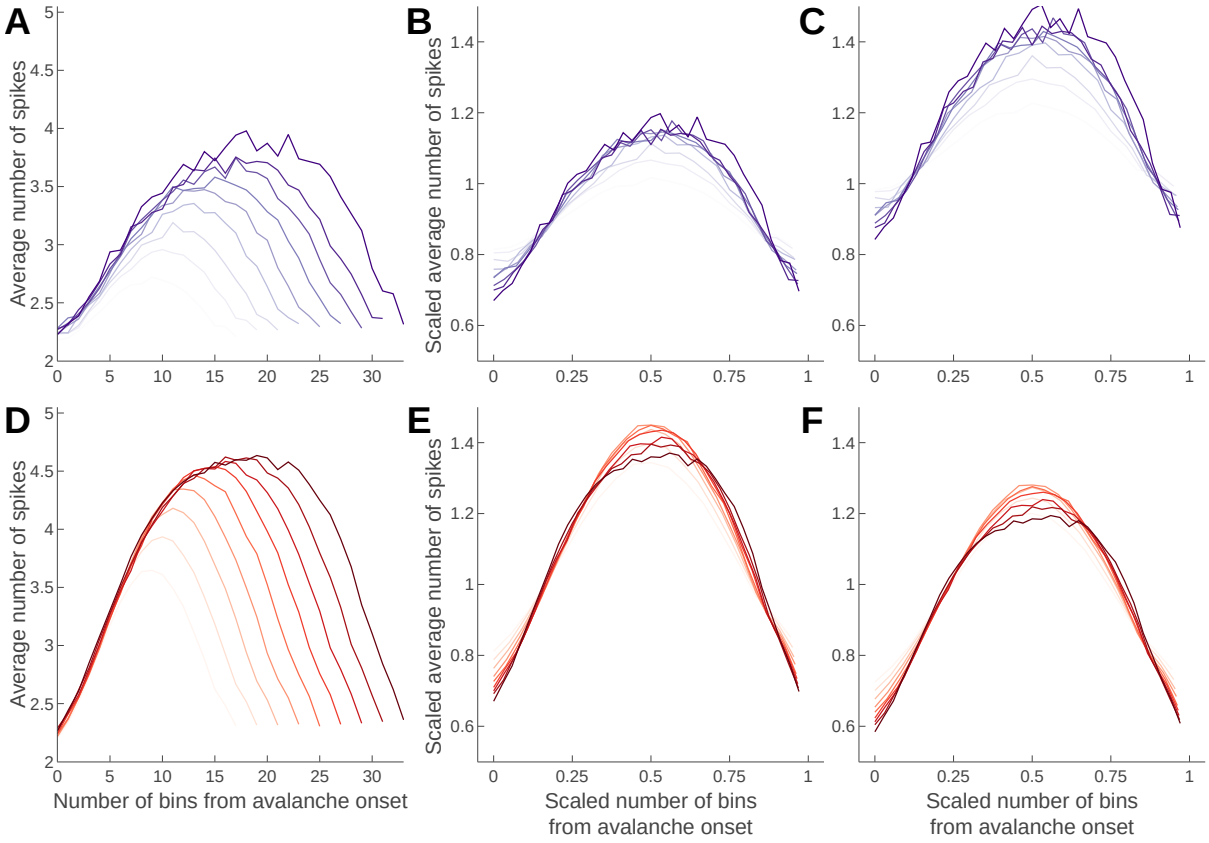

Figure 2.3: *Temporal profiles of neuronal avalanches - avalanche shapes.*

Avalanche shapes for a subset of avalanche durations $\{18, 20, 22, 24, 26, 28, 30, 32, 34\}$, color intensity increases with avalanche duration, from 18 (lightest colors) to 34 temporal bins (darkest colors). Shades of blue indicate avalanche shapes during wakefulness, shades of red during sleep/rest. Averages calculated across avalanches pooled from all recording days. **A** - avalanche shapes during wakefulness, on the x-axis is the number of temporal bins from the onset of avalanche, on the y-axis is the average number of spikes for each temporal bin, **B** - collapsing of avalanche shapes during wakefulness when rescaled with $\frac{1}{\sigma\nu z}$, on the x-axis is the scaled number of temporal bins from the onset of avalanche, on the y-axis is the scaled number of spikes for each temporal bin (details in Methods), **C** - collapsing of avalanche shapes during wakefulness when rescaled with Σ , on the x-axis is the scaled number of temporal bins from the onset of avalanche, on the y-axis is the scaled number of spikes for each temporal bin (details in Methods), **D** - avalanche shapes during sleep/rest, on the x-axis is the number of temporal bins from the onset of avalanche, on the y-axis is the average number of spikes for each temporal bin, **E** - collapsing of avalanche shapes during sleep/rest when rescaled with $\frac{1}{\sigma\nu z}$, on the x-axis is the scaled number of temporal bins from the onset of avalanche, on the y-axis is the scaled number of spikes for each temporal bin (details in Methods), **F** - collapsing of avalanche shapes during sleep/rest when rescaled with Σ , on the x-axis is the scaled number of temporal bins from the onset of avalanche, on the y-axis is the scaled number of spikes for each temporal bin (details in Methods).

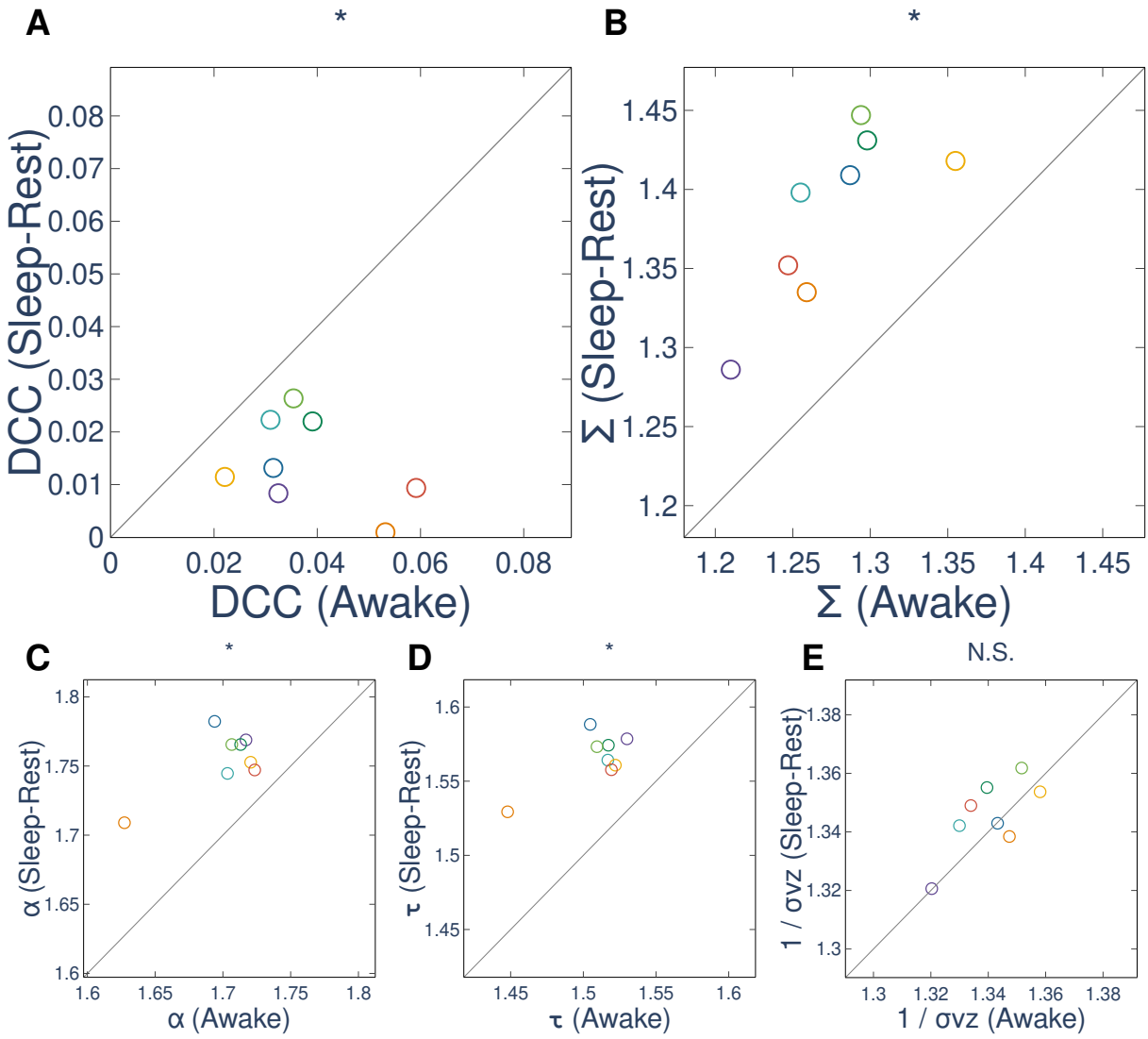

Figure 2.4: *Criticality in wakefulness and sleep/rest.*
A - Distance-to-criticality coefficient in awake and sleep/rest ($p < 0.05$, Wilcoxon Signed-Rank test, Bonferroni correction), **B** - Optimal exponent for collapsing avalanche shapes Σ in awake and sleep/rest (p < 0.05, Wilcoxon Signed-Rank test, Bonferroni correction), **C** - Power law exponent of avalanche duration α in awake and sleep/rest ($p < 0.05$, Wilcoxon Signed-Rank test, Bonferroni correction), **D** - Power law exponent of avalanche size τ in awake and sleep/rest ($p < 0.05$, Wilcoxon Signed-Rank test, Bonferroni correction), **E** - Scaling relation in awake and sleep/rest ($p > 0.1$, Wilcoxon Signed-Rank test, Bonferroni correction). Circle colors correspond to different recording days.

and human LFP, which link prolonged wakefulness to increased deviations from criticality (Meisel et al. 2013). In this study, I find no significant differences in the scaling relation $\frac{1}{\sigma\nu z}$ between wakefulness and sleep ($p = 0.98$, Figure 2.4 E). However, the exponent Σ , which reduces the variance of collapsed avalanche shapes, increases during sleep/rest compared to wakefulness (Figure 2.4 B, $p = 0.039$, Wilcoxon Signed-Rank test; $\Sigma = 1.276 \pm 0.016$ during wakefulness and $\Sigma = 1.384 \pm 0.019$ during sleep/rest). The power law exponents of avalanche distributions, α and τ, show higher values during sleep/rest compared to wakefulness (Figure 2.4 C and D, $p < 0.05$ Wilcoxon Signed-Rank test), indicating that activity spreads farther and for a longer time in both temporal and spatial dimensions during wakefulness.

Taken together, these results indicate that hippocampal activity exhibits a dynamics close

to criticality and that the hippocampus might operate in a regime close to the critical point. Additionally, in wakefulness and sleep/rest, I observed a different dynamics relative to the critical point. This difference is mostly a consequence of slower decaying activity during awake than during sleep/rest, and likely results from different spatiotemporal activity propagation.

2.2 Phenomenological Renormalization Group

In addition to "avalanche criticality," researchers examine critical-like neural dynamics by looking at the activity at a series of different spatiotemporal scales. Meshulam et al. 2019 introduced the Phenomenological Renormalization Group (PRG) by modifying the Renormalization Group procedure (Kadanoff 1966; K. G. Wilson 1975) to apply to neural activity(Meshulam et al. 2019; Morales, Santo, and Muñoz 2023; Munn et al. 2024; Castro et al. 2024). This approach iteratively simplifies the underlying system through a series of coarse-graining steps, observing and measuring macroscopic properties at each step. If the measured properties increase (or decrease) with the coarse-graining procedure, the system exhibits scaling behavior. I applied this method to the same data used for avalanche analysis to provide an alternative perspective on potential critical dynamics in hippocampal activity.

In the traditional Renormalization Group framework, coarse-graining involves averaging over local spatial neighborhoods. However, this method is inapplicable to extracellular recordings due to the lack of precise spatial coordinates and connectivity data for recorded cells. In conventional systems, nearby elements exhibit the strongest correlations, so, for neural recordings, pairwise correlations between cells are utilized as a proxy for distance in the Phenomenological Renormalization Group (PRG).

The PRG procedure begins by binning the activity of N recorded cells into temporal bins (Figure 2.5). The duration of the temporal bins is calculated as the geometric mean ($\sqrt[n]{x_1 x_2 \dots x_n}$) of inter spike intervals for all spikes ($35.125 \pm 2.47ms$ during wakefulness, $46.8 \pm 3.32ms$ during sleep/rest, see Methods and Supplementary figure S.1), considered an effective estimator of the characteristic timescale of the population (Morales, Santo, and Muñoz 2023). Binned spiking activity represents the finest granularity of the system, initiating PRG with $K = 1$, where each cell serves as a unit. I compute pairwise correlations among cells and sort the pairs according to these values, ensuring that each cell belongs to a single pair. The first pair displays the highest correlation, and the last pair the lowest correlation. Pairing cells outlines the initial coarse-graining stage: units at the second PRG step arise from merging the activity of cells in each pair. The merging refers to the sum of activities, followed by renormalization that sets the average non-zero activity to one and preserves zero bins (i.e., activity in temporal bins is divided by the average activity of non-zero bins). The merged activity of units for $K > 1$ is referred to as coarse-grained activity. Applying this to each pair of cells results in $N/2$ coarse-grained units at the second PRG level ($K = 2$) where each coarse-grained unit comprises two original cells. In the next iteration, the procedure produces the third PRG level ($K = 4$) with $N/4$ coarse-grained units, each comprising four original cells. Repeating this procedure iteratively until one unit remains results in a list of PRG steps, denoted by the count of original cells K, as depicted in Figure 2.5.

In a typical population analysis, researchers examine neural activity at the most detailed microscopic level ($K = 1$) by observing single-cell activity over time. The PRG method allows for an iterative increase in scale, with each PRG step K representing a new scale level ('zoom'), averaging out small-scale details of the system along the way. The essence of PRG analysis

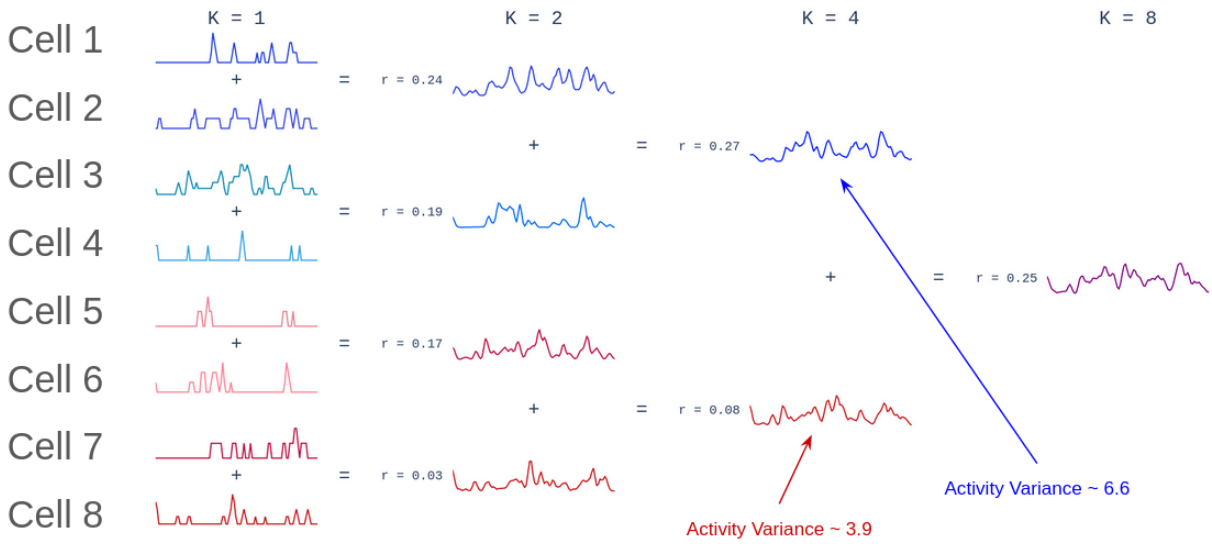

Figure 2.5: *Phenomenological Renormalization Group.*

An illustration of the PRG procedure for a population of $N = 8$ cells. Variable K is used as the index of PRG and denotes the number of original cells that compose a unit at each step of PRG. At the first step of PRG ($K = 1$), units are binned spikes of original cells. The next step ($K = 2$, four units) is obtained by ordering cell pairs by correlation, summing and renormalizing their activity. Repeating this procedure two more times yields the third ($K = 4$, two units) and fourth ($K = 8$, one unit) step of PRG. Activity variance for the blue unit at $K = 4$ is calculated as the total variance of cells $1 - 4$ that participate in that unit.

lies in tracking the evolution of variables that depict collective activity across different scales (PRG steps K).

Progressing through the PRG simplifies the system, allowing expression of the coarse-grained activity distribution at each K as:

$$P^K(x) = P_0^K(x) + (1 - P_0^K(x))Q^K(x)$$

where $P_0^K(x)$ is the probability of silence (zero activity) and $Q^K(x)$ is the distribution of non-zero activity.

As each coarse-graining step merges the activities of the units from previous steps, K increases, and coarse-grained units accumulate more and more summed cells. If the collective activity of all cells was simple and weakly correlated, due to the Central limit theorem, all artificial units in the PRG would be normally distributed. However, throughout PRG, I observed (Figure 2.6) non-normal activity distributions. These distributions have heavy tails as evidenced by the measured excess kurtosis of 15.55 ± 1.65 during awake and 17.87 ± 1.09 during sleep/rest, implying that PRG reflects complex interaction patterns between cells. Moreover, up to a certain value, the distributions $Q^K(x)$ at different steps K assume a similar form and are invariant to coarse-graining, indicating convergence (fixed-point) of the Renormalization Group. Together, the convergence and non-Gaussian form of coarse-grained activity distributions might be interpreted as a signature of critical dynamics (Meshulam et al. 2019).

To examine the second term of the coarse-grained activity distributions, the probability of silence $P_0(x)$, I first calculate its negative logarithm, the "free-energy" ($-ln(P_0)$). Plotting this relationship against K on a double logarithmic scale (Figure 2.7) yields a straight line. This indicates that increasing the number of participating cells results in a proportional and

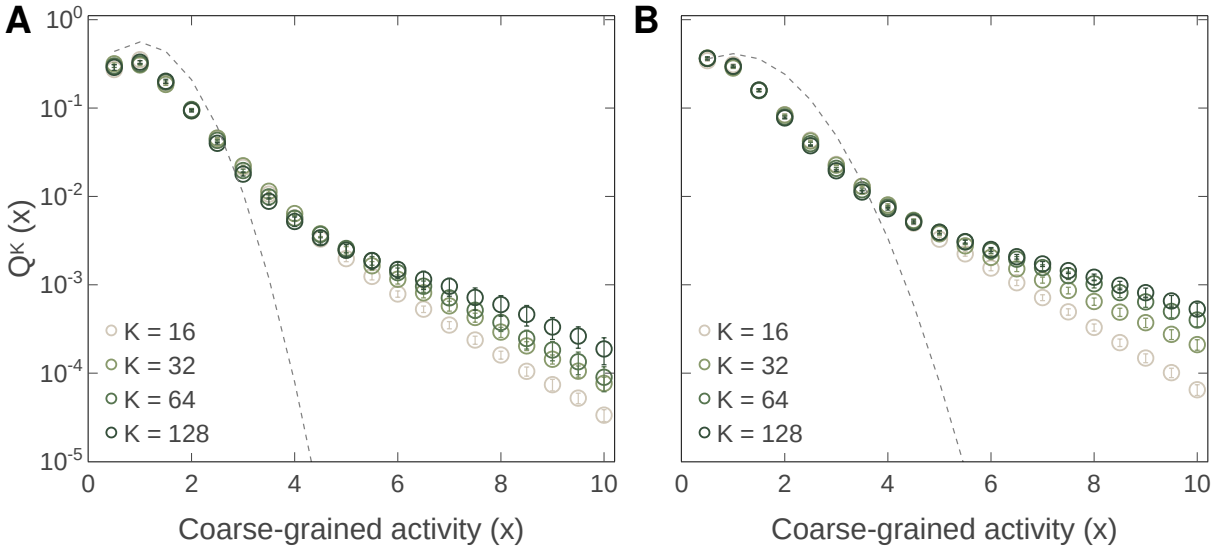

Figure 2.6: *Distribution of non-zero, coarse-grained activity.*

Histograms of non-zero coarse grained activity for different PRG steps $K \in \{16, 32, 64, 128\}$. Coarse-grained activity is renormalized so that the mean of non-zero temporal bins is equal to 1. Histograms are normalized and calculated over equal-width bins, where each bin has width of 0.5. For visualization purposes only coarse-grained activity in the range $[0, 10]$ is shown. For both panels data is pooled from all recording days, circles indicate mean probability, error bars are inside the circles. The dashed gray lines denote normal distribution with mean $\mu = 1$ (the mean of non-zero coarse grained activity) and variance σ^2 equal to the variance of non-zero coarse grained activity. **A** - during wakefulness, **B** - during sleep/rest.

regular increase in free energy, illustrating the concept of free energy scaling. The slope of the fitted line in a log-log plot provides the exponent β, which quantifies the scaling of the free energy. Systems with uncorrelated units exhibit an upper bound of $\overline{\beta} = 1$. This study finds $\beta = 0.79 \pm 0.017$ during wakefulness and $\beta = 0.762 \pm 0.018$ during sleep/rest, aligning with (Meshulam et al. 2019; Morales, Santo, and Muñoz 2023; Munn et al. 2024; Castro et al. 2024).

Next, I measured the activity variance within coarse-grained units (Morales, Santo, and Muñoz 2023). For each coarse-grained unit, as depicted in Figure 2.5, the activity of the original cells that comprise the given unit (before coarse-graining) is summed and the variance is calculated. Figure 2.8 shows how the activity variance scales in the PRG. The scaling exponent of activity variance is denoted as α and should not be confused with the power law exponent of distributions of avalanche duration from the previous section. In systems with entirely uncorrelated units, α equals 1, and the activity variance increases only due to the increase in cell count. For systems with fully correlated units, α becomes 2, serving as the upper limit for α. The analysis of the dataset shows $\alpha = 1.434 \pm 0.015$ during awake periods and $\alpha = 1.497 \pm 0.012$ during sleep/rest, highlighting the complex nature of the CA1 dynamics.

Next, I examined the diagonalized spectrum of the covariance matrix of units in the PRG (Meshulam et al. 2019) (details in the Methods). The eigenvalues λ_i of all covariance matrices, plotted against their fractional rank ($rank(\lambda_i)/K$, Figure 2.9), show power law scalings with an exponent of $\mu = 0.814 \pm 0.055$ in wakefulness and $\mu = 0.819 \pm 0.05$ during sleep/rest. The spectra of covariance matrices from various steps of the coarse-graining procedure align closely with a power law decay, consistent with previous reports (Meshulam et al. 2019; Morales, Santo, and Muñoz 2023).

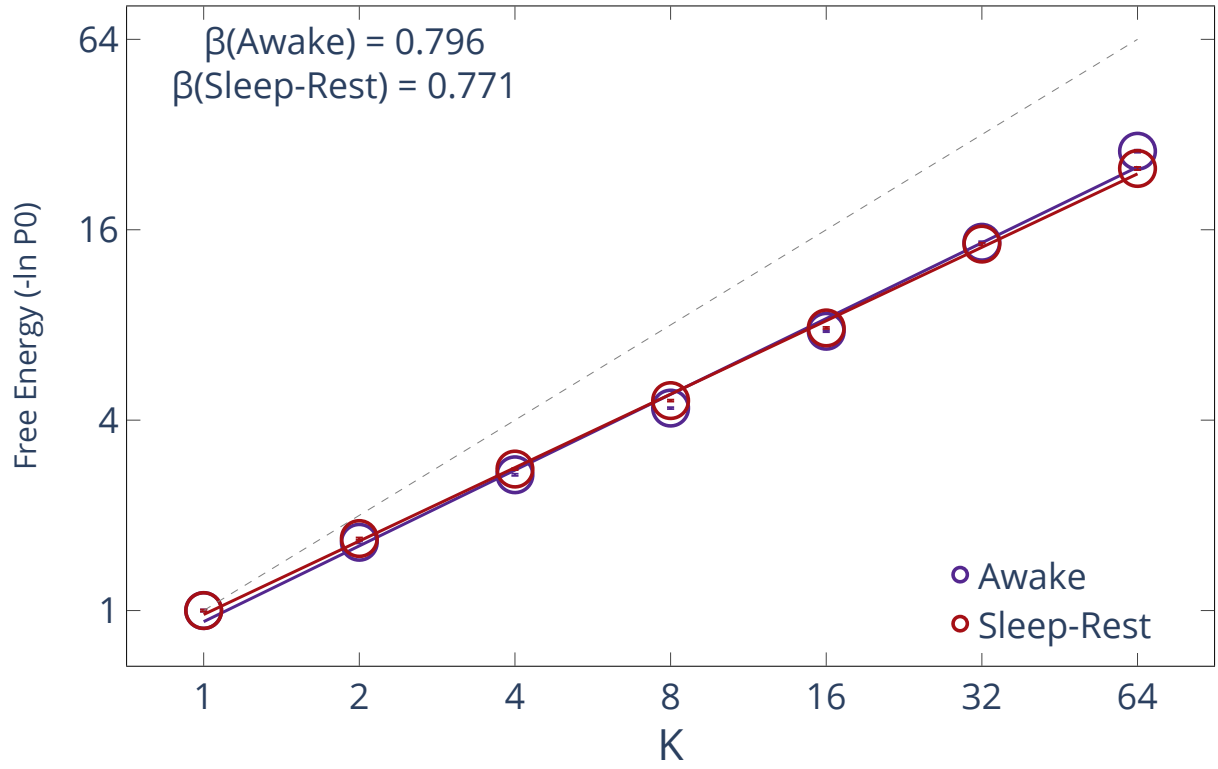

Figure 2.7: *Scaling of free energy under coarse-graining.*
Free energy as a function of the number of units per block K. For each K, data was pooled from all recording days, circles indicate mean free energy, error bars (SEM) are inside the circles. The dashed line denotes scaling with $\beta = 1$.

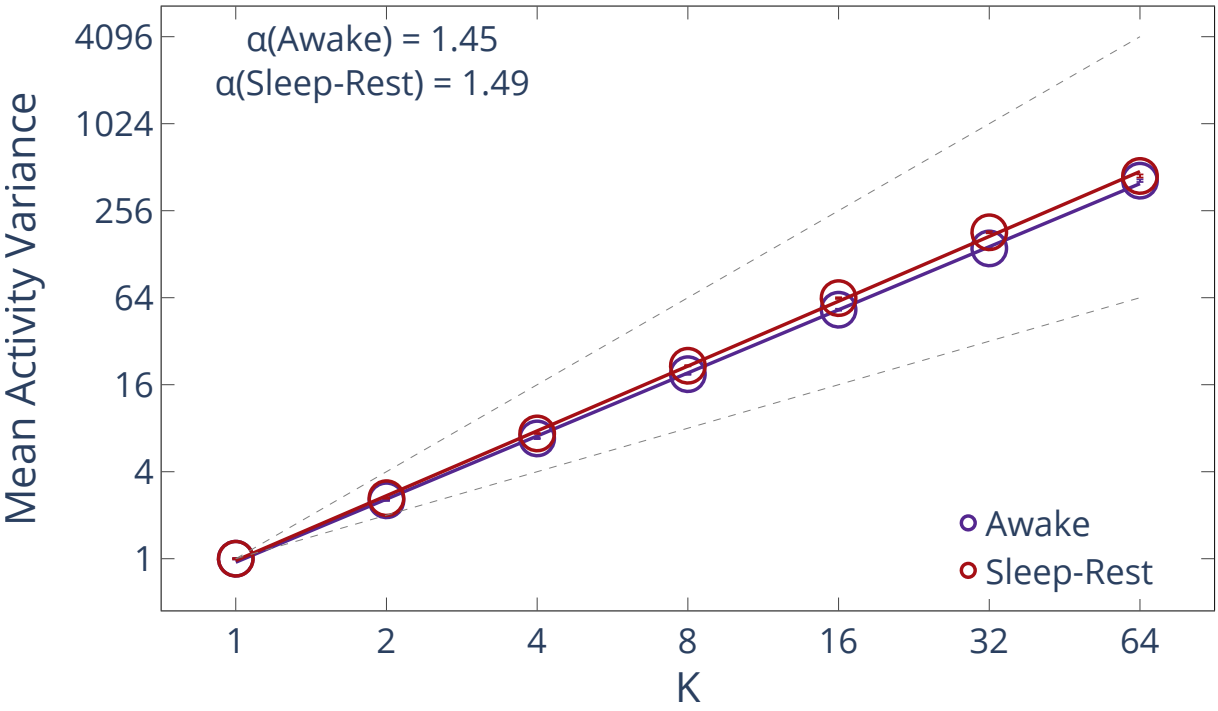

Figure 2.8: *Scaling of activity variance under coarse-graining.*
Variance of the within-block activity as a function of the number of units per block K. For each K, data was pooled from all recording days, circles indicate mean activity variance, error bars (SEM) are inside the circles. Top and bottom dashed lines denote scaling with $\alpha = 2$ and $alpha = 1$.

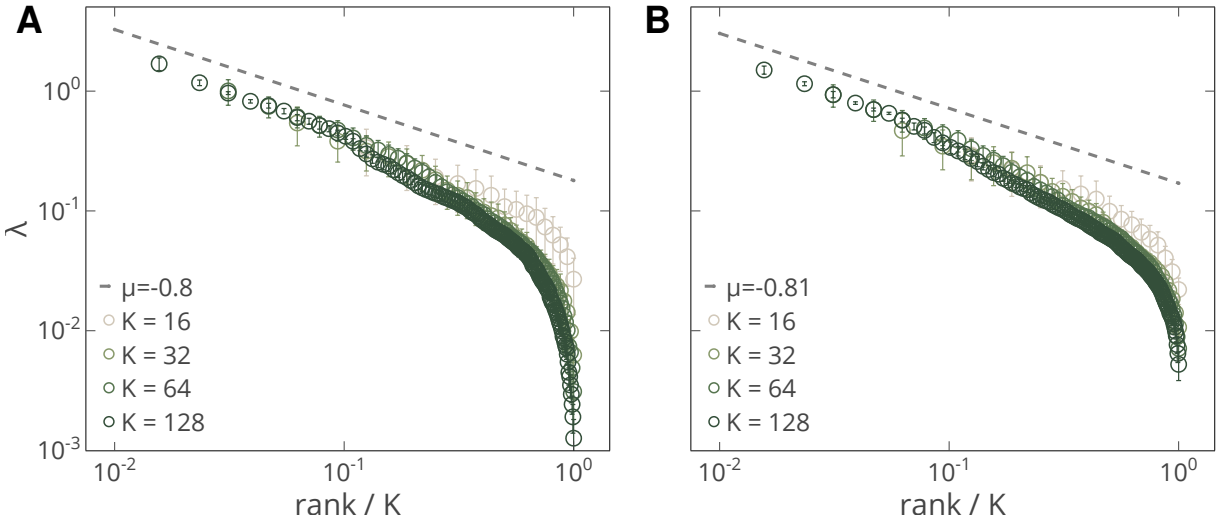

Figure 2.9: *Scaling and collapsing of the covariance matrix spectrum of clustered activity.* **A** - during wakefulness, **B** - during sleep/rest. For different iterations of coarse-graining (K). For both panels, data is pooled from all recording days, circles indicate mean λ, error bars are inside (SEM) the circles. The dashed gray lines represent fitted power law with exponent μ (power law scaling is indicated by dashed lines positioned above scatter plots for visualization purposes).

PRG units consist of multiple original cells, and when the system approaches the critical point, the autocorrelation function for units at higher K values decays more slowly compared to those at lower K values. The decay is quantified through an exponential decay constant τ_c, which scales in systems near the critical point (Meshulam et al. 2019; Meshulam et al. 2018). In my study, when plotted against K (Figure 2.10 B), the results show a clear scaling of the autocorrelation decay constant tau_c, with exponents $z = 0.313 \pm 0.022$ for wakefulness and $z = 0.303 \pm 0.025$ for sleep/rest, aligning with previous findings but differing in exponent values (Morales, Santo, and Muñoz 2023). Additionally, when, within each PRG step K, the autocorrelation time is normalized by the decay constant τ_c, the autocorrelation functions collapse onto a single line (Figure 2.10 A).

So far, PRG analysis revealed scale-free activity patterns akin to those seen in systems approaching a phase transition. This finding supports the presence of universal (quasi-)critical dynamics (Meshulam et al. 2019; Morales, Santo, and Muñoz 2023; Munn et al. 2024; Meshulam et al. 2018) and conceptually aligns with the "avalanche criticality" analysis in Chapter 2.1. However, PRG does not provide a way to quantify the system's distance from the critical point analogous to DCC , and the understanding of PRG's relationship with criticality in neural networks remains unresolved (Nicoletti, Suweis, and Maritan 2020; Nascimento et al. 2025). I explored whether both approaches yield qualitatively consistent results. Specifically, do PRG scaling exponents, like those of DCC , also reveal distinct CA1 criticality-related dynamics during wakefulness versus sleep/rest? Figure 2.11 illustrates that the activity variance scaling exponent (α) differs between sleep and wakefulness, whereas the scaling exponents for free energy (β), autocorrelation time (z), and the covariance matrix spectrum (μ) stay constant.

Sleep and wake states not only affect the scaling of activity variance, but also influence the distance to criticality coefficient (DCC) derived from avalanches (Figure 2.4 A). Although this suggests alignment between these interpretations of critical-like dynamics, the connection between PRG exponents and avalanche criticality remains unclear. I analyzed the mutual relationship between two perspectives of collective dynamics despite having only eight days

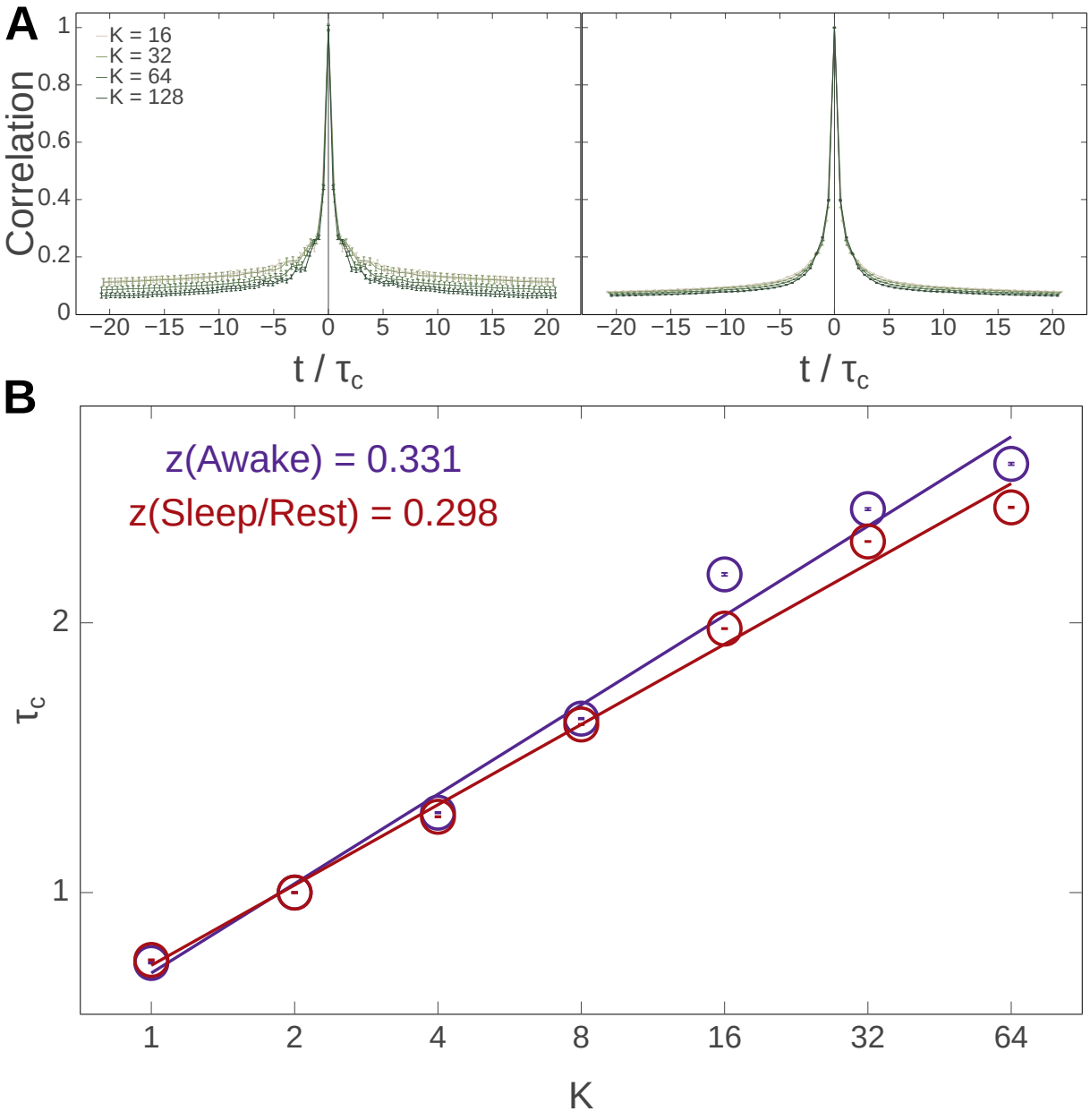

Figure 2.10: *Scaling and collapsing of the autocorrelation function.*
A - autocorrelation function as a function of rescaled time t/τ_c, during wakefulness (left) and sleep/rest (right), **B** - scaling of characteristic correlation timescale under coarse-graining. For each K, data was pooled from all recording days, circles indicate mean τ_c, error bars are inside the circles (SEM).

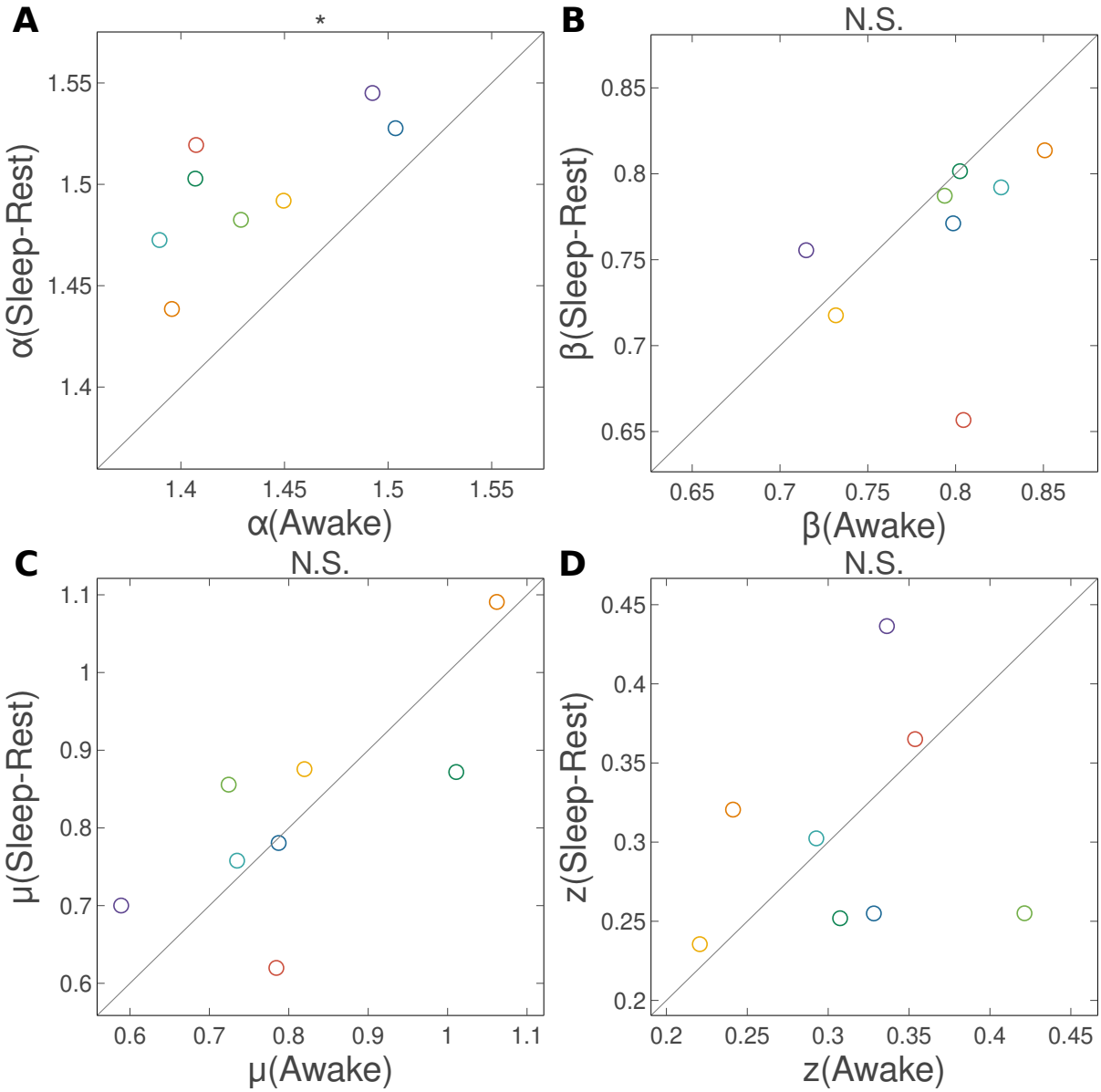

Figure 2.11: *Scaling exponents of PRG during wakefulness and sleep/rest.*
A - scaling exponent of activity variance, **B** - scaling exponent of free energy, **C** - scaling exponent of the covariance matrix spectrum, **D** - scaling exponent of characteristic correlating timescale (Wilcoxon Signed-Rank test and Bonferroni correction for all panels, for $N.S.$, $p > 0.1$, for $*$, $p < 0.05$). Diagonal lines represent $y = x$, circle colors correspond to different recording days.

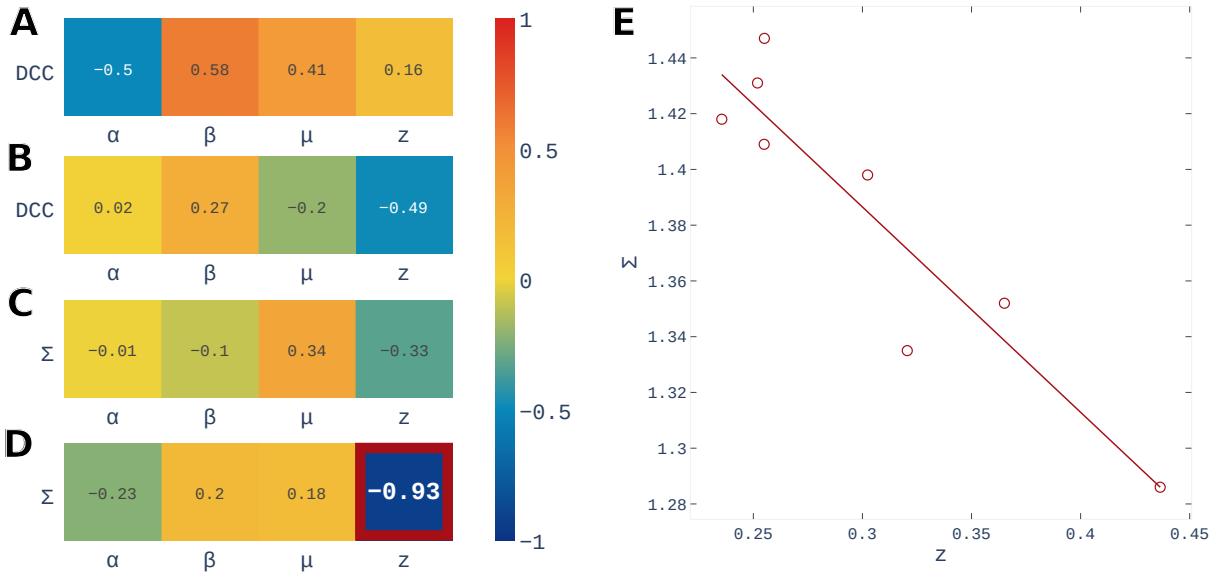

Figure 2.12: *Relation between scaling exponents of PRG and avalanches.*
A - correlation matrix between scaling exponents of PRG and DCC during wakefulness ($p > 0.1$ in all cases, adjusted for multiple comparison), **B** - same as in A, but during sleep/rest ($p > 0.1$ in all cases, adjusted for multiple comparison), **C** - correlation matrix between scaling exponents of PRG and optimal collapsing exponents of avalanche shapes , during wakefulness ($p > 0.1$ in all cases, adjusted for multiple comparison), **D** - same as in **C**, but during sleep/rest ($p > 0.1$, for α, β, μ and $p = 0.001$ for z - red bounding box, adjusted for multiple comparison), **E** - correlation between scaling exponent of autocorrelation timescale z and the optimal collapsing exponent for avalanche shapes Σ .

of recording, which limits statistical power (Figure 2.12). The PRG scaling exponents did not show a significant linear correlation with DCC during wakefulness (Figure 2.12 A) or sleep/rest (Figure 2.12 B). This suggests the presence of potentially complex, non-linear associations between these quantities.

In addition, I explored the link between PRG scaling and activity propagation in avalanches, characterized by their shapes. The optimal collapsing exponent Σ for avalanche shapes varied between awake periods and sleep/rest (Figure 2.4 B) and did not show correlation with the PRG scaling exponents during wakefulness (Figure 2.12 C). During sleep or rest, Σ exhibited a negative correlation with the scaling exponent of the autocorrelation timescale z (Figure 2.12 D and E, $p < 0.001$). This relationship clearly shows the connection between population timescales and cascaded activity propagation in neuronal avalanches.

2.3 Discussion

One of the main challenges in neuroscience is understanding how, amidst ever-changing environmental and internal conditions, the brain directs behavior. This process involves multiple stages: perception through sensory systems, integration of sensory inputs and preexisting memories, and storage of critical information. Each stage has distinct computational demands and is performed by extensive networks of interconnected neurons. Neural networks often appear to be noisy and have complex dynamics that can be studied from different angles (Barabási et al. 2023; Srivastava et al. 2022). In this chapter, I applied tools derived from statistical physics to study hippocampal dynamics in relation to the brain criticality hypothesis.

To start, I detected neuronal avalanches (Beggs and Plenz 2003; Beggs and Plenz 2004) and showed power laws within distributions of their size and duration. The duration distribution power law exponents were different, while the size distribution power law exponents aligned with theoretical predictions for critical systems ($\alpha = 2, \tau = 1.5$), closely resembling the values reported in other studies on avalanche spiking data *in vivo* (Fontenele et al. 2019; Viola Priesemann, Wibral, et al. 2014; Bédard, Kröger, and A. Destexhe 2006; Ma et al. 2019; Hahn, Adrian Ponce-Alvarez, et al. 2017). Next, I showed that the duration and size of hippocampal neuronal avalanches are intertwined by a scaling relation $\frac{1}{\sigma\nu z}$ (Friedman et al. 2012; Fontenele et al. 2019; Sethna, Dahmen, and Myers 2001), corroborating findings from related studies (Friedman et al. 2012; Xu et al. 2024; Fontenele et al. 2019; Ma et al. 2019; Mariani et al. 2021). Using this exponent to rescale avalanche temporal profiles (Marshall et al. 2016; Friedman et al. 2012; Sethna, Dahmen, and Myers 2001), achieved shape collapse of the avalanches, yet without optimal results ($\frac{1}{\sigma\nu z} \neq \Sigma$ [1]). I utilized avalanche properties to assess the deviation of CA1 activity from the critical point using the distance to criticality coefficient (DCC) (Ma et al. 2019). This measurement was positive and near zero, indicating dynamics near, but not precisely at the critical point (Viola Priesemann, Wibral, et al. 2014).

These results indicate a system with critical exponents showing inconsistencies but fulfilling the scaling relation, suggesting quasicritical dynamics (Tian et al. 2022; Williams-García et al. 2014; Fosque et al. 2021). This perspective implies the presence of a critical-like dynamic region where a network might function, which explains the observations presented in this chapter. Additionally, quasicriticality might encompass some earlier evidence of slightly sub-critical operating regimes in the brain (Viola Priesemann, Wibral, et al. 2014; Jens Wilting et al. 2018).

My study focused solely on the hippocampus; therefore, I cannot determine the origin of the hippocampal dynamics resembling criticality. This regime might result from input-dependent modulation (Ribeiro et al. 2010; Hahn, Adrian Ponce-Alvarez, et al. 2017; Viola Priesemann and Shriki 2018; Stewart and Plenz 2006; Stewart and Plenz 2008; Zierenberg, Jens Wilting, and Viola Priesemann 2018; Habibollahi et al. 2023), or it might emerge as "self-organized" criticality due to the inherent circuitry properties of CA1 (Chialvo 2010; Beggs 2007; Hesse and Gross 2014; Plenz et al. 2021; Tkačik, Mora, et al. 2015; A. Levina, J. M. Herrmann, and T. Geisel 2007; Anna Levina, J. Michael Herrmann, and Theo Geisel 2009; Effenberger, Jost, and Anna Levina 2015; Arcangelis and H. J. Herrmann 2010; Arcangelis, Perrone-Capano, and H. J. Herrmann 2006; Lombardi, Wang, et al. 2020; Tkačik, Marre, et al. 2014). Distinguishing these two hypotheses requires complete experimental control of all input to the hippocampus, which is hardly achievable at present *in vivo*.

I must acknowledge alternative explanations for power law avalanche distributions that might not be related to criticality (Bédard, Kröger, and A. Destexhe 2006; Touboul and Alain Destexhe 2017; Touboul and Alain Destexhe 2010; Alain Destexhe 2009; Mia C. Morrell, A. J. Sederberg, and Nemenman 2021; Mia C Morrell, Nemenman, and A. Sederberg 2024; Chintaluri and Vogels 2023). Specifically, signatures of criticality could arise as a result of the interplay of a limited number of latent factors (Mia C. Morrell, A. J. Sederberg, and Nemenman 2021; Mia C Morrell, Nemenman, and A. Sederberg 2024) or stem from intracellular metabolic processes (Chintaluri and Vogels 2023). Thus, one has to refrain from asserting that criticality is the principle that universally governs brain function (Hengen and Shew 2025). However, these reports do not undermine the potential practical contributions of studying brain dynamics

[1] I have not yet investigated the origin of this discrepancy and can only leave this question open for future work.

from the perspective of criticality. Specifically, criticality signatures have been relevant for neural disorders and pathological conditions (Heiney et al. 2021; Zimmern 2020; He 2011; Muñoz 2018; Hengen and Shew 2025), such as epilepsy (Lepeu et al. 2024; Liu, F. Li, and Wan 2023; Müller et al. 2025), and differ between different behavioral states (Cambrainha et al. 2025; Xu et al. 2024; Meisel et al. 2013), suggesting a potential functional role of critical-like dynamics (Cambrainha et al. 2025; Müller et al. 2025).

Using the distance to the critical point during both sleep/rest and awake periods, I found DCC in CA1 to be greater during wakefulness compared to sleep/rest, consistent with findings in the neocortex (Xu et al. 2024). This suggests that awake behavior disrupts critical-like dynamics, whereas sleep restores the brain to its natural state, optimal for learning (Xu et al. 2024; Fosque et al. 2021; Tkačik, Mora, et al. 2015). However, I must note that the dynamics of the CA1 code during learning differs from the dynamics during sleep/rest. During learning, CA1 encodes new place and learning-related information, altering its code in response to external and internal changes (R. U. Muller and J. L. Kubie 1987; Quirk, R. U. Muller, and J. L. Kubie 1990; Bostock, Robert U. Muller, and John L. Kubie 1991; John O'Keefe and Burgess 1996). Meanwhile, CA1 significantly contributes to memory consolidation during sleep. Thus, the distinct critical-like dynamics that I observed in CA1 during awake compared to sleep/rest may also reflect different roles assumed by the hippocampus at different experimental stages.

Finally, I want to note that the power law exponents reported in this chapter are evident only over approximately 1.5 to 2 orders of magnitude. I had to restrict the range of avalanches for fitting power laws due to potentially insufficient representation of events towards the tail of distributions. Since these distributions likely do not have finite variance and possess "fat-tails", the probability of avalanches of extreme durations or sizes is small but significant. Thus, one needs a very good sampling of underlying events, in the case of this study, spikes, to estimate power law decay properly, requiring simultaneous recording from a large number of cells for long periods of time. Otherwise, it is possible to observe the effects of insufficiently good sampling (Nonnenmacher et al. 2017). To overcome some of these challenges, I analyzed only very long recording sessions with a relatively high number of cells (150-200). However, this represents $0.1 - 0.2\%$ of the total cell count in the rat's hippocampus (G. Buzsáki 1989), over time during which rats may experience various global brain states. These methodological limitations make it difficult to assess the temporal evolution of brain states related to criticality or to relate them to learning and memory performance. Thus, for the remainder of the study, I analyzed the data using the Phenomenological Renormalization Group approach (Meshulam et al. 2019).

The initial results of the Phenomenological Renormalization Group analysis, consistent with previous studies (Meshulam et al. 2019; Morales, Santo, and Muñoz 2023; Munn et al. 2024; Jones et al. 2023), show robust scaling across multiple coarse-graining steps for various macroscopic quantities. In particular, I observed scaling in the covariance matrix spectrum, autocorrelation times, negative logarithm of silence probability ("free energy"), and activity variance. The last two exponents capture interest because their values indicate intricate properties of CA1 dynamics. The observed value of the exponent beta was within the bounds provided by a system with only independent units ($\beta = 1$), while alpha took the value within the bounds provided by systems with completely independent units ($\alpha = 1$) and the upper bound in systems with completely correlated units ($\alpha = 2$). In addition to robust scaling exponents, coarse-grained activity showed non-Gaussian distributions. These distributions converged to a uniform form up to a certain limit, demonstrating invariance when coarse-grained. The invariance of coarse-grained probability distributions, together with robust scaling exponents,

during two different behavioral regimes, sleep and wakefulness, is substantial evidence in favor of scale-invariant activity in the hippocampus (Meshulam et al. 2019; Morales, Santo, and Muñoz 2023; Munn et al. 2024).

However, the question of whether this form of scaling is a feature of criticality in the brain remains open. On the one hand, the invariance of the probability distributions of coarse-grained activity can be interpreted as the proof of criticality in the network (Meshulam et al. 2019), and the variability of the scaling exponents can be attributed to the existence of critical regions (Moretti and Muñoz 2013; Morales, Santo, and Muñoz 2023) instead of a singular critical point, conceptually matching a quasi-critical explanation of the avalanche exponents (Williams-García et al. 2014; Fosque et al. 2021). On the other hand, the relation between quantities isolated using PRG and critical systems is not well understood, and one has to carefully interpret the scaling exponents (Nascimento et al. 2025). Computational analyzes show that contact process models, when adjusted for supercriticality, exhibit scaling exponents and coarse-grained activity distributions that have a significantly different form from those produced by the model tuned to criticality (Nicoletti, Suweis, and Maritan 2020). However, there is a lack of understanding between sub-critical dynamics and PRG, especially in more realistic models of brain activity or in experimental data. I tried to bridge this gap by performing a simple analysis between these two views. I did not observe any significant correlation between distance to criticality and PRG scaling exponents. This might indicate a complex, non-linear, and non-monotonic relationship between PRG scaling exponents and criticality. Interestingly, during sleep/rest, PRG and avalanche criticality were mutually entangled through measures of temporal activity propagation. The optimal exponent for collapsing avalanche shapes was Σ negatively correlated with the scaling of characteristic timescales in PRG. The existence of this relation only during sleep/rest might suggest a brain-state-dependent (dis)agreement of the two views of criticality. However, investigating the origin and mechanistic properties leading to this has to be left for future work.

Next, I compared the results of applying PRG to wakefulness and sleep. As with the estimated distance to criticality (DCC), the scaling between these two states was different. The exponents β, μ and z remained robust, while the exponent α differed between wakefulness and sleep/rest. This finding initially appears to contrast with Morales, Santo, and Muñoz (2023), which reported α that does not differ between task-engaged and resting mice. However, that study examined the scaling exponent α throughout the brain, including regions not involved in the task. The varying scaling exponent α between wakefulness and sleep/rest likely results from differing inputs or general activity levels in sleep/rest. Alternatively, consistent with other studies, it could be explained by a dynamics distorted by awake behavior, only to be restored to its natural state during sleep (Xu et al. 2024; Meisel et al. 2013).

I propose an additional interpretation. Different avalanche dynamics and different scaling laws in the hippocampus during awake and sleep/rest may reflect functionally different roles assumed by the hippocampus during these two states. In awake behavior, the hippocampus is engaged in navigation and, in experiments I analyzed, learning. During sleep/rest, it is involved in memory consolidation, where, under the prevailing view, it serves as a source from which short-term memories are transferred to the cortex. Learning and acquiring new information necessitate distinct computational demands compared to transferring that information to the cortex. The former process requires a circuit that can rapidly adapt and encode novel information, while the latter process requires a circuit that produces stable encoding that can be a reliable source of information for the cortex. These two processes may require different underlying dynamics echoed by different scaling of activity variance and different DCC . If

correct, this explanation would imply a direct functional relevance of activity scaling, and that is what I set out to investigate in the next chapter.

CHAPTER 3

Functional role of scaling in the hippocampal activity

Abstract

It has been extensively studied how operating in a scale-free regime would endow neural networks with maximal information processing and storage capabilities. However, the functional role of critical scaling remains highly debated. In this chapter, I applied the Phenomenological Renormalization group (PRG) on the spiking data recorded from the rat's hippocampus during a memory consolidation period and related PRG-derived scaling exponents to memory retention performance. I found that the scaling exponent of activity variance α measured during the sleep/rest session that followed learning correlated with memory retention during the subsequent unrewarded testing session. Moreover, α predicted performance even when controlled for reactivation that also occurs in the same sleep/rest session. Second, α measured in the sleep/rest phase that preceded learning was correlated with the learning speed. To better understand the nature of the scaling exponent α, I analyzed the distributions of the characteristic timescale and burstiness of the cells. The day-to-day variability of these distributions, during sleep/rest that followed learning, correlated with the scaling exponent of activity variance α. Interestingly, the same distributions predicted subsequent memory retention. These findings confirmed that the scaling of activity variance provides a behaviorally meaningful perspective on hippocampal activity, as it is directly related to memory retention. Furthermore, these results indicate the importance of hippocampal activity outside of reactivation periods, and beyond sharp wave-ripples, for the memory consolidation process.

Introduction

In the previous Chapter, I have demonstrated signatures of dynamics close to criticality in the hippocampus CA1. My findings align with other studies in slice cultures (Beggs and Plenz 2003; Mazzoni et al. 2007; Pasquale et al. 2008), *in vivo* (Petermann et al. 2009; Gireesh and Plenz 2008; Hahn, Petermann, et al. 2010; Yu et al. 2011; Xu et al. 2024), and across species (Adrián Ponce-Alvarez, Kringelbach, and Deco 2023; Freeman et al. 2003; Meisel et al. 2013; Solovey et al. 2012; Poil et al. 2012; Lombardi, Shriki, et al. 2021; Mainali, Azeredo da Silveira, and Burak 2025). However, the origin and nature of these neural dynamics remain a topic of debate (Bédard, Kröger, and A. Destexhe 2006; Touboul and Alain Destexhe 2017;

Touboul and Alain Destexhe 2010; Alain Destexhe 2009; Mia C. Morrell, A. J. Sederberg, and Nemenman 2021; Mia C Morrell, Nemenman, and A. Sederberg 2024; Chintaluri and Vogels 2023). Although it is not certain whether criticality is the principle that universally governs brain activity, the results of the previous chapter, together with earlier studies Xu et al. 2024; Meisel et al. 2013, reveal distinct scaling dynamics between sleep and wakefulness. This distinction is a basis for one of the objectives of this study: to determine the functional relevance of scaling exponents and criticality-like dynamics.

Previous research focused on the theoretical aspects and computational properties of critical systems (Shew and Plenz 2013). Studies have demonstrated that operating at or near criticality enhances long-range correlations (Lombardi, Shriki, et al. 2021), maximizes dynamic range (Shew, Yang, Petermann, et al. 2009; Kinouchi and Copelli 2006), improves adaptability to task demands (Jens Wilting et al. 2018), and optimizes information transmission (Beggs and Plenz 2003; Shew, Yang, Yu, et al. 2011; Avramiea et al. 2022). Although these are functionally relevant network characteristics, earlier studies did not link criticality to the ultimate task of the brain ¯ to guide behavior. There is only a minimal amount of evidence linking criticality and task performance measures (Cambrainha et al. 2025), none focusing on the hippocampus. In this Chapter, I will attempt to address this gap by demonstrating how scaling in the $CA1$ activity is related to animal performance in a spatial memory task.

3.1 Scaling of activity variance predicts retention of spatial memory

I analyzed a different group of animals compared to the first chapter, focusing on their performance during the "Cheeseboard" task (Dupret et al. 2010; Boccara et al. 2019). I combined existing datasets in the lab and extended them with novel recordings. On each recording day, the animals learned to locate and remember three novel food-rewarded goal locations (refer to Figure 3.1, Methods for additional details). After training, they were transferred to a separate box for a sleep/rest session labeled "*Post-Sleep*". Afterwards, the animals underwent performance evaluation during an unrewarded session termed "*Post-Probe*". During this task two important processes take place, learning and memory consolidation, the latter occurring primarily during sleep/rest immediately after learning. Importantly, both memory retention performance and learning performance are straightforward to measure.

I assess memory retention (Figure 3.2 A) by measuring the duration rats spend near the goals during the first 2 minutes of the "*Post-Probe*". Furthermore, I normalized the duration by computing the difference between time around goals and the mean time around randomly sampled non-goal locations, divided by the sum of the two (Figure 3.2 B; Supplementary Figure S.2; see Methods for details). Comparing these metrics with those of the "*Pre-Probe*" control session reveals that the rats recall newly baited locations without prior knowledge. In this chapter, I use normalized time around goals to quantify memory retention.

To quantify learning performance (Figure 3.2 C), I assessed the distance covered in each trial and plotted it throughout the learning session. A reduction in distance per trial signifies effective learning, with its speed measured by the number of trials required to achieve 20% the distance of the first trial.

The structure of the cheeseboard task allows me to investigate the potential relationship between scale-free dynamics and spatial learning and memory performance. In this section, I will demonstrate how scaling of hippocampal activity, measured during sleep and learning,

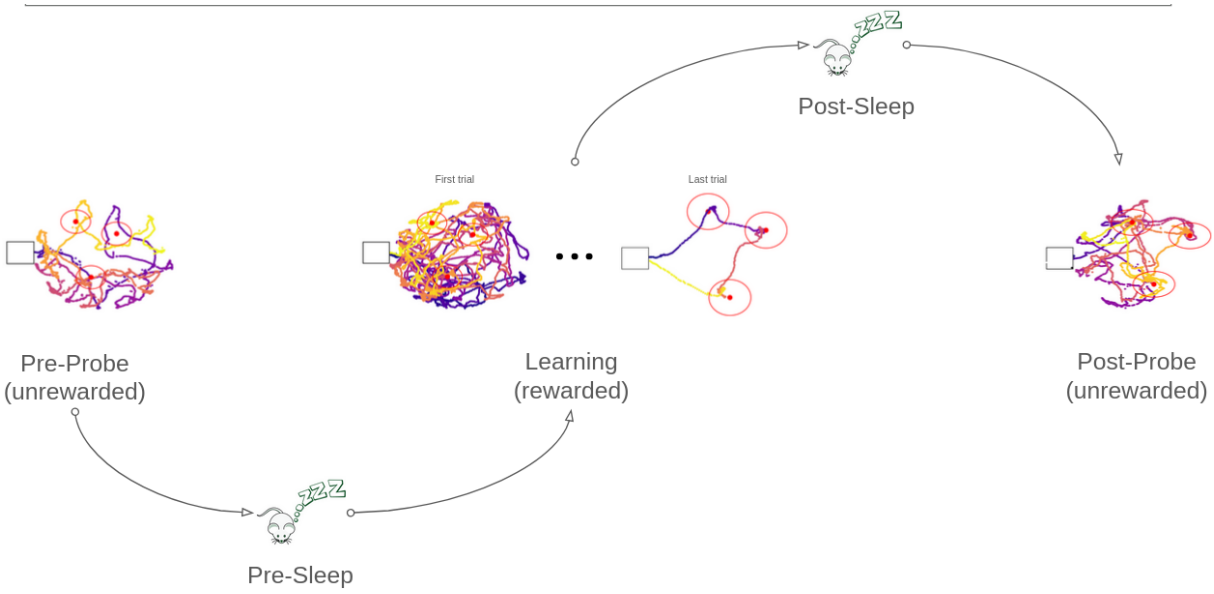

Figure 3.1: *Behavioral paradigm.*
Order of sessions throughout a day. Each awake session contains an example animal trajectory, color-coded so that blue shades indicate the start and yellow the end of the trial. Red dots indicate goal location, red circles indicate $10cm$ goal zones.

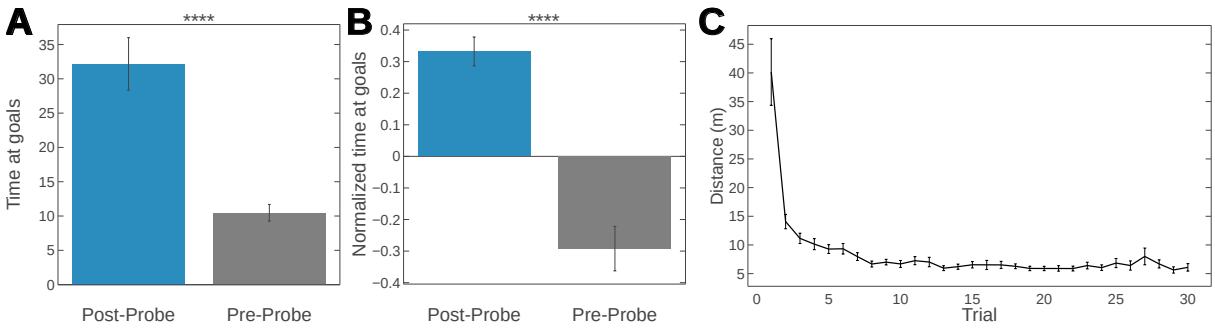

Figure 3.2: *Performance on the cheeseboard task.*
A - Time spent in goal zones during first three minutes of *Post-Probe* ($p < 0.001$, Wilcoxon-Signed rank test), **B** - normalized time spent around goals ($p < 0.001$, Wilcoxon-Signed rank test), **C** - learning curve, distance covered per trial.

is related to the memory retention performance measured in *Post-Probe*, using the same measure in *Pre-Probe* as a control. Next, I will show how the same scale-free quantities are related to learning performance. Crucially, I will link the scale-free activity to another important process for memory consolidation — reactivation. Moreover, I will show that scale-free dynamics predict memory performance independent of reactivation. Finally, to improve our understanding of scale-free dynamics, I will establish a relationship between scale-free dynamics and functional/physiological variability between hippocampal cells.

Hippocampal activity during sleep/rest immediately after learning is essential for certain types of memories (Stickgold 2005; Diekelmann and Born 2010; Rasch and Born 2013; Klinzing, Niethard, and Born 2019; Girardeau and Lopes-dos-Santos 2021; Lutz, Harkotte, and Born 2025). Therefore, the functional relevance of activity scaling in the hippocampus implies that the day-to-day variability of scaling exponents observed in *Post-Sleep* should account for some variation in memory retention performance. If there is a relation between activity scaling during *Post-Sleep* and memory retention, it would imply necessity since, in the experimental

paradigm, the *Post-Sleep* session precedes the *Post-Probe* session.

I calculated a linear correlation between the PRG scaling exponents of *Post-Sleep* and the normalized time around the goals on *Post-Probe* (Figure 3.3). Since, for each scaling exponent, the relative differences between different recording days are more important than the absolute values (Supplementary Figure S.3), I performed an analysis of rank correlation [1]. Scaling exponents of free energy (β), autocorrelation times (z) and the spectrum of the covariance matrix (μ) were not significantly correlated with memory retention (Figure 3.3 B, C, D). On the other hand, the scaling exponent of activity variance (α) correlated negatively with the normalized time around the goals in *Post-Probe*(Figure 3.3 A) and did not correlate with the same measure in *Pre-Probe*. Essentially, a rapid scaling in variance within coarse-grained clusters during *Post-Sleep* results in poorer memory retention.

As α was the sole scaling exponent that predicted memory retention performance, I investigated its relationship with other scaling exponents. The correlation plots in Figure 3.4 A-C show a lack of linear correlation among α and other PRG scaling exponents. Nevertheless, the combined use of multiple scaling exponents might enhance the prediction of memory retention performance. I tested this by fitting multiple regression models with different combinations of input exponents (Figure 3.4 D). To compare models while accounting for different numbers of parameters, I used the Bayesian information criterion (BIC, lower is better, details in Methods). BIC being the lowest for the model using only α as a predictor indicates that including more scaling exponents does not enhance prediction quality. Together with the results in Figure3.3, I conclude that under coarse-graining during *Post-Sleep*, only the scaling of activity variance (α) was related to memory retention performance.

The scaling of activity variance is a complex measure based on intuition coming from statistical physics and is not derived from the physiological or biological properties of the brain. The connection between α and memory retention might result from its correlation with another biologically relevant property of network activity. I examined whether the properties of the network activity that are more straightforward and frequently assessed are related to α or the animal's behavior. The mean firing rate, mean synchrony, coefficient of variation of the instantaneous firing rate, mean pairwise correlation, and inhibition/excitation ratio did not show correlation with α or with normalized time surrounding the goals (Supplementary Figure S.4). This analysis eliminated these measures as potential linear confounders.

[1] For the same reason, rank correlation is used in the rest of the thesis.

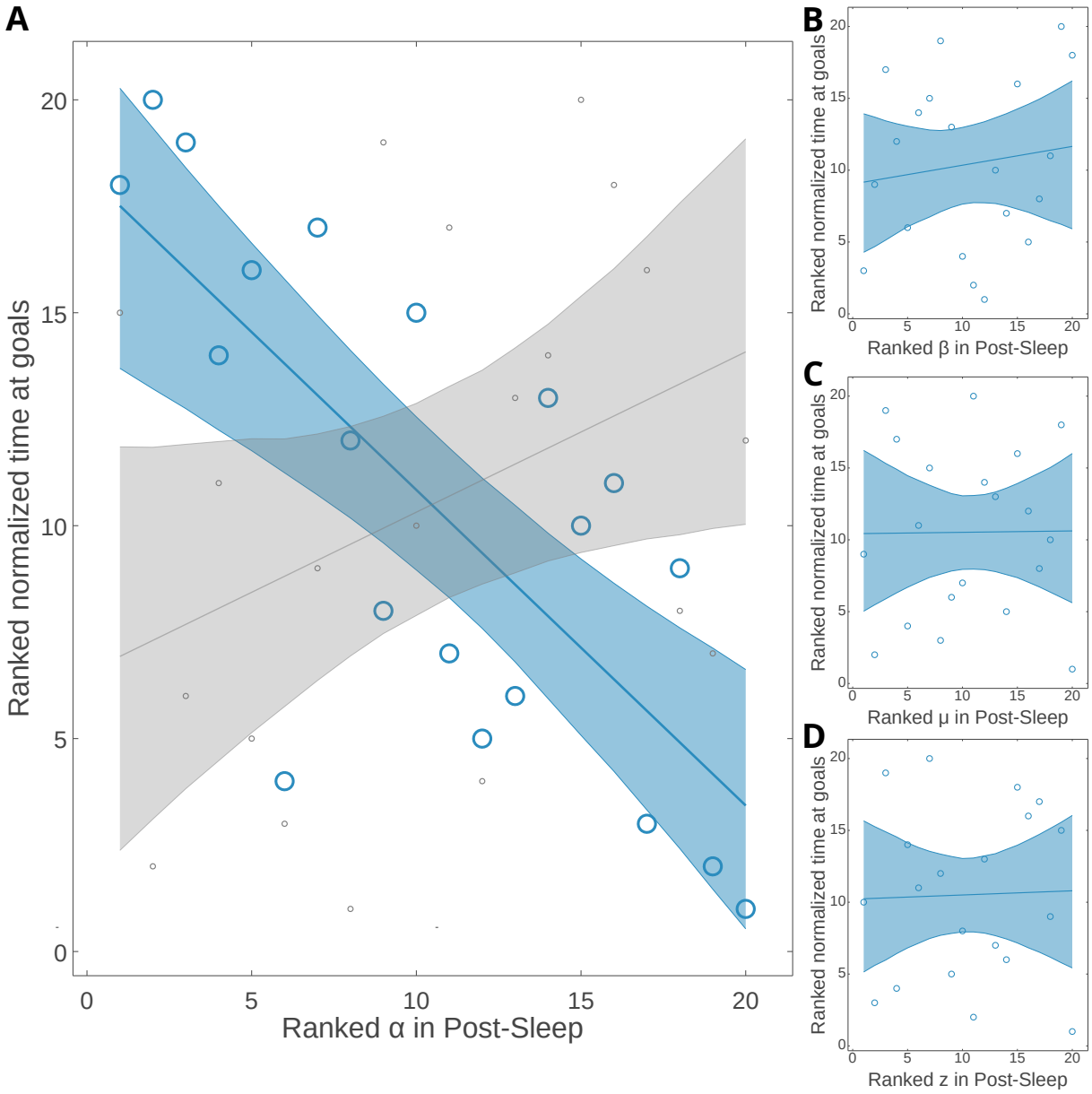

Figure 3.3: *Scaling of activity variance during Post-Sleep predicts memory retention.*
Scaling exponents measured during *Post-Sleep* versus normalized time around goals during *Post-Probe* (Blue) and during *Pre-Probe* (grey). **A** - scaling exponent of activity variance (correlation with *Post-Probe*: $R = -0.737$, $CI = [-0.937, -0.329]$, non-significant correlation with *Pre-Probe*: $R = 0.36$, $CI = [-0.145, 0.754]$), **B** - scaling exponent of free energy (non-significant correlation with *Post-Probe*: $R = 0.135$, $CI = [-0.474, 0.611]$, **C** - scaling exponent of covariance matrix spectrum (non-significant correlation with *Post-Probe*: $R = 0.01$, $CI = [-0.574, -0.618]$), **D** - scaling exponent of characteristic autocorrelation time (non-significant correlation with *Post-Probe*: $R = 0.034$, $CI = [-0.531, 0.628]$) Lines represent linear fits, confidence intervals are obtained by bootstrapping 5000 times.

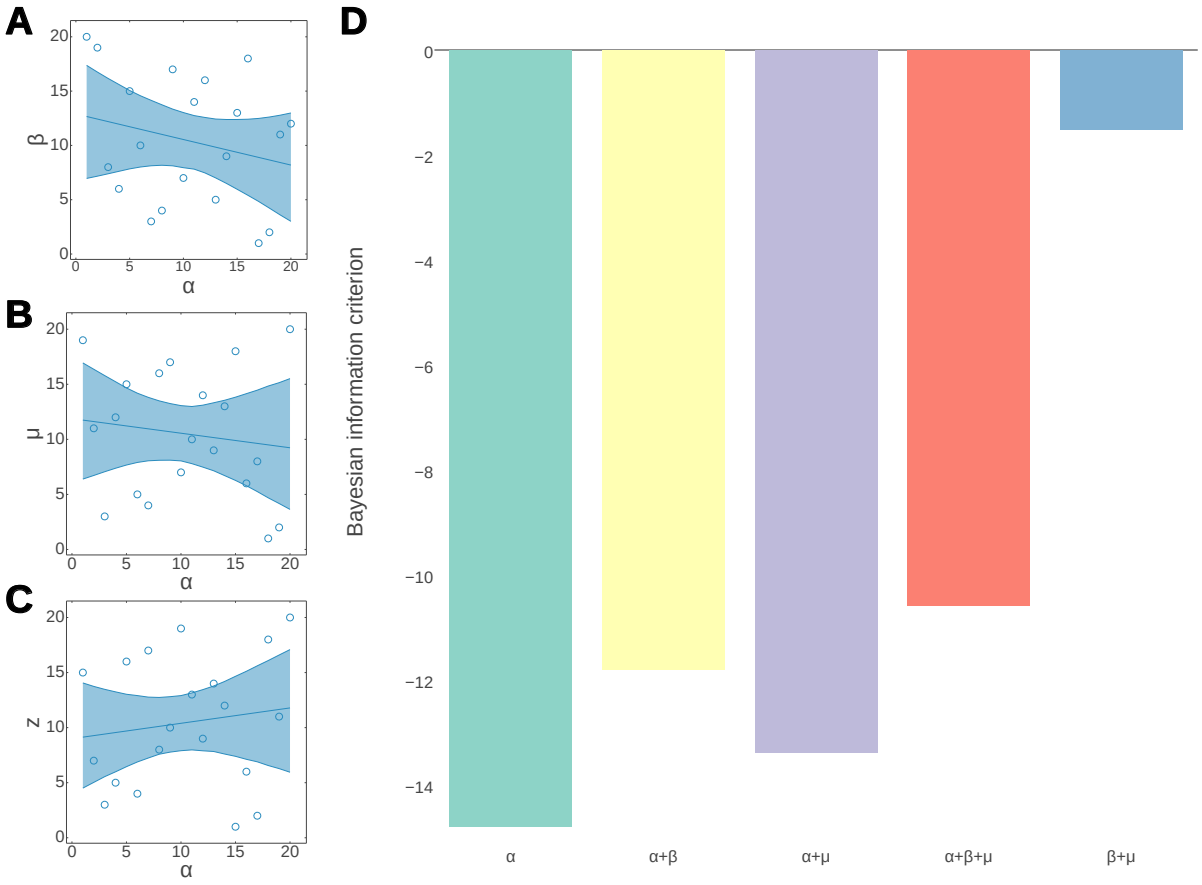

Figure 3.4: *Relations between PRG scaling exponents.*
A - non-significant correlation between the scaling of activity variance and the scaling of free energy ($R = -0.228$, $CI = [-0.684, 0.388]$), **B** - non-significant correlation between the scaling of activity the variance and scaling of correlation matrix spectrum ($R = -0.135$, $CI = [-0.71, 0.509]$), **C** - non-significant correlation between the scaling of activity variance and the scaling of autocorrelation time ($R = 0.143$, $CI = [-0.443, 0.688]$), **D** - Bayesian information criterion of linear models with different input parameters (lower is better).

3.2 Scaling of activity variance predicts spatial memory retention together with reactivation

I demonstrated in the preceding section that the scaling of activity variance during *Post-Sleep* predicts memory retention performance during *Post-Probe*. However, another process in the hippocampus provides similar predictive abilities —reactivation (M. Wilson and B. McNaughton 1994; Louie and M. A. Wilson 2001; Lee and M. A. Wilson 2002; Joseph O'Neill et al. 2010). Memory reactivation is a process in which neural activity patterns observed during awake behavior are observed again during quiet immobility, occurring mostly during sharp-wave ripples (SWRs) (Buzsaki et al. 1992; M. Wilson and B. McNaughton 1994), even though the animals are not reproducing the same behavior. Research demonstrated the causal role of reactivation in memory consolidation by disrupting SWR-related hippocampal reactivation during sleep (Girardeau, Benchenane, et al. 2009; Ego-Stengel and M. A. Wilson 2009), thereby affecting memory consolidation and recall. Additionally, in a dual-environment task, targeting reactivation associated with one environment exclusively hinders the recall of that particular disrupted environment, while the recall performance of the undisturbed environment remains unaffected (Gridchyn et al. 2020). Crucially for my work, the reactivation process is known to

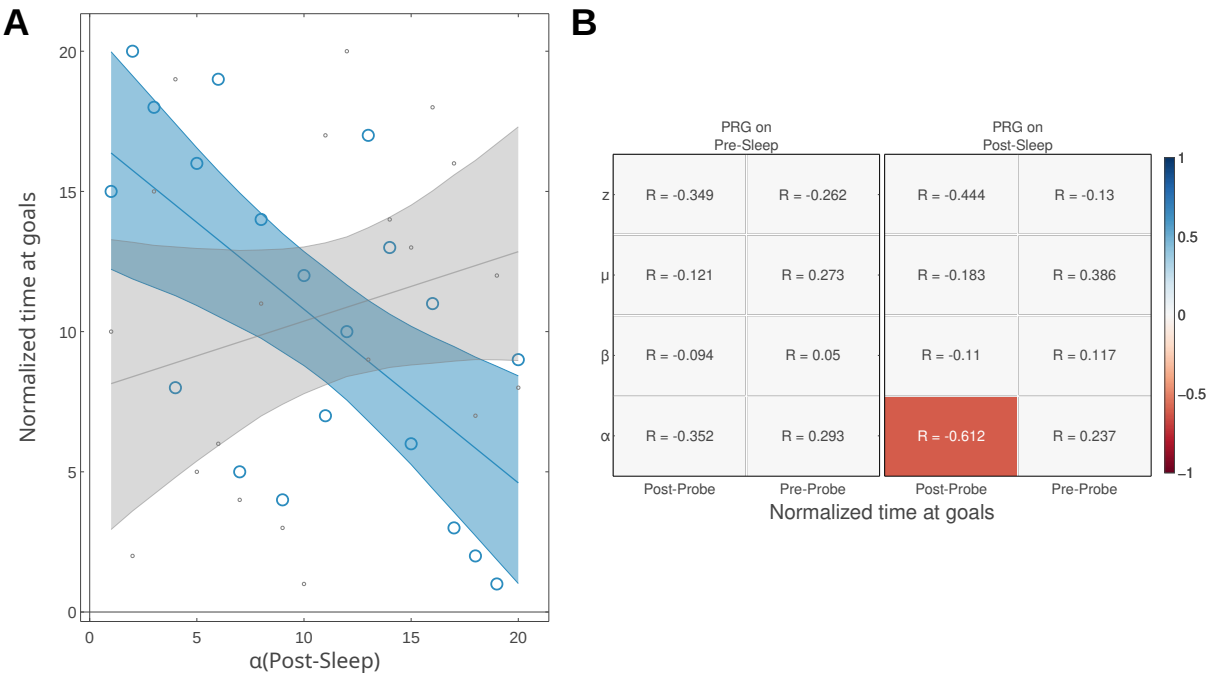

Figure 3.5: *Excluding SWRs and HSEs does not influence behavioral predictions of PRG scaling exponents.*

A - scaling exponent of activity variance versus normalized time around goals, with excluded SWRs and HSEs (correlation with Post-Probe: $R = -0.612$, $CI = [-0.891, -0.145]$, non-significant correlation with Pre-Probe: $R = 0.237$, $CI = [-0.251, 0.684]$]) **B** - summary of correlation between PRG scaling exponents and normalized time around goals, with excluded SWRs and HSEs; grey fields indicate non-significant correlation, colored square a indicates significant correlation.

support spatial memory and correlates with subsequent memory retention performance (Dupret et al. 2010). Two questions arise: 1) does the scaling of activity variance during *Post-Sleep* relate to memory reactivation; 2) does the predictive effect of the scaling exponent α result from reactivation.

To find these answers, I began the investigation with a straightforward analysis. Eliminating SWR periods from the data retained the prediction outcomes, as the scaling of activity variance remained correlated to the normalized time around the goals (Figure 3.5).

Next, I conducted reactivation analysis (Figure 3.6). I calculated the Pearson correlation between population vectors (**PVs**) based on the initial three minutes of *Post-Probe* and SWR activity during *Post-Sleep*. This yielded a reactivation map for each SWR (Figure 3.6 B). To pinpoint SWRs with task-relevant reactivation, I focused only on the Pearson correlation between **PVs** in reward zones and SWR activity during sleep/rest. If the actual value surpasses the correlation of spatially shuffled surrogate data (Figure 3.6 C), I designated the SWR as an event that contained reactivation. Analogously to the findings presented in (Dupret et al. 2010), the proportion of SWRs that exhibit reactivation during *Post-Sleep* correlated with the normalized time around the goals in *Post-Probe* (Figure 3.6 D). However, it did not correlate significantly with the normalized time around the goals measured before learning, in *Pre-Probe* (Figure 3.6 E). Furthermore, the fraction of SWRs that exhibited reactivation during *Pre-Sleep*, before learning, did not correlate significantly with the normalized time around the goals in *Post-Probe* (Figure 3.6 F).

The scaling exponent α also correlated with the fraction of reactivating events (Figure 3.7 A), but did not correlate with the average correlation between SWR activity and **PVs** of the reward

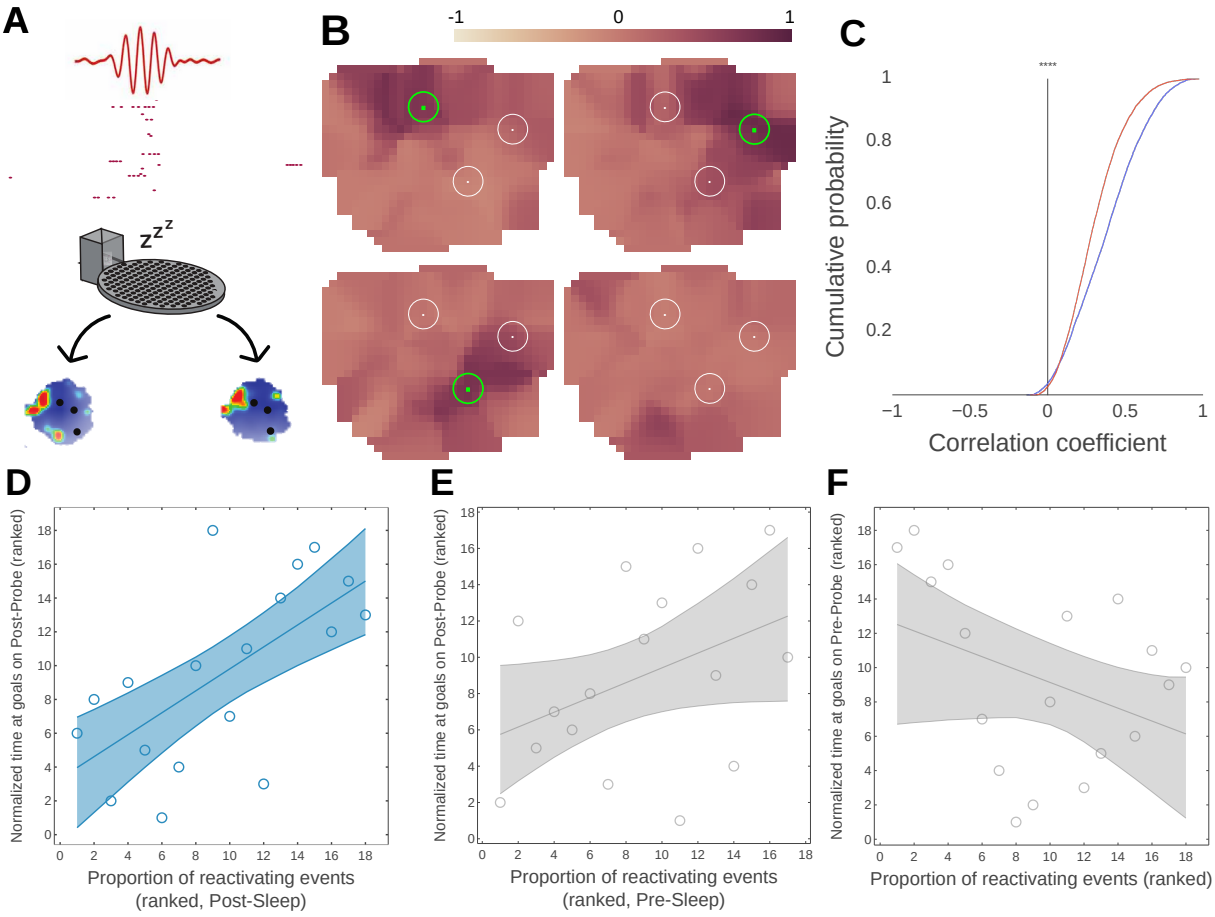

Figure 3.6: *Goal-related reactivation in CA1.*

A - Pearson correlation between the activity during SWRs (top, LFP + spike rasters) and population vectors during awake periods, **B** - Example reactivation maps during four different SWRs, shades of brown indicate correlation coefficient $r \in [-1, 1]$ between a given SWR and each spatial bin, with green are marked goals that are reactivated in each SWR, during the SWR event at bottom right no goals were reactivated, **C** - CDFs of Pearson correlation scores between PVs around goals and SWRs, shuffled distribution in red (details in Methods), **D** - correlation between fraction of events that are reactivating during *Post-Sleep* and memory retention during *Post-Probe* ($R = 0.644$, $CI = [0.312, 0.87]$), **E** - non-significant correlation between fraction of events that are reactivating during *Post-Sleep* and memory retention during *Pre-Probe* ($R = 0.404$, $CI = [-0.171, 0.828]$), **F** - non-significant correlation between the fraction of events that are reactivating during *Pre-Sleep* and memory retention during *Post-Probe* ($R = -0.372$, $CI = [-0.757, 0.265]$).

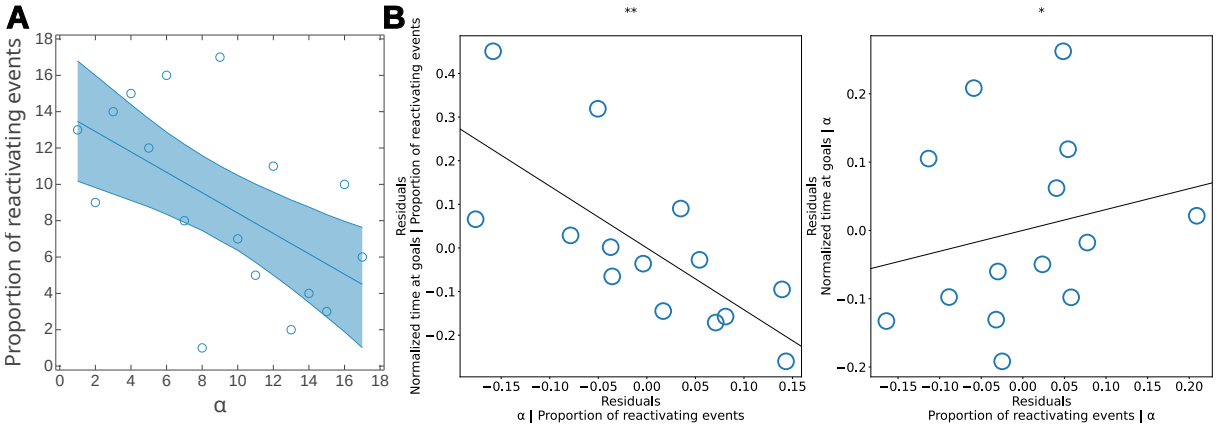

Figure 3.7: *Scaling of activity variance and goal-related reactivation.*
A - Correlation between scaling of activity variance during *Post-Sleep* and proportion of SWRs that reactivated reward zones ($R = -0.555$, $CI = [-0.798, -0.26]$), **B** - Partial regression plots, left: scaling of activity variance versus normalized time around goals, when controlled for proportion of reactivating SWRs ($R = -0.817$, $p = 0.002$), left: proportion of reactivating SWRs versus normalized time around goals, when controlled for scaling of activity variance ($R = 0.637$, $p = 0.038$).

zones (Supplementary Figure S.5). Next, I conducted partial correlation analysis between α and the normalized time around the rewards, while using the fraction of reactivation events as the control variable. The results indicated that α predicted memory retention independently of reactivation ($R = -0.817$, p 0.002, Figure 3.7 B left). Similarly, the fraction of reactivating SWRs significantly correlated with the normalized time around the goals, when using α as the control variable ($R = 0.637$, $p = 0.038$, Figure 3.7 B right). Together, these results indicate a complex interplay between the scaling of activity variance and reactivation, leading to independent contributions to memory consolidation.

3.3 The scaling of activity variance predicts the speed of learning

I wondered if memory-related scaling of activity variance is a hallmark of hippocampal activity or a consequence of learning-induced transformation of the hippocampal code. To investigate this, I examined the relationship between the exponent α calculated during *Post-Sleep* and the exponent α calculated during learning (see Figure 3.8 A) and found a correlation. Consequently, the exponent α during learning also correlated negatively with the normalized time around the rewards in *Post-Probe*, but not in *Pre-Probe* (Figure 3.8 B). This shows that, although affected by behavioral states, the exponent α is fairly robust throughout the recording day.

Given that the scaling exponent α predicted memory retention regardless of reactivation, could it also indicate daily learning capability? Indeed, α in *Pre-Sleep* negatively correlated with the number of trials required to reach a threshold on the learning curve (Figure 3.9).

The negative correlation between the scaling exponent α and the number of trials necessary for good learning performance indicates a qualitatively opposite relation compared to that with memory retention. That is, larger exponent values imply fewer trials needed to reach optimal performance, indicating that quicker scaling of activity variance facilitates faster learning. In contrast, this rapid scaling of activity variance decreases memory performance. This contrast

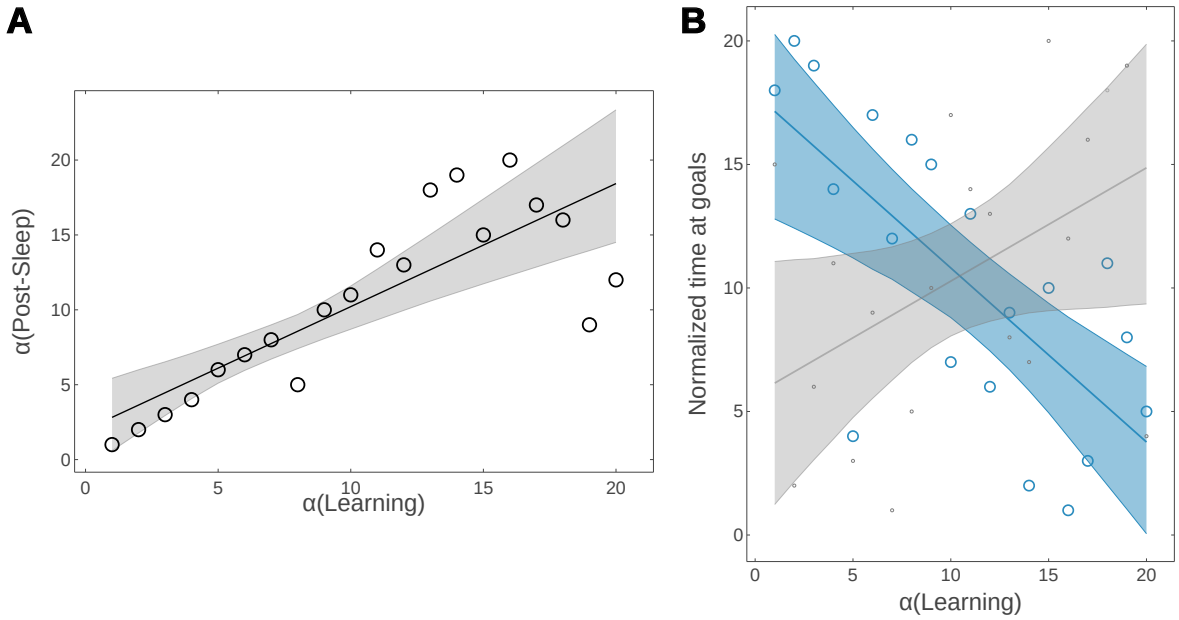

Figure 3.8: *Scaling of activity variance during learning predicts memory retention.*
A - Correlation between scaling of activity variance during learning and during *Post-Sleep* ($R = 0.808$, $CI = [0.602, 0.965]$), **B** - Correlation between during learning and normalized time around goals on *Post-Probe* (blue, $R = -0.699$, $CI = [-0.913, -0.302]$) and on *Pre-Probe* (gray, $R = 0.442$, $CI = [-0.152, 0.861]$).

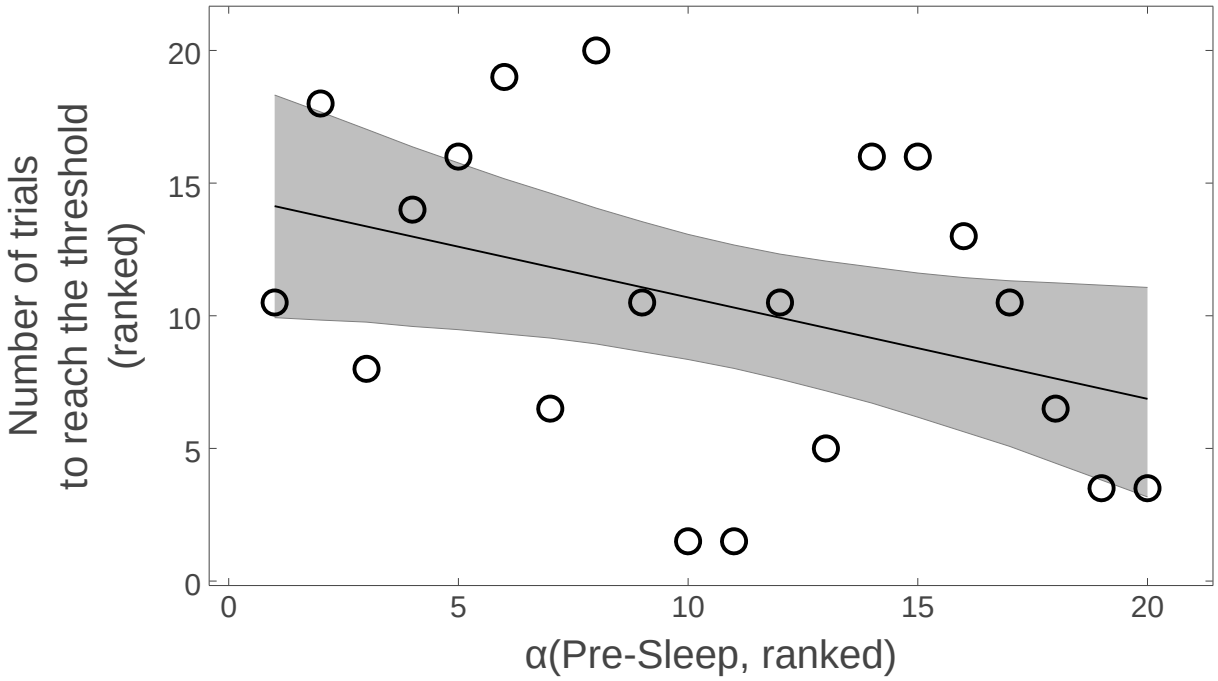

Figure 3.9: *Scaling of activity variance predicts the speed of learning.*
Correlation between scaling of activity variance during *Pre-Sleep* and number of trials necessary for reaching good performance ($R = -0.381$, $CI = [-0.671, -0.017]$).

might indicate distinct physiological processes within the hippocampus during learning and sleep.

3.4 Scaling of activity variance during sleep/rest and functional heterogeneity of hippocampal cells

The above findings demonstrated a direct link between hippocampal scaling exponents and task performance, yet they raise more questions than they resolve. Scaling of macroscopic properties along iterative coarse-graining does not have a foothold in the underlying biological properties of the brain, and to date has only been explained in terms of abstract statistical models (Mia C. Morrell, A. J. Sederberg, and Nemenman 2021). It is not established how these quantities are related to elementary units of computation in the brain. On the other hand, there have been accounts of genetic (Yao et al. 2021), anatomical (Soltesz and Losonczy 2018; Cembrowski and Spruston 2019) and functional (Wasmuht et al. 2018; Perez-Nieves et al. 2021; Mainali, Azeredo da Silveira, and Burak 2025; Cohen and Drugowitsch n.d.) cell heterogeneity in the brain.

In particular, two functional characteristics of single cells are relevant: intrinsic cellular timescales and burstiness. Intrinsic temporal profiles of cortical cells have been linked to working memory processes (Wasmuht et al. 2018; Sean E Cavanagh et al. 2016; Sean E. Cavanagh, Hunt, and Kennerley 2020), while modeling studies demonstrate learning benefits associated with a diverse pool of computational units that process information on slightly different timescales (Perez-Nieves et al. 2021; Kurikawa 2025). In the hippocampus, cell burstiness has been correlated with replay properties (Grosmark and György Buzsáki 2016). Thus, I investigated whether the scaling of activity variance is related to these two functional characteristics of hippocampal cells, in particular, to the cell-to-cell variability of these properties.

I examined the cell-specific characteristic time scales, defined as the exponential decay constant τ of the autocorrelation function (Figure 3.10 A, Methods). The lower values of τ indicate rapid decay of the autocorrelation function, while the higher values of τ signal a prolonged influence of current activity on future behavior. Histograms of τ distributions during *Post-Sleep* (Figure 3.10 B) revealed heavy-tailed distributions with notable day-to-day variability. During *Post-Sleep*, these distributions had tails fatter than expected from the normal distribution ($excess\,kurtosis = 25.55 \pm 6.43$, Figure 3.10 D, bottom) and substantial variability indicated by the quartile coefficient of dispersion (QCD) of 0.24 ± 0.02 (Figure 3.10 D, bottom). Indeed, the QCD of the τ distribution correlated with the scaling of activity variance (Figure 3.10 E). Interestingly, QCD of τ during *Post-Sleep* also predicted memory retention (Figure 3.10 F). However, α still correlated with memory retention even when controlled for QCD (partial correlation coefficient $R = -0.542, p = 0.025$).

Next, I looked at cell burstiness, defined as the proportion of interspike intervals (**ISI**) shorter than $6ms$ (Grosmark and György Buzsáki 2016). The cell burstiness distributions were more spread than the τ distributions (Figure 3.10 B, C). Again, during *Post-Sleep*, the burstiness distribution had high variability ($QCD = 0.59 \pm 0.03$, Figure 3.10 D, top) and positive excess kurtosis (1.82 ± 0.42, Figure 3.10 D, top). The scaling exponent α correlated with the excess kurtosis of burstiness (Figure 3.10 H), which also correlated with the normalized time in the goals during *Post-Probe* (Figure 3.10 I). However, α still predicted memory retention even when controlled for excess kurtosis of burstiness (Figure 3.10 J, partial correlation coefficient $R = -0.58, p = 0.0154$). Interestingly, α exhibited a strong trend towards a negative correlation with median burstiness, while median burstiness showed a strong trend towards correlation with normalized time around goals in *Post-Probe* (Supplementary figure S.6). These results, together with the positive correlation between excess kurtosis, imply a complex

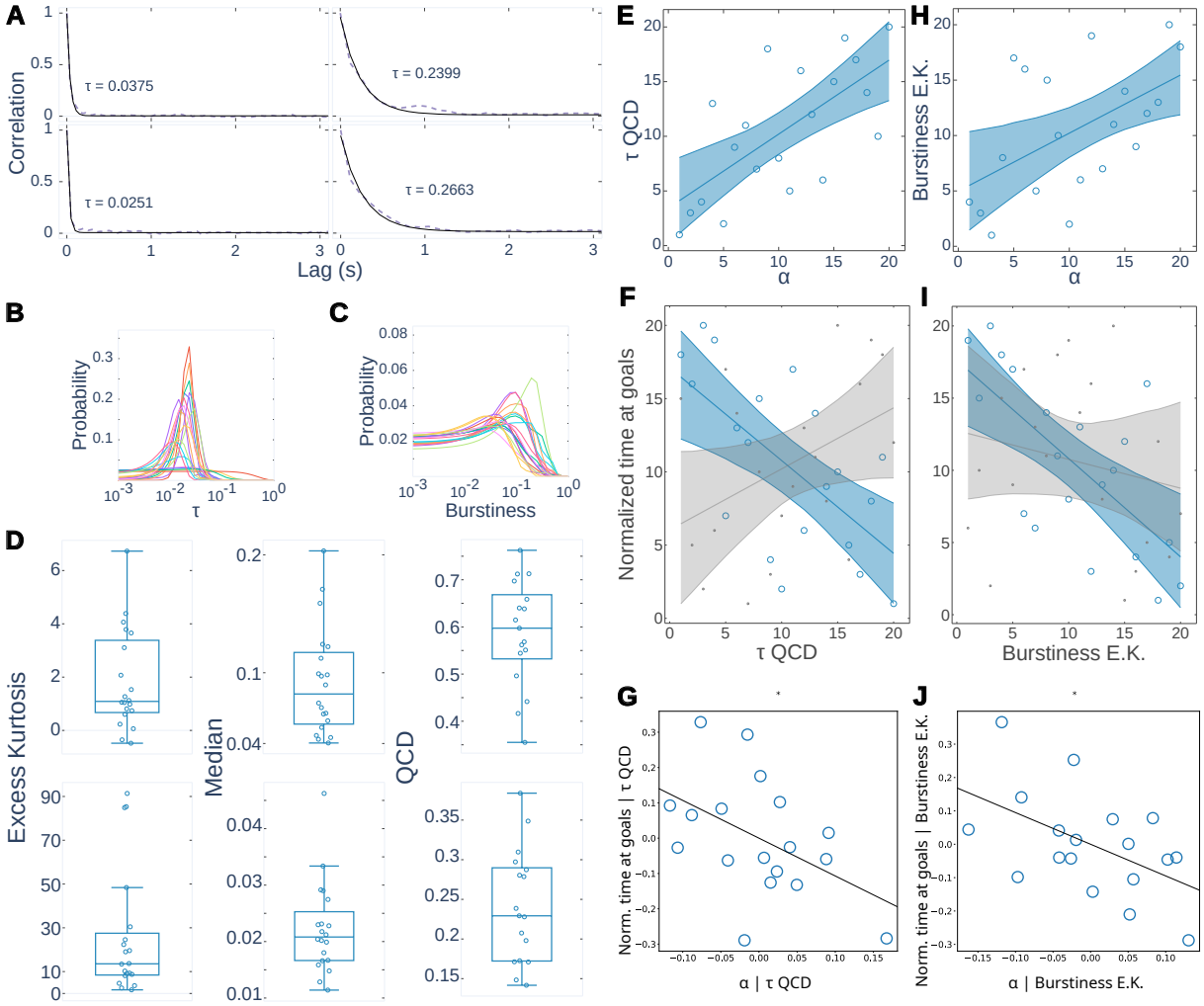

Figure 3.10: *Scaling of activity variance reflects functional variability of hippocampal cells.*
A - autocorrelation function of four different cells, **B** - distribution of characteristic timescale during *Post-Sleep*, kernel density estimate, colors correspond to recording sessions, **C** - distribution of pyramidal cell burstiness, kernel density estimate, colors correspond to recording sessions, **D** - excess kurtosis, median and quartile coefficient of dispersion (QCD) of burstiness (top) and characteristic timescale τ (bottom), **E** - correlation between scaling of activity variance and τ QCD ($R = 0.67$, $CI = [0.352, 0.879]$), **F** - rank correlation between QCD and normalized time around goals on *Post-Probe* (blue, $R = -0.629$, $CI = [-0.898, -0.154]$), non-significant correlation with *Pre-Probe* (grey, $R = 0.405, CI = [-0.182, 0.837]$)), **G** - partial correlation plot between scaling exponent alpha and normalized time around goals during *Post-Probe*, controlled for QCD ($R = -0.542$, $p = 0.025$), **H** - rank correlation between scaling of activity variance and burstiness excess kurtosis ($R = 0.524$, $CI = [0.143, 0.804]$), **I** - rank correlation between burstiness excess kurtosis and normalized time around goals on *Post-Probe* (blue, $R = -0.675$, $CI = [-0.941, -0.152]$), non-significant correlation with *Pre-Probe* (grey, $R = -0.196$, $CI = [-0.727, 0.426]$), **J** - partial correlation plot between scaling exponent alpha and normalized time around goals during *Post-Probe*, controlled for burstiness excess kurtosis ($R = -0.58, p = 0.015$).

relationship between the scaling of activity variance, burstiness, and memory consolidation.

In summary, I found that the scaling of hippocampal activity variance correlated with the variability of characteristic timescales and the propensity for bursting among hippocampal cells. These quantities also predict task performance, demonstrating the relationship between functional heterogeneity and the memory consolidation process.

3.5 Discussion

This chapter demonstrates how scaling of activity variance in the rat hippocampus predicts spatial memory task performance. The scaling exponent α predicts performance in two ways: first, α measured during the sleep/rest session that followed learning (*Post-Sleep*) correlated with memory retention during the unrewarded *Post-Probe* session (Figure 3.3); second, in the sleep/rest phase preceding learning (*Pre-Sleep*), α correlated with learning speed (Figure 3.8). Other scaling exponents examined did not predict task performance (Figure 3.4). To my knowledge, this is the first study connecting hippocampal activity's critical scaling exponents with spatial memory performance.

This result complements very recent findings linking non-Gaussian scaling dynamics in the mouse visual cortex to visual recognition task performance (Cambrainha et al. 2025). The study also noted varying scaling dynamics between the active and passive task phases, indicating that scaling may modulate task engagement. However, the scaling dynamics observed during the task may depend on other factors such as input statistics and dopaminergic reward signaling (Dommett et al. 2005; Noudoost and Moore 2011; Mueller et al. 2020; Stalter, Westendorff, and Nieder 2020). Considering this, my result contributes to this line of research by offering prediction "in the future", from sleep/rest to subsequent learning or memory evaluation session.

By analyzing the scaling dynamics during *Post-Sleep*, I showed that the scaling of activity variance is related to the reactivation process (M. Wilson and B. McNaughton 1994; Dupret et al. 2010). I demonstrate that α and reactivation both independently account for variability in memory retention, even when controlling for each other. This finding indicates a complex interconnection between the scaling of activity variance and reactivation, which warrants further study. These results underscore the importance of activity scaling in the hippocampus and emphasize its functional role.

The results in this chapter extend the findings of Chapter 2, where I reported a different scaling of activity variance during sleep/rest versus wakefulness. Similarly, α influences learning and memory reactivation differently. An increase in α values during sleep/rest enhances learning speed and impairs memory retention. This contrast suggests different processing requirements of the sleeping/resting and awake hippocampus. During learning, the hippocampus quickly reconfigures and encodes new information (R. U. Muller and J. L. Kubie 1987; Quirk, R. U. Muller, and J. L. Kubie 1990; Bostock, Robert U. Muller, and John L. Kubie 1991; John O'Keefe and Burgess 1996). Networks with rapidly scaling activity variance may accelerate this process, although the exact mechanism remains unclear.

Since scaling under coarse-graining might result from simple processes (Mia C. Morrell, A. J. Sederberg, and Nemenman 2021), these results do not establish the necessity of (quasi-)criticality in the hippocampus for the consolidation of spatial memories. However, these results demonstrate the practical importance of scaling-exponents and their relation to the process of memory consolidation. This is especially relevant since the scaling exponent α provides predictive power beyond the reactivation and physiological properties of hippocampal

cells. Therefore, an analysis motivated by the brain criticality hypothesis has the potential to uncover functionally relevant aspects of brain activity that have not yet been extensively studied.

The hippocampus plays a pivotal role in memory consolidation during sleep, actively transferring learned information to the cortex (M. Wilson and B. McNaughton 1994; Louie and M. A. Wilson 2001; Lee and M. A. Wilson 2002; Joseph O'Neill et al. 2010). High α values may suggest more varied CA1 spatial representations, resulting in a noisier input for downstream cortical areas. Conversely, a larger α, representing more correlated cells, may indicate inadequate differentiation in hippocampal representations, which presents challenges for cortical processing. Smaller α values could imply more orthogonal CA1 representations, which could facilitate downstream decoding. This hypothesis requires separate investigation.

Through my investigation, I found that the scaling of activity variance is correlated with variability in cells' characteristic timescales and their tendencies for extreme (both low and high) levels of bursting. This reveals that the scaling of activity variance can indicate network configuration. Specifically, high α values indicate networks with cell populations having diverse operating timescales and mixtures of non-bursty and very bursty cells. Interestingly, these configurations also predict memory retention performance and potentially affect spatial representations or the attractor landscape.

Notably, both scaling and functional heterogeneity offer coding-agnostic perspectives on hippocampal activity that elucidate internal operational regimes and reflect computational principles. The opposing effects of the scaling of activity variance on learning and memory consolidation suggest that the hippocampus balances between two extremes ($\alpha = 1$ and $\alpha = 2$) in order to support both processes. The correlation between memory retention and measures of functional heterogeneity, only during sleep/rest after learning, indicates the network flexibility and relevance of non-average cells for learning adaptations. Meanwhile, the relationship between the scaling of activity variance and functional heterogeneity of the cell population during post-learning sleep/rest indicates that activity scaling facilitates and governs this adaptation. Collectively, these findings underscore the importance of both dynamics close to criticality and functional heterogeneity for the functioning of the hippocampus.

CHAPTER 4

Functional heterogeneity and CA1-mEC encoding dynamics

Abstract

In the prevailing view, the hippocampus acquires short-term memories that are later transferred to the cortex for long-term storage, during the memory consolidation process. However, the details of this process, in particular, the transfer of task-specific information, are still not fully understood. To expand the existing understanding, I investigated the process of memory acquisition and the consolidation process between the CA1 hippocampus and the mEC. In the experiments, rats performed a goal-directed spatial learning task that allowed me to focus only on activity around the goals. During learning, CA1 cells shifted their firing field towards the goals, while mEC cells remained mostly stable, shifting their firing fields towards the goals during sleep/rest that followed learning. This shift during sleep/rest was supported by the reactivation process, which occurred in two ways, synchronously with CA1 (during SWRs) and independently of the hippocampal SWRs. Both types of reactivation predicted subsequent memory retention, as well as the amount of goal-related remapping. Using statistical modeling, I gained insight into the temporal interactions of these two reactivation processes. For the acquisition of goal-related firing in mEC cells, SWRs were more important in the beginning of sleep/rest and independent reactivation at the end of the sleep/rest period. This suggests a model in which SWRs perform information transfer from CA1 to mEC, until mEC acquires relevant encoding and begins to reactivate autonomously. Finally, the day-to-day variability of the distribution of the cell characteristic timescales correlated with the goal-related remapping, in CA1 during the learning session and in mEC during sleep/rest. These results suggest that in spatial navigation tasks, the distribution of cells' characteristic timescales represents a network configuration that corresponds to the state of information acquisition.

Introduction

I finished the previous chapter showing the relationship between the functional diversity of hippocampal cells and memory consolidation. However, the learning part of the task was less investigated because sleep/rest was the main focus of that investigation. It also did not consider another brain area involved in spatial navigation, the medial entorhinal cortex (mEC).

The mEC is closely connected to the hippocampus, acting as both an input via the trisynaptic and perforant pathways, while also receiving direct CA1 output (Osanai, Nair, and Kitamura 2023; Hernández-Frausto and Vivar 2024). Functionally, both areas are similar in the sense that their cells exhibit spatial tuning, although with substantial differences. Hippocampal place cells activate within distinct place fields in specific environments (Edvard I Moser, M.-B. Moser, and Bruce L McNaughton 2017). In contrast, mEC grid cells display multiple firing fields in systematic hexagonal patterns that cover all environments (Hafting et al. 2005), likely providing an invariant metric for spatial cognition (Edvard I. Moser and M.-B. Moser 2008). Beyond spatial selectivity, activity in both CA1 and mEC undergoes replay (Lee and M. A. Wilson 2002; J. O'Neill et al. 2017), complementing the current view under which the hippocampus establishes new memories before transferring them to the cortex. In addition, spatial coding in both areas is modulated by rewards (Boccara et al. 2019; Butler, Hardcastle, and Giocomo 2019), further indicating the importance of both areas in goal-directed navigation.

However, the dynamic interaction between CA1 and mEC in the memory encoding and consolidation processes, along with its underlying mechanisms, is still not sufficiently understood. Moreover, given the findings in section 3.4, the relationship between functional heterogeneity and CA1-mEC encoding dynamics becomes a subject for further investigation. To investigate these, I examined a different set of thirteen recordings (Boccara et al. 2019) compared to the previous two chapters (although five sessions analyzed in Chapter 3 are the same as here). In this dataset, CA1 and mEC activity was recorded simultaneously from rats while they performed the same cheeseboard task. This protocol allowed me to investigate the temporal dynamics of goal-related spatial memory encoding in CA1 and mEC during both learning and sleep/rest.

4.1 Differential functional heterogeneity during learning and sleep/rest

I resumed my investigation from the previous chapter by exploring functional heterogeneity among CA1 (purple) and mEC (green) cells during learning and sleep/rest. My analysis focused on the characteristic timescale τ (Figure 4.1 A, B). Observing the histograms of τ (Figure 4.1 C, D), I noted a bimodal distribution during learning, while sleep/rest presented a singular, strong peak. I quantified this using Sarle's bimodality coefficient (Figure 4.1 E, Methods). Additionally, the quartile coefficient of dispersion (QCD) of these distributions revealed a different spread between sleep/rest and learning (Figure 4.1 F $p < 0.01$ for both CA1 and mEC, Wilcoxon signed-rank test). This highlights that the functional configuration of the network in both CA1 and mEC depends on the brain state.

Continuing the train of thought from Section 3.4 and the discussion in the previous Chapter, I propose that distributions of cells' characteristic timescales represent network configurations that reflect information acquisition. In particular, during Post-Sleep, mEC shows more varied distributions of characteristic timescales τ compared to CA1 (distinct QCD, $p < 0.01$, Wilcoxon Signed-rank test, Figure 4.1 F). Could this indicate different operational modes in these regions at various stages of the experiment? Given that CA1 is involved in learning and memory consolidation, while mEC shows a similar configuration later during sleep/rest, could this suggest that the coding in CA1 and mEC evolves differently? In the remainder of the chapter, I explore this in more detail.

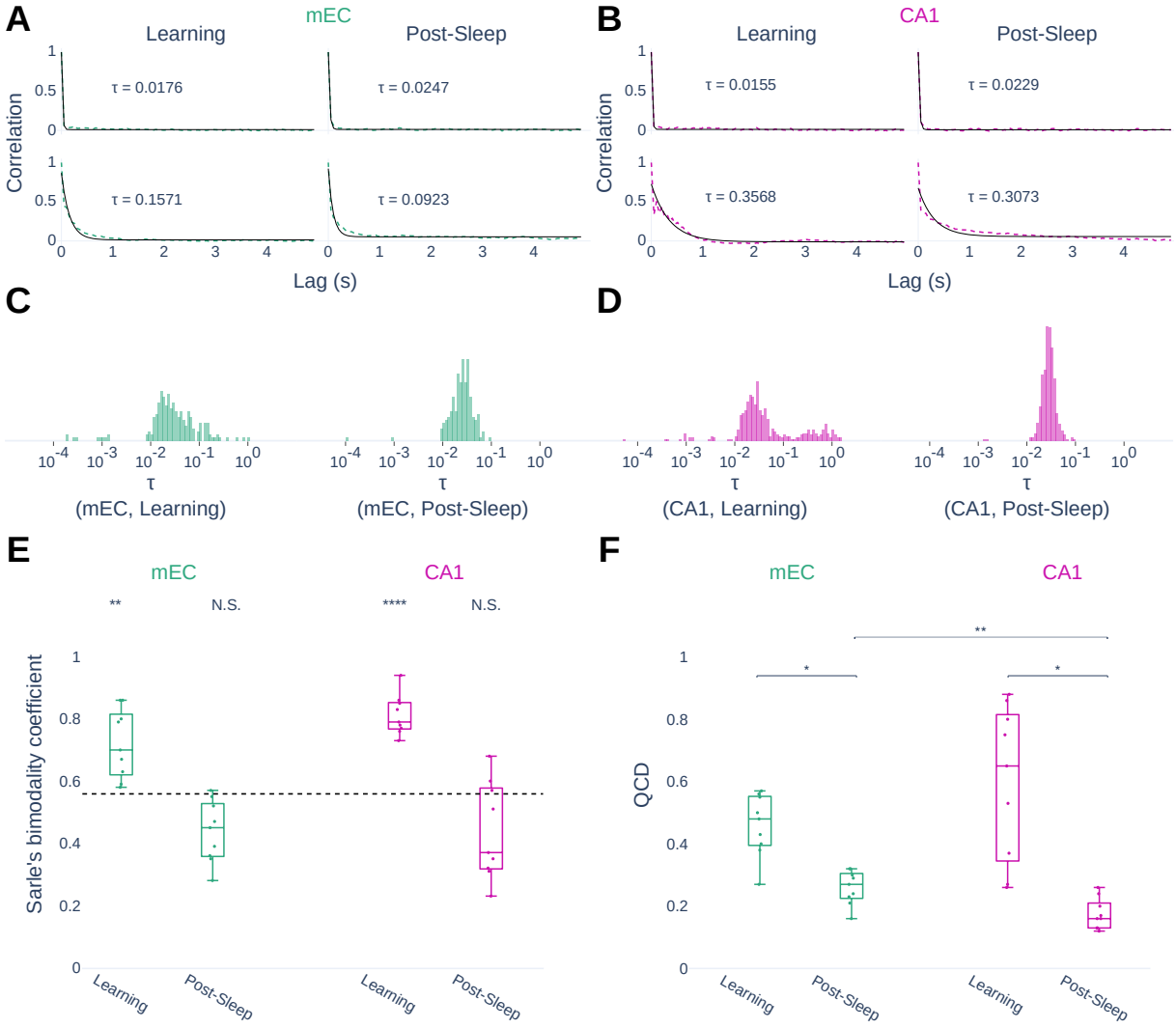

Figure 4.1: *Distribution of characteristic timescales during learning and Post-Sleep.*
A - example autocorrelation function of four different mEC cells, during *Learning* (left) and *Post-Sleep* (right), black lines represent exponential fit, **B** - same as A but for CA1 cells, during *Learning* (left) and *Post-Sleep* (right), **C** - histogram of characteristic timescale τ of mEC cells, during *Learning* (left) and *Post-Sleep* (right), **D** - histogram of characteristic timescale τ of CA1 cells, during *Learning* (left) and *Post-Sleep* (right), **E** - Sarle's bimodality coefficient of τ distribution in mEC (green) and CA1 (purple), dashed line indicates value of Sarle's coefficient for uniform distribution ($\frac{5}{9}$), **F** - Quartile coefficient of dispersion of τ distribution in mEC (green) and CA1 (purple). Each box on panels **E** and **F** spans from the first quartile to the third quartile, the median is marked by a line inside the box, the whiskers correspond to the box' edges $\pm$ 1.5 times the interquartile range (each group compared against 5/9, 1-sample t-test, $N.S.\ p > 10$, $**\ p < 0.01$, $****\ p < 0.0001$.

4.2 Online goal-oriented remapping in CA1, offline goal-oriented remapping in mEC

I investigated the evolution of goal-related remapping of individual cells, as has been observed both in CA1 and in mEC (Boccara et al. 2019; Butler, Hardcastle, and Giocomo 2019). I quantified it using a "goal-related remapping score," which represents a normalized firing rate within goal zones (Methods, Boccara et al. 2019). This score allows me to assess goal-related remapping with fine temporal resolution, offering insights into goal-related coding dynamics. Figure 4.2 A illustrates the temporal dynamics of goal-related remapping alongside relative performance increases. In CA1, rapid goal-oriented remapping occurs during learning (Figure 4.2 A, middle), matching the total goal-related remapping observed throughout a recording day (Figure 4.2 E and Supplementary Figure S.7 C). In contrast, in mEC, the goal-related remapping remains minimal during learning (Figure 4.2 A, C and Supplementary Figure S.7 D), and it is lower than the total remapping observed between *Pre-Probe* and *Post-Probe* (Figure 4.2 F). The goal-related remapping between the first and last learning block ("during learning", each learning block comprises five trials) was greater in CA1 than in mEC (Figure 4.2 B). In contrast, from the end of learning to *Post-Probe* ("during *Post-Sleep*"), mEC exhibited higher goal-related remapping than CA1 (Figure 4.2 C).

After the initial learning phase and during *Post-Probe*, the animal trajectories are biased towards the goals, implying that the observed effect might result from an increased time spent in the goal zones. I controlled for that by measuring the goal-related remapping in data that was randomly downsampled using two strategies. In the first strategy, I aimed for uniform occupancy within the session by randomly downsampling trajectories ("within," details in Methods). This method produced results that were qualitatively similar to those on the original data (Figure 4.2 G, H). In the second strategy ("across", Methods), I randomly downsampled trajectories to match the occupancy between two sessions (*Pre-Probe* and *Post-Probe*, and the first and last learning blocks). This approach also yielded qualitatively similar results to those on the original data (Supplementary Figure S.7 A, B).

Finally, I observed that the dynamics of learning performance are correlated with the dynamics of goal-related remapping in CA1, but not with those in mEC (Figure 4.2 D). This observation confirms that online goal-related coding is task-relevant, with CA1 functioning as an online learner, while mEC provides representations that, with respect to goals, change marginally during learning.

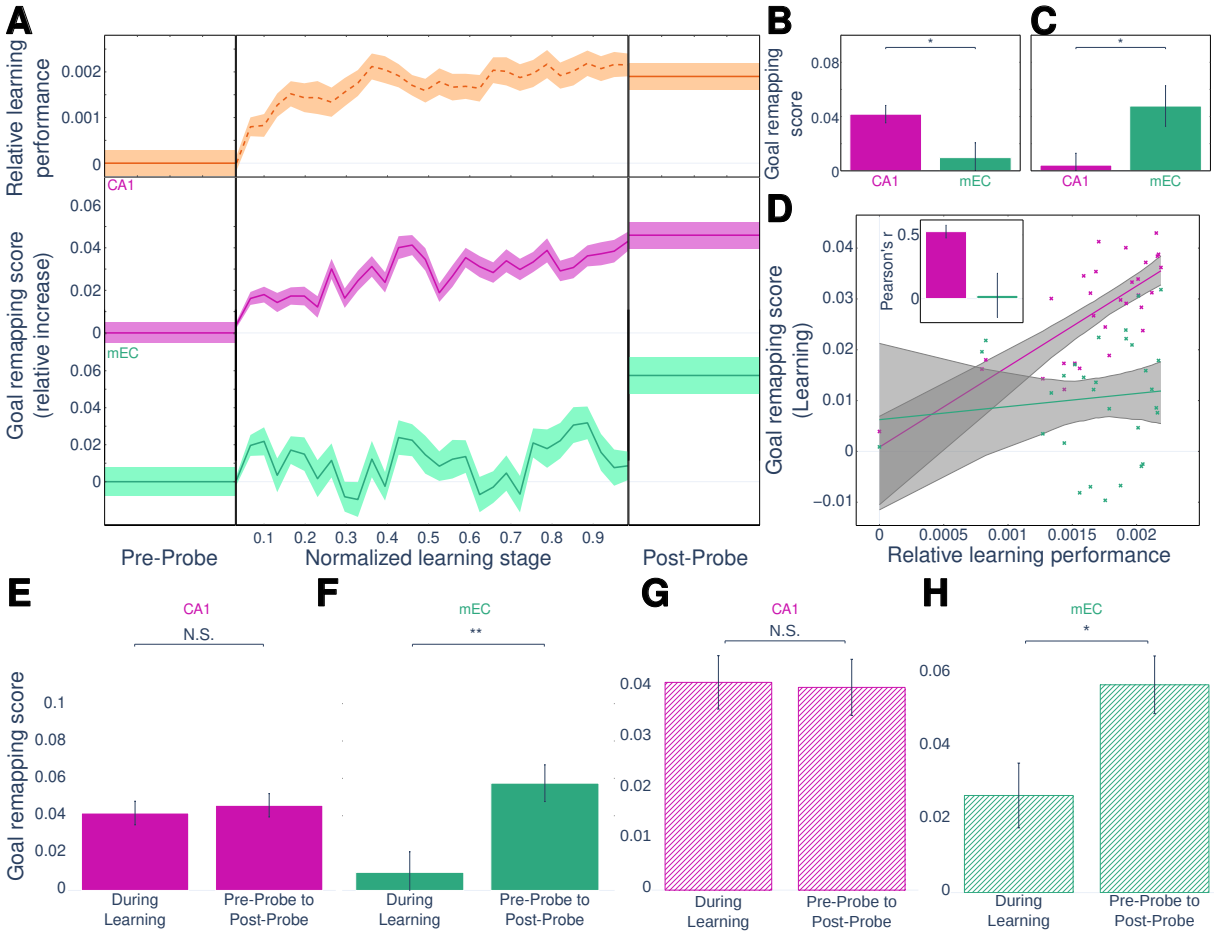

Figure 4.2: *Goal-related remapping in the CA1 and mEC.*

A - top: performance increase, middle: goal-related remapping in CA1, bottom: goal-related remapping in mEC, all three curves are normalized relative to the first learning block, or relative to *Pre-Probe*, **B** - goal-related remapping between the beginning and end of learning ("During learning"), in CA1 (purple) and mEC (green) ($p = 0.0277$, Mann-Whitney U rank test), **C** - goal-related remapping from the end of learning to *Post-Probe* ("during *Post-Sleep*") in CA1 (purple) and mEC (green) ($p = 0.0189$, Mann-Whitney U rank test), **D** - goal-related remapping versus performance increase, each point is one learning block, averaged across all recording days (CA1: $R = 0.743$, $CI = [0.548, 0.871]$, mEC: $R = 0.103$, $CI = [-0.246, 0.378]$, not significant), inset shows Pearson r for individual recording days, **E** - goal-related remapping score in CA1 during learning and from *Pre-Probe* to *Post-Probe* ($p > 0.1$, Wilcoxon signed-rank test), **F** - goal-related remapping score in mEC during learning and from *Pre-Probe* to *Post-Probe* ($p < 0.0001$, Wilcoxon signed-rank test), **G** - goal-related remapping score in CA1 during learning and from *Pre-Probe* to *Post-Probe* on data subsampled using "within" strategy ($p > 0.1$, Wilcoxon signed-rank test, details in Methods), **H** - goal-related remapping score in mEC during learning and from *Pre-Probe* to *Post-Probe* on data subsampled using "within" strategy ($p < 0.05$, Wilcoxon signed-rank test, details in Methods)

4.3 Offline reactivation in mEC supports spatial memory consolidation

Having established that CA1 and mEC modify their codes in different behavioral states, CA1 during learning and mEC during sleep/rest, I explored the potential mechanism for this adjustment in mEC. Hippocampal reactivation plays a vital role in memory consolidation (M. Wilson and B. McNaughton 1994; Girardeau, Benchenane, et al. 2009; Ego-Stengel and M. A. Wilson 2009) and is believed to facilitate the transfer of memories to other cortical areas. Therefore, I investigated the reactivation of the *Post-Probe* map using the same method described in section 3.2 (Figure 4.3). First, in CA1, I observed reactivation during the SWR periods (Figure 4.3 A). In line with the previous chapter and earlier studies (Dupret et al. 2010), this analysis showed that hippocampal reactivation during SWRs predicts memory retention performance during *Post-Probe* (Figure 4.3 B). Interestingly, I also observed a similar effect in mEC, its population activity during SWRs reflected the learned goals (Figure 4.3 C), and the reactivation rate in mEC predicted spatial memory retention on *Post-Probe* (Figure 4.3 D). For both areas, the reactivation analysis on *Pre-Sleep* did not produce a significant correlation with memory retention (Supplementary figure S.8 A, B). This shows a synchronous reactivation between CA1 and mEC. To investigate this synchrony further, I calculated the SWR-mEC coupling by measuring the cross-correlation between SWR power and mEC multi-unit activity. In *Post-Sleep*, SWRs with mEC reactivation were more strongly coupled to mEC than those with only CA1 reactivation (Figure 4.3 E). During *Pre-Sleep* (see Supplementary figure S.8 D), I did not observe the same phenomena, suggesting that learning might trigger synchronized reactivation. Furthermore, I measured similarity between the PVs near the goals and the activity of the population during SWRs (in both cases temporal bins were $102.4ms$ long). The similarity in mEC peaked after the similarity in CA1 (Figure 4.3 F), indicating the potential flow of information from CA1 to mEC during SWRs.

However, mEC can replay independently from the hippocampus (J. O'Neill et al. 2017). Therefore, I isolated high synchrony events (HSE, Methods) in mEC that did not overlap with hippocampal SWRs. During independent HSEs, the activity of the mEC resembled that of goal zones (Figure 4.4 A), and the reactivation rate predicted memory retention (Figure 4.4 B) on *Post-Probe*. However, the reactivation analysis on *Pre-Sleep* did not produce a significant correlation with memory retention (Supplementary figure S.8 C). This suggests that mEC reactivation also occurs independently of the hippocampus, supporting memory consolidation.

With two independent mechanisms of reactivation streams in mEC, a question arises about their role in goal-related remapping in mEC during sleep/rest after learning. To investigate this, I developed a model that predicts single-cell goal-related remapping score during *Post-Sleep* using as input the increase of cell's firing rate during goal reactivation events relative to the firing outside of reactivation (Figure 4.4 C, Methods). I built two models: one on data from the beginning of sleep (first 40%) and another on data from the end of sleep/rest (last 40%). Both models predicted goal-related remapping better than chance, but the model trained on end-of-sleep data performed better (Figure 4.4 D, E, F). As a control, models trained on periods between two reactivating events did not perform better than chance (Supplementary Figure S.8 E). To delve deeper, I analyzed the weights each model assigned to SWR-related reactivation and independent reactivation (Figure 4.4 G). At the beginning of *Post-Sleep*, SWR-related reactivation was more important than mEC reactivation, whereas by the end of *Post-Sleep*, independent reactivation became more dominant and crucial for goal-related remapping. This result shows that memory transfer involves complex temporal dynamics,

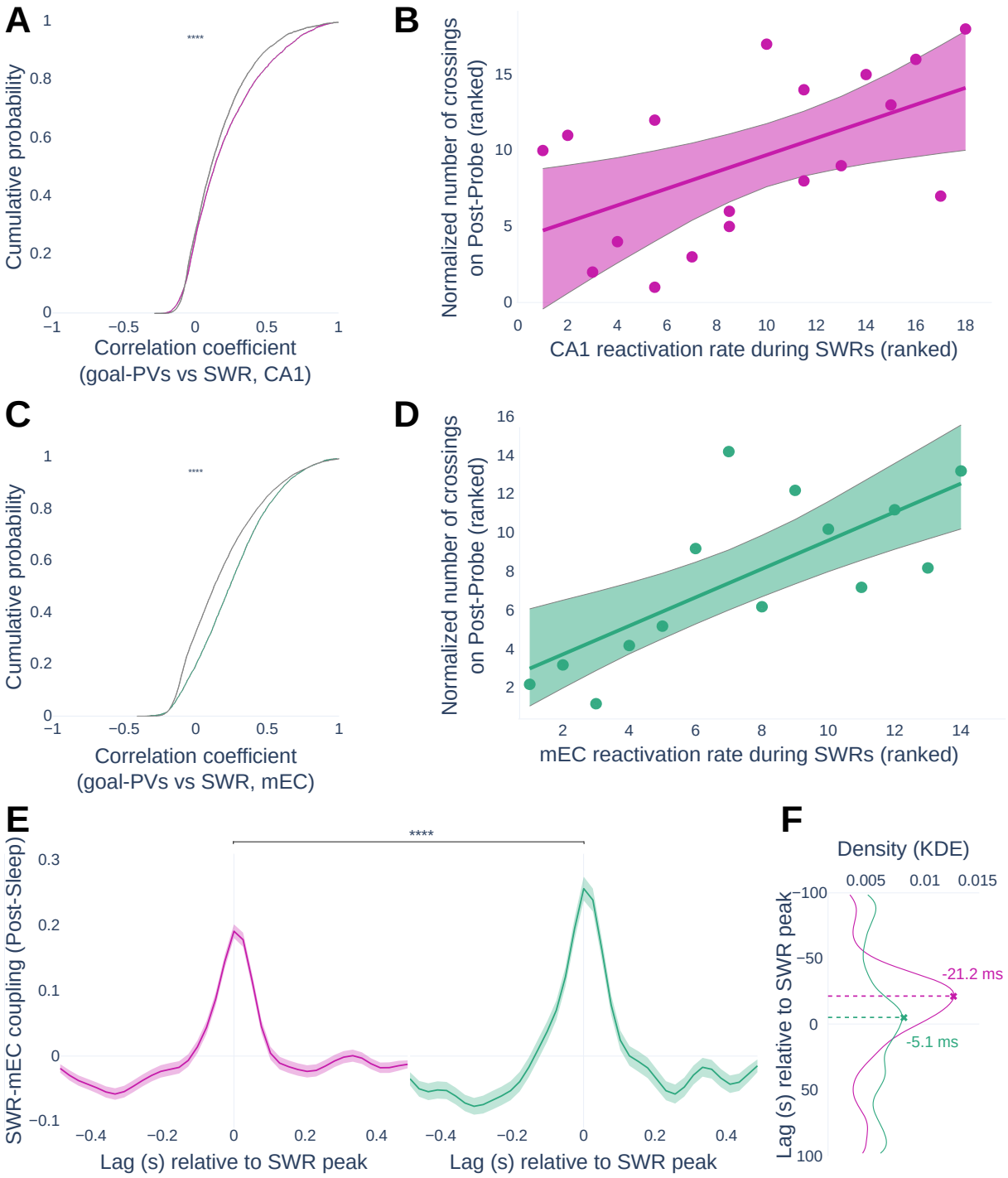

Figure 4.3: *Reactivation during SWRs in CA1 and mEC.*
A - CDF of Pearson correlation scores between PVs around goals and activity during SWRs, in CA1, shuffled distribution in grey ($p < 0.0001$), **B** - rank correlation between CA1 reactivation rate during SWRs and normalized number of goal crossings ($R = 0.53$, $CI = [0.173, 0.822]$]), **C** - CDF of Pearson correlation scores between PVs around goals and activity during SWRs, in mEC, shuffled distribution in grey ($p < 0.0001$), **D** - rank correlation between mEC reactivation rate during SWRs and normalized number of goal crossings ($R = 0.733$, $CI = [0.39, 0.933]$), **E** - SWR-mEC coupling score in *Post-Sleep* during SWRs in which CA1 reactivated (left, purple) and during SWRs in which (mEC reactivated (right, green) ($p < 0.0001$, Fisher transformation and t-test), **F** - kernel density estimation of peak similarity between goal zone PVs and SWR activity during *Post-Sleep*, dashed lines indicate time of the peak relative to SWR peak power (CA1 in purple, mEC in green).

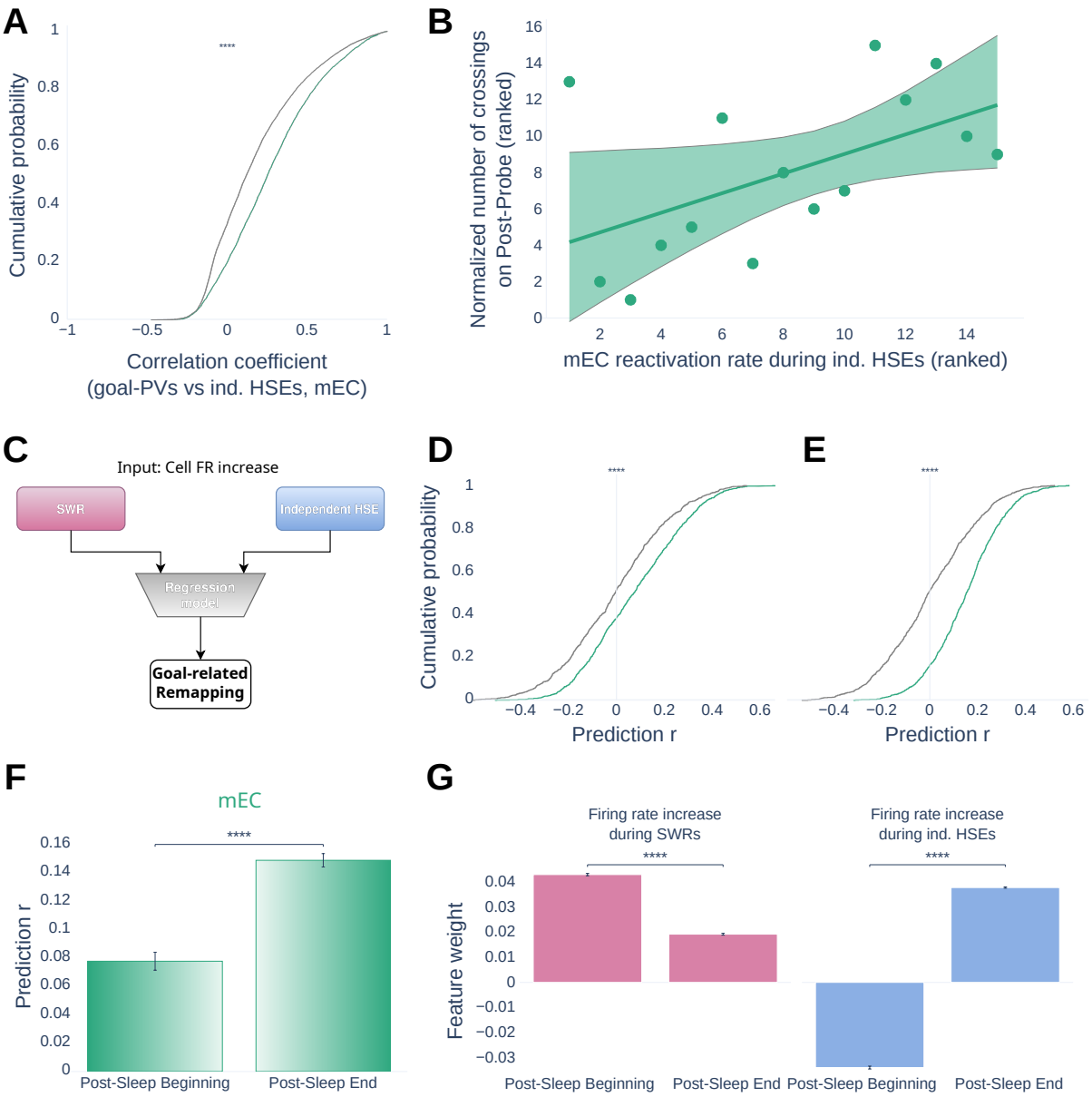

Figure 4.4: *Goal-related remapping in the CA1 and mEC.*

A - CDF of Pearson correlation scores between PVs around goals and activity during independent HSEs in mEC, shuffled distribution in grey ($p < 0.0001$), **B** - rank correlation between mEC reactivation rate during independent HSEs and normalized number of goal crossings ($R = 0.516$, $CI = [0.015, 0.883]$), **C** - illustration of the model that predicts goal-related remapping per cell from firing during reactivation events, **D** - CDF of cross-validated prediction score of a model trained on the beginning of *Post-Sleep*, gray line indicates CDF of prediction score on shuffled data, **E** - CDF of cross-validated prediction score of a model trained on the end of *Post-Sleep*, gray line indicates CDF of prediction score on shuffled data, **F** - comparison of cross-validated prediction score between models ($p < 0.0001$), **G** - weights assigned to each feature in both models ($p < 0.0001$ in both cases).

where hippocampal reactivation initiates the process, before mEC takes over and consolidates autonomously.

4.4 Distribution of characteristic timescale correlates with goal-related remapping

At the beginning of the chapter, I demonstrated that the distribution of characteristic timescales among cells depends on the state of the brain and hypothesized that it might resemble a network configuration (Figure 4.1). If the former is the case, the encoding dynamics of each area should be related to the distribution of population timescales. During learning, the excess kurtosis of the timescale distribution in CA1 correlated with goal-related remapping in CA1 (Figure 4.5 B), but not in mEC (Figure 4.5 D). In contrast, during *Post-Sleep*, excess kurtosis of the mEC timescale distribution correlated with the mEC goal-related remapping during *Post-Sleep* (Figure 4.5 A), unlike in *Pre-Sleep* (Supplementary figure S.8 F) or in CA1 during *Post-Sleep* (Figure 4.5 E). Notably, these relationships are the result of the learning process, as the pre-learning session measures did not show a correlation with the goal-related remapping (Supplementary figure S.8 F, G). The correlation between the extent of remapping and the tendency of cells to exhibit slow/fast decay of autocorrelation time highlights the importance of this trait for coding and functioning in CA1 and mEC, supporting the findings in section 3.4.

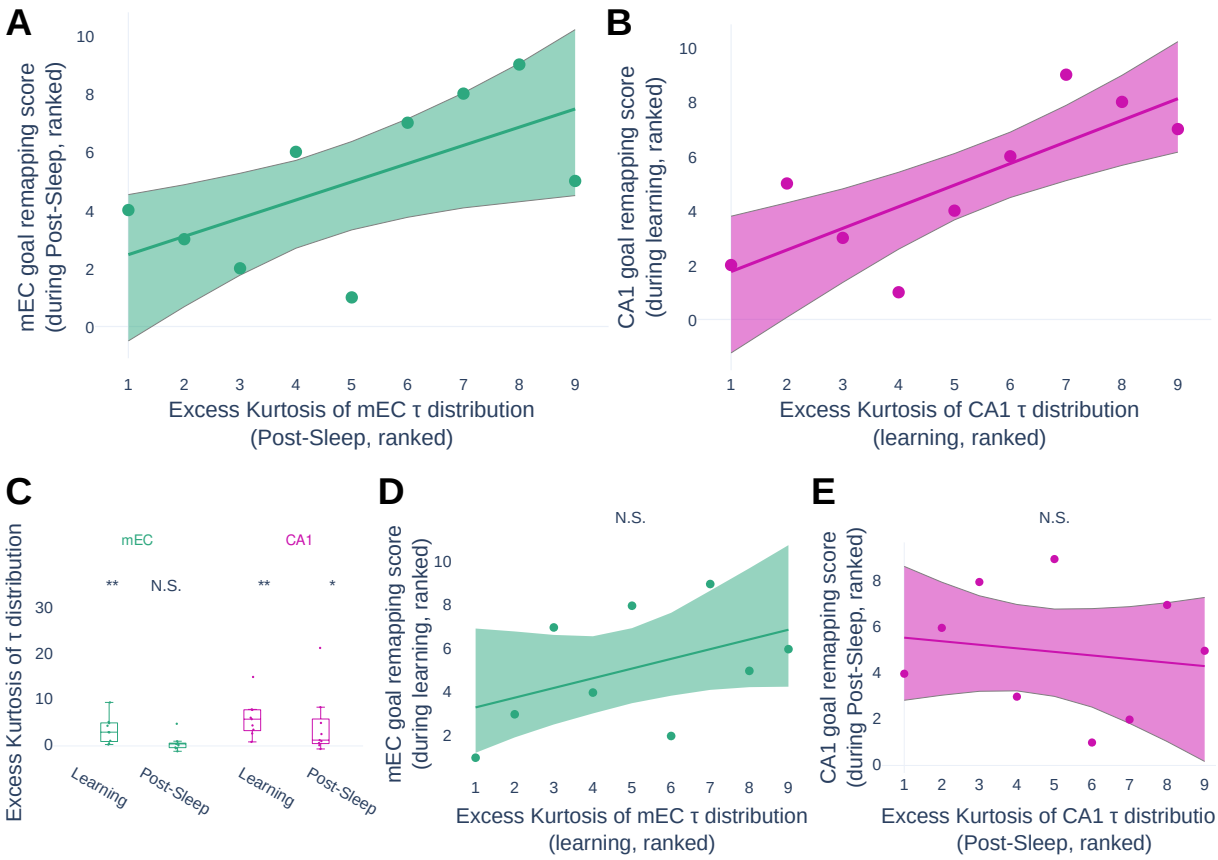

Figure 4.5: *Distribution of characteristic timescales and goal-related remapping.*
A - correlation between the excess kurtosis of the distribution of τ and goal-related remapping in mEC during *Post-Sleep* ($R = 0.591$, $CI = [0.177, 0.957]$), **B** - correlation between the excess kurtosis of the distribution of τ and goal-related remapping in CA1 during learning ($R = 0.773$, $CI = [0.478, 0.952]$), **C** - excess kurtosis of the distribution of τ ($p < 0.01$ during learning in both CA1 and mEC, $p < 0.05$ during *Post-Sleep* in CA1, $p > 0.1$ in mEC during *Post-Sleep*, 1-sample t-test), **D** - non-significant correlation between the excess kurtosis of the distribution of τ and goal-related remapping in mEC during learning ($R = 0.438$, $CI = [-0.194, 0.868]$), **E** - non-significant correlation between the excess kurtosis of the distribution of τ and goal-related remapping in CA1 during *Post-Sleep* ($R = -0.121$, $CI = [-0.659, 0.427]$)

4.5 Discussion

I started this chapter by showing state-dependent changes in functional heterogeneity among CA1 and mEC cells. This was reflected in the shift of the distribution of characteristic timescales of cells from bimodal during learning to unimodal during sleep/rest. Since, in addition to brain state, these changes may be a consequence of different operating regimes during the two phases of the task, I next investigated the coding dynamics of CA1 and mEC.

I assessed the different dynamics of the encoding between CA1 and mEC through goal-related remapping. During learning, CA1 pyramidal cells reorganized their preferred firing fields and shifted towards goals, concurrently with improved learning performance. In contrast, the firing of the pyramidal cells of mEC remained relatively stable during learning and was not modulated by the goals. The *Post-Probe* revealed a different remapping dynamics that occurred during sleep/rest that follows learning: the preferred firing fields of mEC cells shifted closer to the goals (Boccara et al. 2019). On the other hand, CA1 pyramidal cells maintained a goal-related firing similar to that at the end of learning. These observations indicate the online acquisition

of spatial representation in the hippocampus CA1, and offline coding adaptation in mEC. As such, this result supports two-stage memory theories, stating that long-term memory formation involves hippocampal-cortical representation transfer (Marr 1971; G. Buzsáki 1989; Larry R Squire and Alvarez 1995; Frankland and Bontempi 2005; Larry R. Squire et al. 2015; Diekelmann and Born 2010; Klinzing, Niethard, and Born 2019).

Furthermore, I explored reactivation as a potential mechanism responsible for memory transfer. During post-learning sleep/rest, CA1 and mEC reactivated synchronously during SWRs, and this reactivation predicted memory retention levels. This finding underlies the crucial role of the CA1-mEC dialog in spatial memory consolidation, providing additional evidence for the significance of SWR-related reactivation (Buzsaki et al. 1992; György Buzsáki 2015; Klinzing, Niethard, and Born 2019; Girardeau and Lopes-dos-Santos 2021).

In addition, similar to J. O'Neill et al. 2017, I identified high synchrony periods in mEC where reactivation functions independently of the hippocampus. I observed that independent mEC reactivation during sleep/rest after learning also correlated with enhanced memory retention on *Post-Probe*. This novel finding suggests that the mEC network autonomously contributes to memory consolidation and that mEC function extends beyond merely relaying spatial information to the hippocampus.

I also examined interactions between the two reactivation pathways and how they support memory transfer from CA1 to mEC. At the onset of sleep/rest, SWR-related mEC reactivation primarily drove goal-related remapping in mEC. By the end of this period, independent mEC reactivation outweighed SWR-related reactivation in importance. The finding suggests that the mEC gradually acquires goal-related information with support from both the hippocampus and the local circuit. Early in the consolidation phase, novel goal-related coding is sourced from the hippocampus until the local mEC circuits restructure sufficiently and start to independently reactivate newly acquired representations. Independent mEC reactivation, may be part of a broad process that spans multiple regions of the brain, and may be supported by local cortical recurrent circuits (Zutshi et al. 2018; Zheng et al. 2024; Douglas, Koch, et al. 1995; Douglas and Martin 2007; Shin et al. 2025) in a manner similar to recurrent pattern completion in the neocortex (Peron et al. 2020; Shin et al. 2025) and pattern separation (Zheng et al. 2024).

The scaling of hippocampal activity variance, as detailed in Chapter 3, may directly affect the process discussed above. This is because the scaling exponent α might be related to the stability of hippocampal representations (Section 3.5). Additionally, stable CA1 representations during initial consolidation likely benefit the transfer of goal-related information from CA1 to mEC. With a 30-minute sleep/rest session in this data set, these results do not conflict with the CA1 representation drift seen over longer periods (Bollmann et al. 2025). Two plausible explanations are: goal-related hippocampal information endures despite drift, or hippocampal offline reorganization occurs after the initial memory consolidation phase. Confirming exact details requires *in vivo* manipulation of both synchronized CA1-mEC and independent mEC reactivation.

Finally, I demonstrated how functional heterogeneity, reflected through evolving distribution of characteristic cell timescales, was related to goal-related remapping in both CA1 and mEC. For the former, the propensity for slow/fast decaying cells was correlated with goal-related remapping during learning. For the latter, the excess kurtosis of the distribution of characteristic timescales correlated with goal-related remapping during *Post-Sleep*. This suggests that to acquire new representations, both networks could benefit from shared global traits, indicating that the distribution of the characteristic cell timescale might be viewed as a (incomplete) network configuration.

The qualitatively similar relationship between functional heterogeneity and goal-related remapping in CA1 and mEC suggests that, for the brain region forming new representations, learning and consolidation might not be fundamentally different. When the hippocampus, during the learning session of the task, reorganizes its code relative to the target locations, it does so by integrating input and reward signals from other areas of the brain and performing online reactivation (Jadhav et al. 2012). As mEC serves as one of the major inputs to hippocampal formation, potentially providing an internal metric for space (Edvard I. Moser and M.-B. Moser 2008), rapid alterations in its code during online states would likely be detrimental to the hippocampus, and hence, the mEC code remains mostly stable during learning and adapts during sleep/rest. This adaptation occurs in a way similar to the online adaptation in the hippocampus. In sleep/rest after learning, mEC acquires goal-related information by processing hippocampal inputs during SWRs, and by performing autonomous reactivation. In this view, the hippocampus might function as a student during learning and as a teacher during sleep/rest, as reflected in the different dynamics with respect to criticality (Chapter 2). At the same time, mEC can be viewed as a guiding post during learning and as a student during sleep/rest.

CHAPTER 5

Conclusion and outlook

In my thesis, I investigated the process of memory storage and consolidation between the hippocampus and other cortical areas. However, I approached this topic from the point of view of brain dynamics in relation to criticality, while in the process relating my main results to functional heterogeneity with CA1 and mEC. Here, I summarize a few novel insights and open questions that resulted from this research project.

5.1 Summary of results

In Chapter 2, I employed methodologies informed by the principles of statistical physics to investigate the dynamics of the hippocampus. For the analysis, I used an existing dataset (Bollmann et al. 2025) consisting of very long extracellular recordings from rat dorsal CA1 during both sleep and awake state. To begin with, I took the "avalanche criticality" approach, detected neuronal avalanches (Beggs and Plenz 2003; Beggs and Plenz 2004) and studied their properties in awake and sleep/rest. The most interesting results of the avalanche analysis can be summarized in two measures, the estimated distance to criticality (DCC, Ma et al. 2019) and the exponent Σ (Marshall et al. 2016; Friedman et al. 2012) that optimally collapses the avalanche shapes. During wakefulness DCC was higher than during sleep/rest, indicating a dynamics that is further from criticality, similarly to the recent report from the neocortex (Xu et al. 2024). The exponent Σ was also higher during the awake state compared to sleep/rest, revealing differences in the evolution and propagation of activity in these two states. Next, I assessed the criticality by analyzing coarse-grained activity within the framework of the Phenomenological Renormalization Group (Meshulam et al. 2019). This allowed me to observe hippocampal activity from different scales and to identify scale-free features of hippocampal activity. Here, also, two values were particularly interesting: the scaling exponent of activity variance α and the scaling exponent of autocorrelation time z. The scaling exponent α was higher during sleep/rest than during awake, indicating different scaling dynamics between these two states and conceptually aligned with the differences observed in avalanche criticality. The scaling exponent z correlated during sleep/rest with the exponent Σ indicating the intimate relation between the propagation of activity in the network and the scaling of characteristic timescales. These results confirm the existence of signatures of dynamics similar to criticality and the dependence of these signatures on the state of the brain. Brain state-dependent differences in critical dynamics may reflect functionally different roles

assumed by the hippocampus during wakefulness and sleep/rest and provide the foundation for the next chapter of the thesis.

In Chapter 3, I continued the work on criticality and investigated the relationship between the scaling of hippocampal activity and memory performance. I used the Phenomenological Renormalization Group (Meshulam et al. 2019) method as in the Section 2.2. The results revealed that of the four scaling exponents that I analyzed, spatial memory performance was predicted only by α, the scaling exponent of activity variance (Morales, Santo, and Muñoz 2023). It predicted performance in two ways: first, α measured during the sleep/rest session after learning correlated with memory retention during the unrewarded testing session, second, α measured in the sleep/rest phase that preceded learning correlated with learning speed. Moreover, in sleep after learning, I conducted a reactivation analysis and demonstrated that the exponent α predicts performance even when reactivation frequency is taken into account. This finding established the importance of variance scaling for memory consolidation and confirmed that it provides a functionally meaningful perspective when analyzing the activity of the hippocampus. Next, I analyzed the diversity of functional properties of neurons in the hippocampus CA1. For each cell, I estimated the characteristic timescale, based on the cell's autocorrelation function. For pyramidal cells, I measured their burstiness as a fraction of inter spike intervals shorter than $6ms$. When I analyzed the distributions of these features within the CA1 population, I observed significant day-to-day variability. Then I observed that the scaling exponent α was correlated with kurtosis and dispersion of these distributions, showing that the scaling of activity variance is related to the functional diversity of the underlying population of cells. Interestingly, these measures also predicted memory retention, demonstrating the importance of functional heterogeneity for the functioning of the hippocampus and brain-wide memory consolidation. The finding that the diversity of cell burstiness is related to memory retention may reflect the importance of synaptic plasticity. The correlation between timescale distributions and memory performance is an experimental confirmation of the idea that timescale diversity among computational units determines learning performance learning and memory (Perez-Nieves et al. 2021; Kurikawa 2025), and agrees with previous studies linking this property to working memory (Wasmuht et al. 2018; Sean E Cavanagh et al. 2016; Sean E. Cavanagh, Hunt, and Kennerley 2020). The distributions of burstiness and characteristic timescales can be interpreted as a "network configuration" assumed by the CA1 while performing specific behavioral functions.

In Chapter 4, I investigated the memory acquisition and consolidation process by analyzing activity in the hippocampus CA1 and the median entorhinal cortex (mEC) during the learning phase and during sleep/rest that followed learning. During learning, the hippocampus cells shift their firing field towards the goals and this shift is correlated with learning performance. At the same time, the spatial tuning of the mEC cells remained mostly stable. Yet, mEC cells also exhibit a shift towards goals (Boccara et al. 2019; Butler, Hardcastle, and Giocomo 2019), however, this shift in mEC occurred during sleep/rest that followed learning. This observation indicated that the hippocampus acquires novel task-relevant information during the behavioral phase, while mEC acquires similar information offline after learning. Since sleep/rest after learning is important for memory consolidation (Klinzing, Niethard, and Born 2019), primarily through reactivation, I next investigated this process. During sharp wave-ripples (SWR), in both CA1 and mEC, I observed reactivation of the goal zones. The rate of reactivation of each goal correlated with the memory retention of that particular goal, measured as the number of crossings of the goal zone. During SWRs that reactivated in mEC, the coupling between mEC and CA1 was significant and stronger than during SWRs that reactivated only in CA1. Next, I found mEC reactivation independent of CA1, during high-synchrony events

in mEC that did not co-occur with hippocampal SWRs. The rate of this reactivation also correlated with memory retention. Then I investigated how mEC reactivation contributes to goal-related remapping, which, in mEC, occurs during sleep after learning. I observed that at the beginning of sleep/rest, SWR-associated reactivation drove goal-related remapping, while at the end of sleep independent reactivation in mEC contributed more. These findings suggest that at the beginning of a consolidation period, CA1 leads the memory transfer to mEC until, after a certain amount of time, mEC acquires enough new information and starts to reactivate independently. All of the results so far suggest that, in spatial navigation tasks, the functional responsibilities of CA1 and mEC change between learning and sleep/rest. During learning, mEC provides robust navigational code, while CA1 performs rapid acquisition of task-related variables, possibly as a result of reward-related signaling. Afterwards, during sleep/rest after learning, with it already encoded representations, CA1 serves as a source of task-related information that is transferred to mEC. With this in mind, I once again analyzed the "network configuration", expressed through the functional properties of CA1 and mEC cells. During learning, the variability of the distribution of cell timescales in CA1 correlated with the goal-related remapping in CA1. In mEC, I observed the same type of correlation during sleep after learning. These two observations suggest that, for the brain region that acquires new information, learning and consolidation might not be conceptually different processes. Both processes involve the formation of representations that represent entities relevant for the underlying task, which in both cases benefits from increased functional heterogeneity among cells.

5.2 Open questions

The results from all chapters jointly expanded our understanding of criticality dynamics and memory consolidation, but also opened several novel questions with potential for new research projects. Few of these questions are specific and meant to expand and round up the currently presented results, but there are also common larger themes that can be investigated more broadly.

To discuss more specific open questions, I start with the results reported in Chapter 2. According to my results, during sleep/rest, the hippocampus operates close to the critical point; however, sleep is a brain state with diverse dynamics and it is likely that sleep stages have different dynamics in relation to criticality. Therefore, in terms of criticality, it is worth to compare REM and slow-wave sleep (SWS), as they are very different in terms of associated brain activity and primary functions (Klinzing, Niethard, and Born 2019). Furthermore, this line of analysis can help to better understand the coexistence of avalanches and oscillations. Oscillatory activity during REM is dominated by theta rhythm, while during slow-wave sleep is dominated by slow oscillations and delta. At the same time, there is a computational framework (Lombardi, Pepić, et al. 2023) that binds oscillations and avalanches using an Ising model with added external negative feedback. Models similar to those may help investigate computational motifs necessary to reproduce avalanches and oscillations of the hippocampus during sleep, while producing alternating periods of REM and SWS. This type of analysis has the potential to deepen our understanding of the interplay of endogenous and exogenous factors that guide activity in the hippocampus. From the functional side, REM and SWS have opposing roles in representation drift (Bollmann et al. 2025) and are involved in synaptic scaling (Puentes-Mestril and Aton 2017; Klinzing, Niethard, and Born 2019). Thus, analyzing scale-free activity in the sleep stages can provide novel links between self-organized criticality

and synaptic properties of neural networks (A. Levina, J. M. Herrmann, and T. Geisel 2007; Anna Levina, J. Michael Herrmann, and Theo Geisel 2009).

Next, the differences in activity propagation between wakefulness and sleep/rest, as evident through the different values of the exponent Σ and different avalanche shapes (which must be quantified), are interesting on its own for further investigation. Although this may be a consequence of (lack of) locomotion, it may reflect different operational modes of the hippocampus. To support the latter, the correlation between the exponent Σ that optimally collapses the avalanche shapes and the scaling exponent z was observed only during sleep/rest and not during wakefulness. This might indicate differences in the underlying dynamics that are intimately related to the operating timescales of the hippocampal population. In addition, the activity of inhibitory interneurons should be investigated as they have a role in the regulation of network activity and it is known that their manipulation can be used to tune the network away from criticality (Shew, Yang, Yu, et al. 2011; J. Li and Shew 2020). I have some preliminary data with optogenetic manipulation of interneurons which, in the future, I may use to analyze how interneurons regulate the propagation of network activity across different scales.

Predicting memory retention, as reported in Chapter 3, is interesting because the scaling of activity variance and functional heterogeneity among cells are quantities that do not consider cells' spatial tuning. Thus, they represent a coding-agnostic snapshot of hippocampal activity that reflects internal operational regimes and can be understood as a sort of network configuration. However, thinking of a network configuration only in terms of individual cell properties is incomplete, as it does not consider the interaction between cells, which shape collective neural activity (Schneidman et al. 2006). Consequently, to dive deeper into this line of reasoning, it is essential to examine interactions between cells with variable functional characteristics, and especially between interneurons and pyramidal cells. The simplest way is to start from a pairwise correlation matrix and observe if the correlation between cells depends on the properties of each participating pair. Observing changes in network configuration, from the session before to the session of the acquisition of novel representations, can provide additional insights into this domain. Ultimately, an analysis in the described direction can provide additional insight into the properties of the network that are desirable for different functional roles that brain areas can assume (Panzeri et al. 2022). Furthermore, relating this type of analysis to spatial tuning of individual cells can give us a unique peak at cell assemblies and expand our understanding of them.

Looking at the coding properties of hippocampal cells is the next natural step in analyzing the functional benefits of activity scaling. I have speculated that the scaling exponent α may reflect the stability and discriminability of the hippocampus assemblies. This would mean that particular values of α are more beneficial for downstream areas that have to "acquire" memories from the hippocampus. Thus, I intend to try and relate α to the place coding properties of hippocampal cells, as well as to the coding specificity and discriminability of cell assemblies. Moreover, since lower values of α during sleep/rest after learning lead to better memory retention, and lower α implies weaker correlation between cells, α may be related to orthogonality in hippocampal representations (Malvache et al. 2016). In general, this line of investigation can lead to a better understanding of coding related to the scaling of hippocampal activity and potentially provide a connection between criticality and the efficient coding hypothesis (Denève and Machens 2016; Safavi et al. 2024).

Next, α correlates with functional heterogeneity measures and predicts memory retention even when controlled for functional heterogeneity. This opens the question whether scale-free activity is a principle that enables networks to develop the observed structure (Hesse and Gross

2014). Thus, investigating how to reproduce scale-free activity (e.g., particular values of the exponent α) using modern modeling approaches, such as simulation-based inference (Cranmer, Brehmer, and Louppe 2020), can help us better understand the connections between scaling and functional heterogeneity among the cell population. Complementarily, similar methodology of investigation can provide an insight into the benefits of scaling for reaching a particular attractor state (e.g. whether a particular scaling regime leads to faster convergence), thereby linking criticality to theoretical models of memory, while being based on experimental data.

The results in Section 4.3 suggest that the memory transfer between CA1 and mEC is a process that, at its initial stage, depends on the hippocampus and that after mEC acquires novel representation "well enough" it takes over the reactivation process. Experimental manipulation during reactivation periods is necessary to confirm the implied causalities of these results. The first step would be to optogenetically inhibit reactivation during SWRs in CA1 and mEC separately and observe the effects on mEC goal-related remapping and memory retention. The expectations are that the disruption of CA1 would impair both synchronous and independent reactivation in mEC, and consequently the goal-related remapping of mEC cells. Similarly, disrupting mEC reactivation during SWRs is expected to impair hippocampus-independent mEC reactivation along with goal-related remapping. Disruption of SWR-related reactivation in both areas should affect memory retention (demonstrated for CA1 (Girardeau, Benchenane, et al. 2009; Ego-Stengel and M. A. Wilson 2009; Gridchyn et al. 2020), but not for mEC). On the other hand, it is not straightforward to formulate the exact expectation from the disruption of independent reactivation in mEC. There are several possible effects that have to be analyzed, ranging from (possibly) partial disturbance of goal-related coding in mEC to unclear consequences on memory retention.

The next open question that arises from the results in Chapter 4 is related to the organization of memory transfer. This question has a few important aspects. First, what is the amount of synchronous reactivation that is necessary for the appearance of independent reactivation in mEC? This is something for which SWR disruption can provide insight and can be further investigated with careful modeling. Next, since mEC reactivates only in a fraction of all SWRs, how does it "decide" when and what to reactivate? Do roles assumed by each cell depend on the cell's characteristic timescale? Since there are inhibitory projections between mEC and CA1, do interneurons play a role in the process of memory consolidation? Maybe they serve as "a gate" and help decide the content of synchronous reactivation in mEC?

Notably, in Chapter 4, I investigated the effects of reactivation on memory consolidation on a relatively short timescale only. The mechanism and importance of this process over multiple days or weeks are not understood and require novel studies with a longer recordings spanning several days or weeks.

5.3 Broad research themes

Finally, there are common and broad themes that emerged from my research that I find interesting enough for future work. Scale-free activity has been observed across species and brain areas (Morales, Santo, and Muñoz 2023; Munn et al. 2024). Similarly, cells across brain regions exhibit a wide range of genetic (Yao et al. 2021), anatomical (Soltesz and Losonczy 2018; Cembrowski and Spruston 2019), and functional (Wasmuht et al. 2018; Perez-Nieves et al. 2021; Mainali, Azeredo da Silveira, and Burak 2025; Cohen and Drugowitsch n.d.) heterogeneity. All of these areas of the brain have distinct functional characteristics and perform a variety of functions. Therefore, a few broad questions emerge. What are possible

functions and computations that can be performed by scale-free heterogeneous networks? What local principles enable the emergence of specific information processing capabilities in such networks? How can these properties be utilized when dealing with brain disorders or when developing artificial information processing systems? One way to investigate these is to decide on a brain region and observe its configuration and activity under multiple conditions in which the chosen brain region exhibits different physiological or functional characteristics. Analyzing developmental stages, characterized by complex neuron migration and specialization processes, provides snapshots of different circuit architectures, each exhibiting its own patterns of neural activity. To do this, lineage tracing techniques (Chen, Liao, and Peng 2022) can be used to attach calcium or voltage indicators to cells belonging to specific groups. This would allow *in vivo* functional imaging of their activity, in different stages of development and behavioral conditions. Furthermore, a genetic perturbation of the network can be achieved by basing the same framework on methods that allow simultaneous labeling and gene knockout (Zong et al. 2005). An approach like this would allow functional imaging of a network in different architectural conditions, each condition with its own functional characteristics. Afterward, methods from network science (Peel, Peixoto, and De Domenico 2022; Barabási et al. 2023; Srivastava et al. 2022) and large scale modeling (Cranmer, Brehmer, and Louppe 2020) can be used to connect the functional configuration of brain circuits to their operation. This type of research can expand our understanding of the computations that are possible in complex networks and the principles that enable them. This knowledge can then be used in dealing with brain disorders, or transferred to non-biological systems, such as brain implants or novel machine learning techniques.

APPENDIX S

Supplementary materials

S.1 Supplementary figures related to Chapter 2

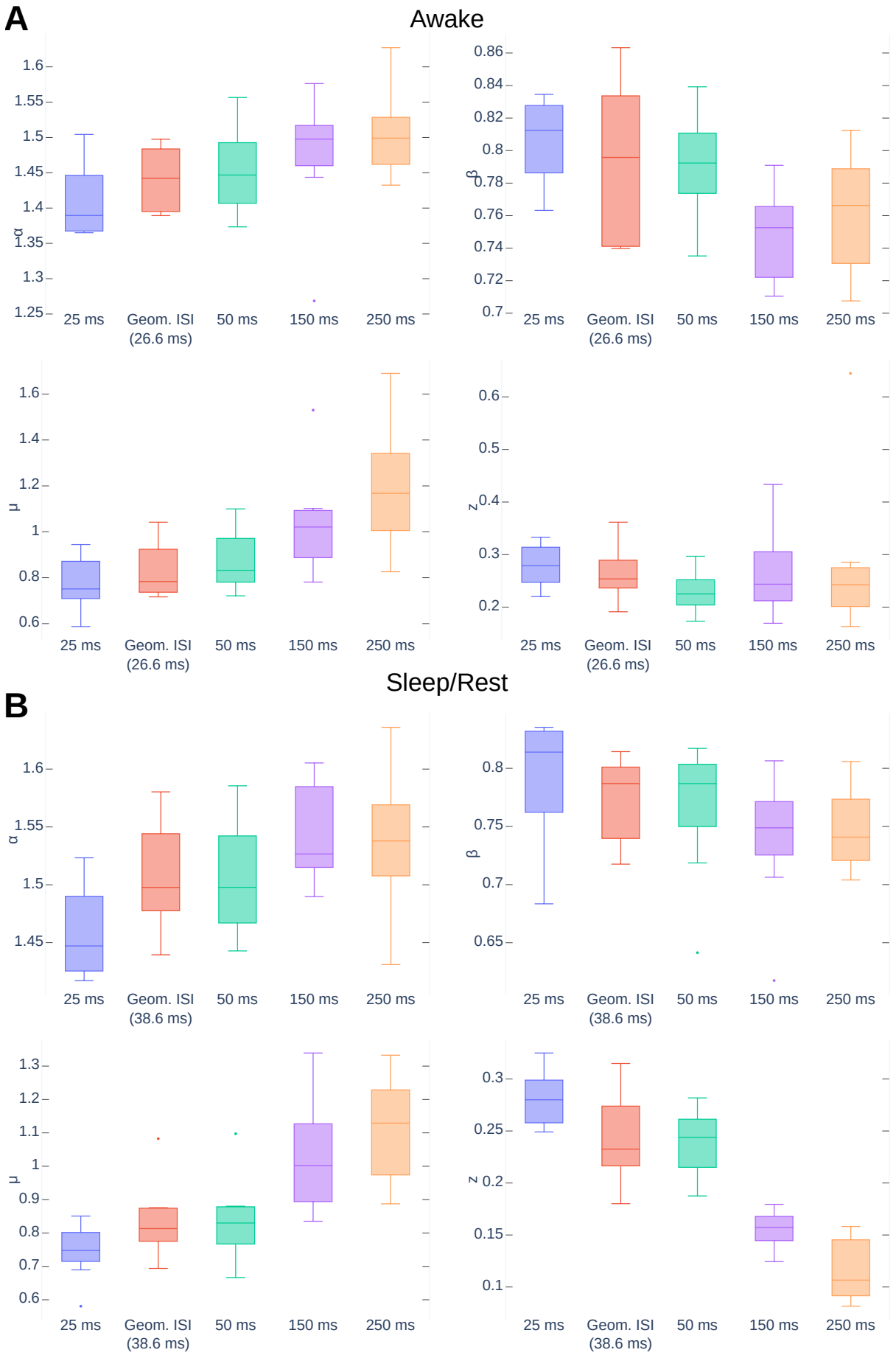

Figure S.1: *PRG exponents for different duration of temporal bins.*

A - in wakefulness, **B** - in sleep/rest. Boxes span from the first quartile to the third quartile, the median is marked by a line inside the box, the whiskers correspond to the box' edges $\pm$ 1.5 times the interquartile range.

S.2 Supplementary figures related to Chapter 3

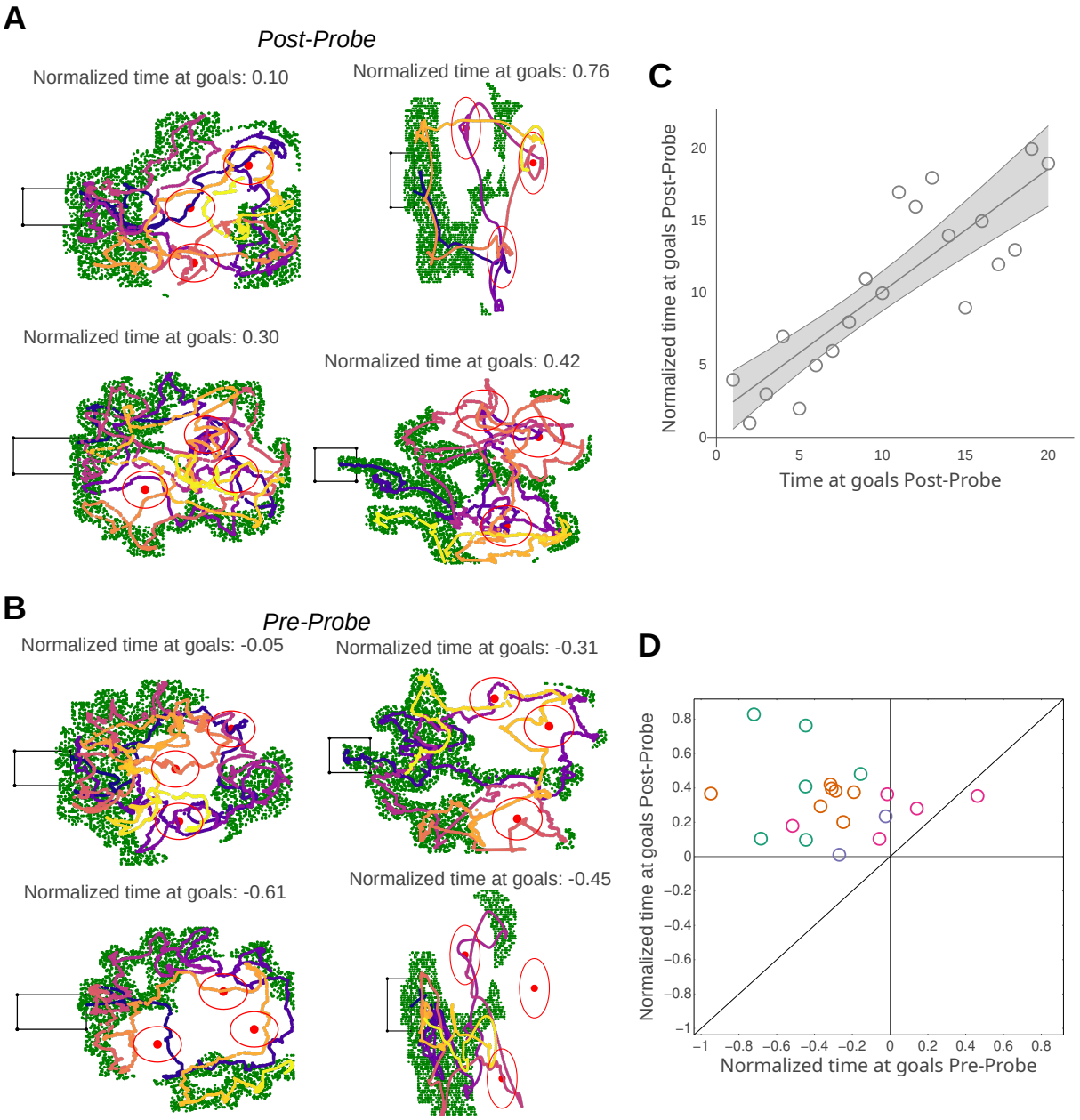

Figure S.2: *Memory retention performance.*

A - example trajectories on *Post-Probe*, red circles denote goal zones, green dots denote randomly sampled goal locations. **B** - example trajectories on *Pre-Probe*, red circles denote goal zones, green dots denote randomly sampled goal locations. **C** - correlation between time around goals and normalized time around goals ($R = 0.846$, $CI = [0.7, 0.936]$ **D** - normalized time around goals during *Post-Probe* vs during *Pre-Probe*, diagonal line is identitiy, colors correspond to different experimenters (details in Table 1.1.

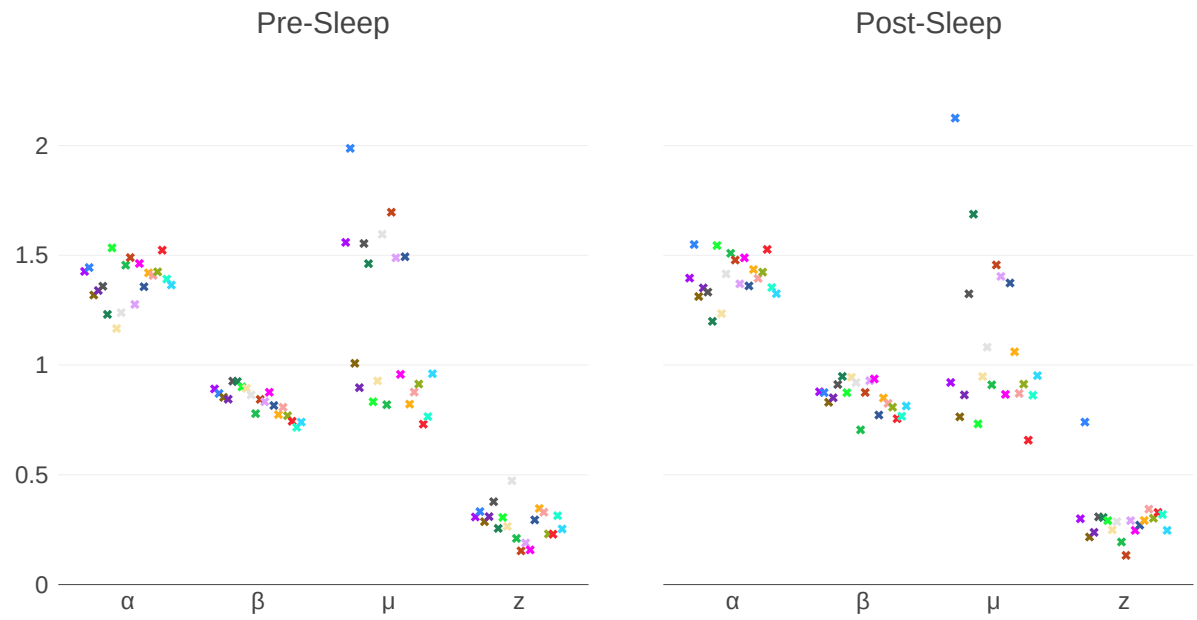

Figure S.3: *PRG scaling exponents.*
Scaling exponents in the Phenomenological Renormalization Group, in *Pre-Sleep* and *Post-Sleep*. Colors correspond to different recording days.

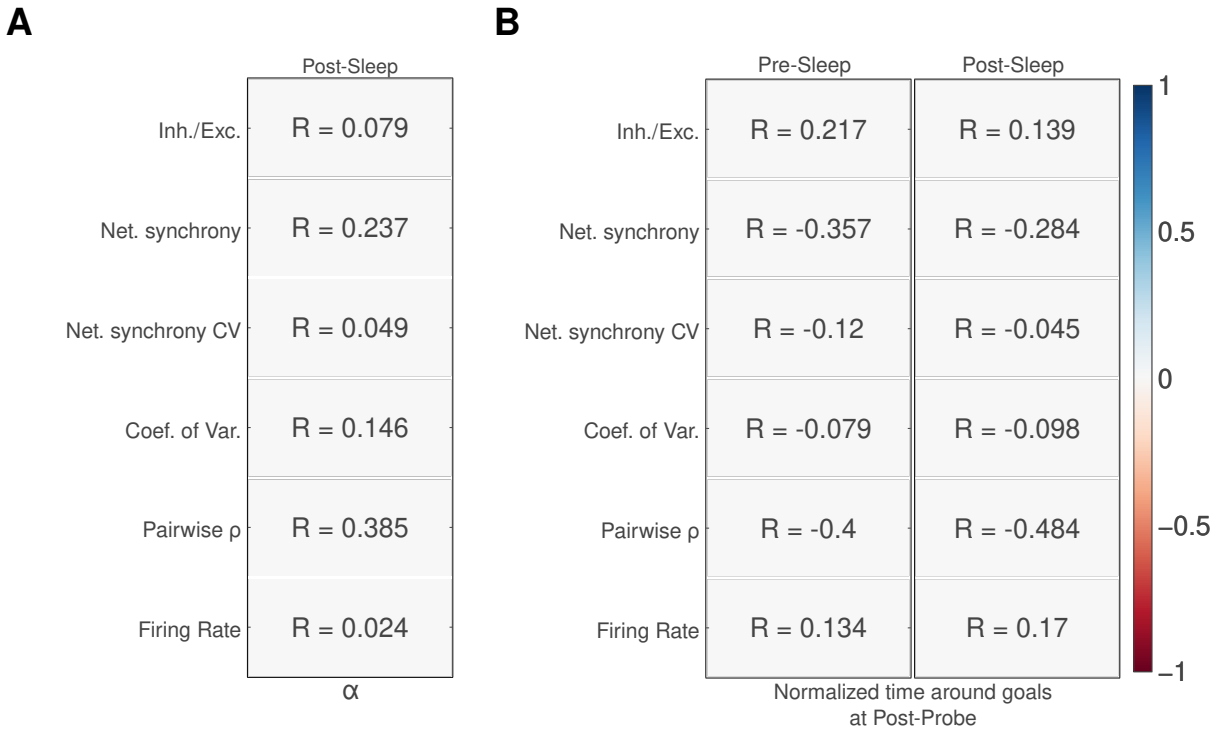

Figure S.4: *Scaling of activity variance and network activity measures.*
A - correlation coefficients between α and statistics of network activity, no correlations were significant, **A** - correlation coefficients between statistics of network activity and memory retention, no correlations were significant.

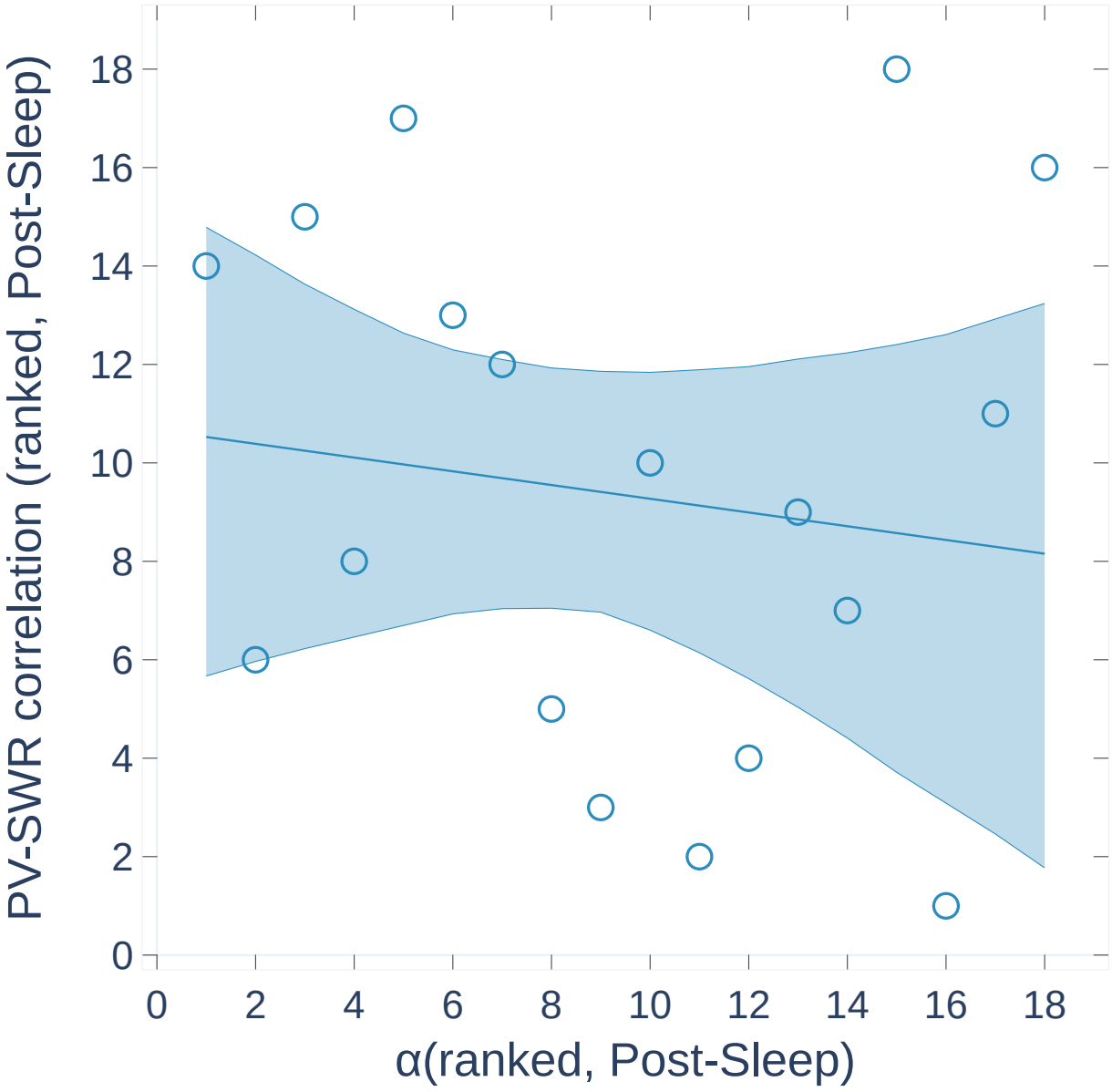

Figure S.5: *Scaling of activity variance does not correlate with reactivation quality.* non-significant correlation between α and PV-SWR reactivation quality ($R = -0.132$, $CI = [-0.641, 0.36]$).

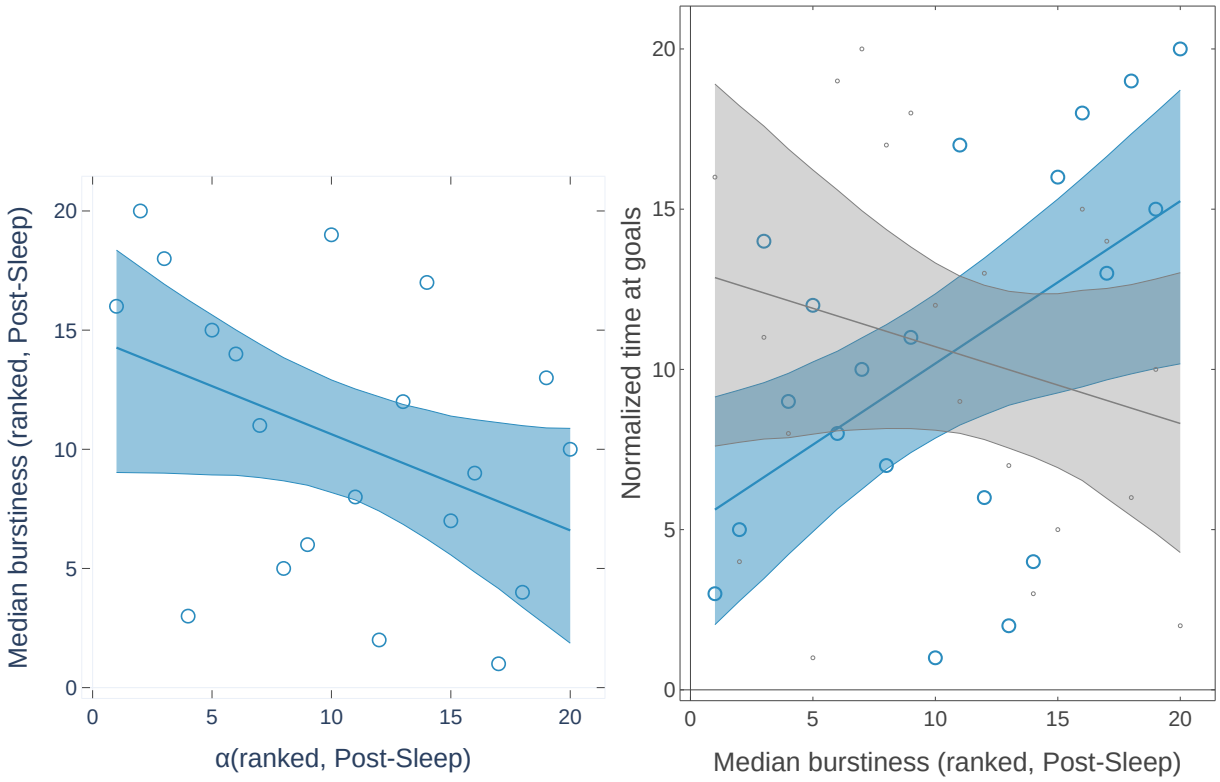

Figure S.6: *Scaling of activity variance vs median burstiness.*
A - α versus median burstiness of pyramidal cells ($R = -0.401, CI = [-0.737, 0.02]$), **B** - median burstiness of pyramidal cells versus normalized time around goals (*Post-Probe*: $R = 0.51\, CI = [-0.076, 0.869]$, *Pre-Probe*: $R = -0.235\, CI = [-0.769, 0.381]$).

S.3 Supplementary figures related to Chapter 4

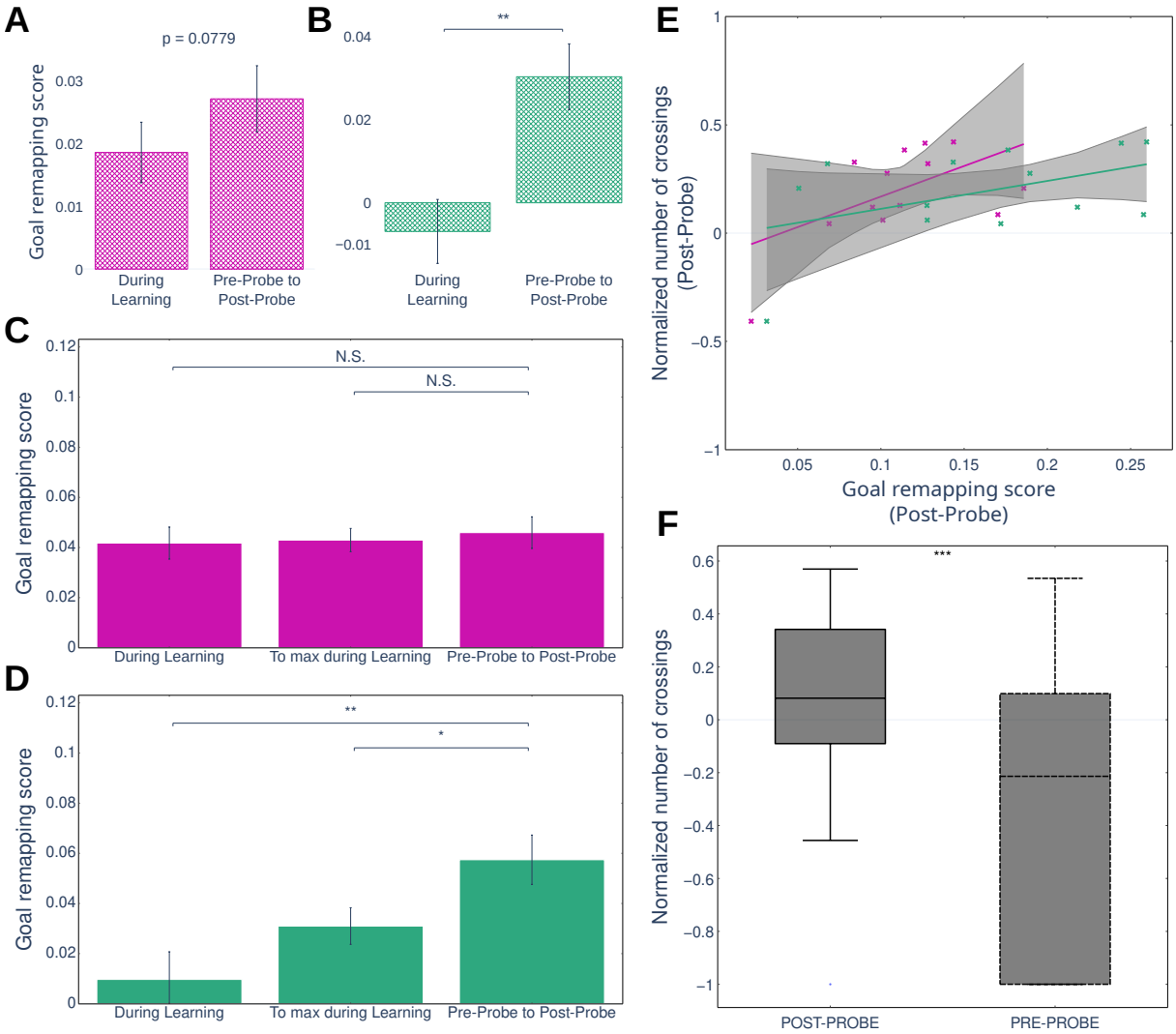

Figure S.7: *Goal-related remapping*.

A - goal-related remapping score in CA1 during learning and from *Pre-Probe* to *Post-Probe* on data subsampled using "across" strategy ($p = 0.0779$, Wilcoxon signed-rank test, details in Methods), **B** - goal-related remapping score in mEC during learning and from *Pre-Probe* to *Post-Probe* on data subsampled using "across" strategy ($p < 0.01$, Wilcoxon signed-rank test, details in Methods) **C** - goal-related remapping in CA1: between the beginning to end of learning ("During learning"), from the beginning of learning to maximum during learning, and from *Pre-Probe* to *Post-Probe* ($p > 0.1$, Wilcoxon signed-rank test), **D** - goal-related remapping in mEC: goal-related remapping between the beginning to end of learning ("During learning"), from the beginning of learning to maximum during learning, and from *Pre-Probe* to *Post-Probe* ($p > 0.1$, Wilcoxon signed-rank test), **E** - non-significant correlation between goal remapping score and normalized number of crossings, during *Post-Probe* ($R = 0.488$, $CI = [-0.309, 0.939]$ for CA1, $R = 0.408$, $CI = [-0.318, 0.825]$), **F** - normalized number of crossings in *Post-Probe* and in *Pre-Probe* ($p < 0.001$, Wilcoxon signed-rank test).

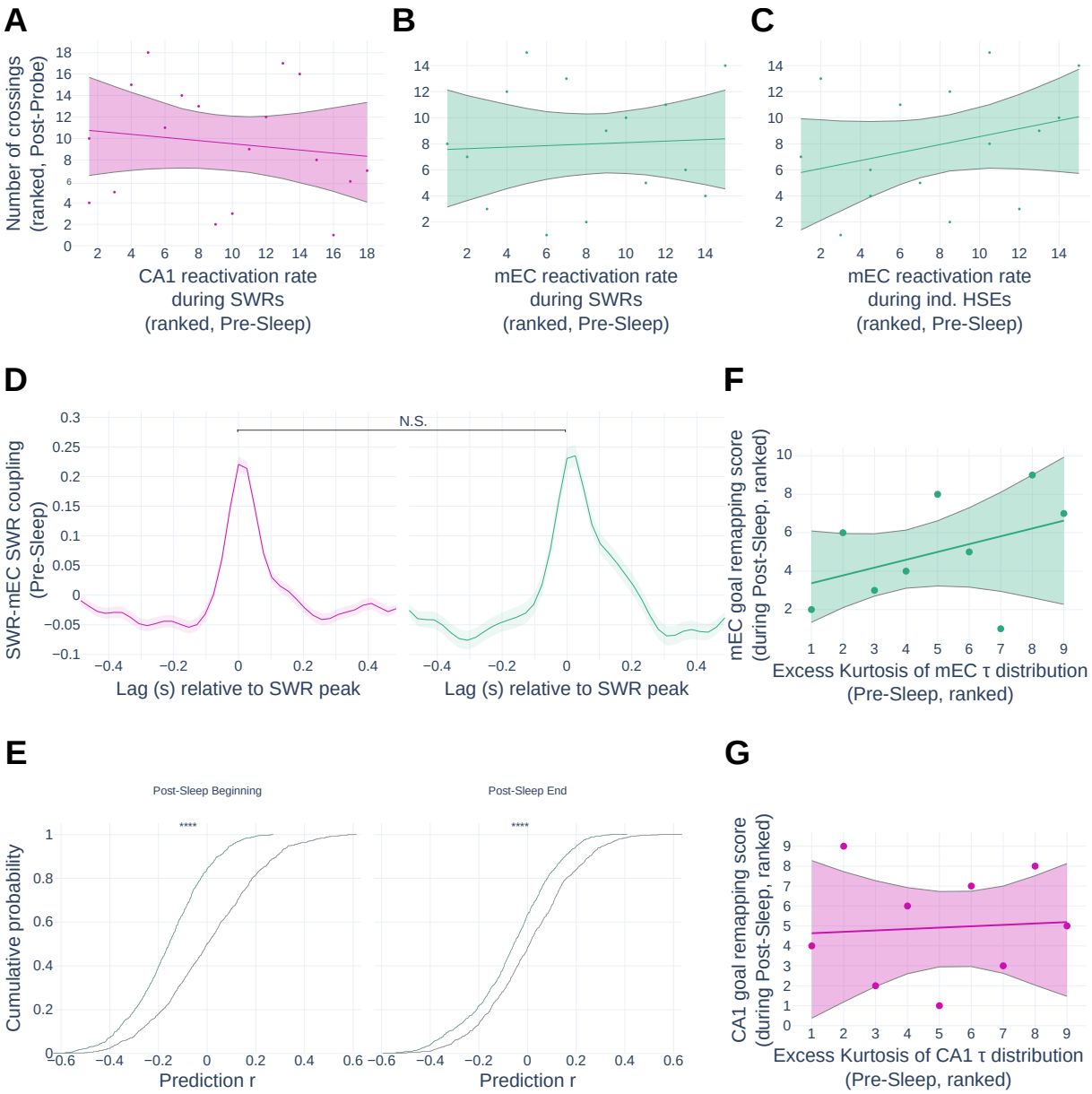

Figure S.8: *Reactivation and functional heterogeneity in CA1 and mEC.*

A - non-significant rank correlation between CA1 reactivation rate during SWRs on *Pre-Sleep* and normalized number of goal crossings on *Post-Probe* ($R = -0.142$, $CI = [-0.567, 0.318]$), **B** - non-significant rank correlation between mEC reactivation rate during SWRs on *Pre-Sleep* and normalized number of goal crossings on *Post-Probe* ($R = 0.06$, $CI = [-0.41, 0.518]$), **C** - non-significant rank correlation between mEC reactivation rate during independent HSEs on *Pre-Sleep* and normalized number of goal crossings on *Post-Probe* ($R = 0.299, CI = [-0.217, 0.709]$), **D** - SWR-mEC coupling score in *Pre-Sleep* during SWRs in which CA1 reactivated (left, purple) and during SWRs in which (mEC reactivated (right, green) ($p > 0.1$, Fisher transformation and t-test), **E** - CDF of cross-validated prediction score of a model whose input is firing rate increase during a period between two reactivation events, trained on the beginning of *Post-Sleep* (left) and the end of *Post-Sleep*, **F** - non-significant correlation between the excess kurtosis of the distribution of τ during *Pre-Sleep* and goal-related remapping in mEC during *Post-Sleep* ($R = 0.419$, $CI = [-0.315, 0.915]$), **G** - non-significant correlation between the excess kurtosis of the distribution of τ during *Pre-Sleep* and goal-related remapping in CA1 during *Post-Sleep* ($R = 0.079$, $CI = [-0.555, 0.686]$),

Bibliography

Adams, P. et al. (Dec. 2002). "The role of the thalamus in the flow of information to the cortex". In: *Philosophical Transactions of the Royal Society of London. Series B: Biological Sciences* 357.1428. Publisher: Royal Society, pp. 1695–1708. DOI: 10.1098/rstb.2002.1161.

Alme, Charlotte B. et al. (Dec. 2014). "Place cells in the hippocampus: Eleven maps for eleven rooms". en. In: *Proceedings of the National Academy of Sciences* 111.52, pp. 18428–18435. ISSN: 0027-8424, 1091-6490. DOI: 10.1073/pnas.1421056111.

Amaral, D. G. and M. P. Witter (Jan. 1989). "The three-dimensional organization of the hippocampal formation: A review of anatomical data". In: *Neuroscience* 31.3, pp. 571–591. ISSN: 0306-4522. DOI: 10.1016/0306-4522(89)90424-7.

Arcangelis, Lucilla de and Hans J. Herrmann (Mar. 2010). "Learning as a phenomenon occurring in a critical state". In: *Proceedings of the National Academy of Sciences* 107.9. Publisher: Proceedings of the National Academy of Sciences, pp. 3977–3981. DOI: 10.1073/pnas.0912289107.

Arcangelis, Lucilla de, Carla Perrone-Capano, and Hans J. Herrmann (Jan. 2006). "Self-Organized Criticality Model for Brain Plasticity". In: *Physical Review Letters* 96.2. Publisher: American Physical Society, p. 028107. DOI: 10.1103/PhysRevLett.96.028107.

Avramiea, Arthur-Ervin et al. (Mar. 2022). "Long-Range Amplitude Coupling Is Optimized for Brain Networks That Function at Criticality". en. In: *Journal of Neuroscience* 42.11. Publisher: Society for Neuroscience Section: Research Articles, pp. 2221–2233. ISSN: 0270-6474, 1529-2401. DOI: 10.1523/JNEUROSCI.1095-21.2022.

Backus, Alexander R. et al. (Feb. 2016). "Hippocampal-Prefrontal Theta Oscillations Support Memory Integration". English. In: *Current Biology* 26.4. Publisher: Elsevier, pp. 450–457. ISSN: 0960-9822. DOI: 10.1016/j.cub.2015.12.048.

Barabási, Dániel L. et al. (Aug. 2023). "Neuroscience Needs Network Science". en. In: *Journal of Neuroscience* 43.34. Publisher: Society for Neuroscience Section: TechSights, pp. 5989–5995. ISSN: 0270-6474, 1529-2401. DOI: 10.1523/JNEUROSCI.1014-23.2023.

Basu, Jayeeta et al. (Jan. 2016). "Gating of hippocampal activity, plasticity, and memory by entorhinal cortex long-range inhibition". In: *Science* 351.6269. Publisher: American Association for the Advancement of Science, aaa5694. DOI: 10.1126/science.aaa5694.

Bédard, C., H. Kröger, and A. Destexhe (Sept. 2006). "Does the $1/f$ Frequency Scaling of Brain Signals Reflect Self-Organized Critical States?" In: *Physical Review Letters* 97.11. Publisher: American Physical Society, p. 118102. DOI: 10.1103/PhysRevLett.97.118102.

Beggs, John M. (Dec. 2007). "How to build a critical mind". en. In: *Nature Physics* 3.12. Publisher: Nature Publishing Group, pp. 835–835. ISSN: 1745-2481. DOI: 10.1038/nphys799.

Beggs, John M. and Dietmar Plenz (Dec. 2003). "Neuronal Avalanches in Neocortical Circuits". en. In: *The Journal of Neuroscience* 23.35, pp. 11167–11177. ISSN: 0270-6474, 1529-2401. DOI: 10.1523/JNEUROSCI.23-35-11167.2003.

— (June 2004). "Neuronal Avalanches Are Diverse and Precise Activity Patterns That Are Stable for Many Hours in Cortical Slice Cultures". en. In: *Journal of Neuroscience* 24.22. Publisher: Society for Neuroscience Section: Behavioral/Systems/Cognitive, pp. 5216–5229. ISSN: 0270-6474, 1529-2401. DOI: 10.1523/JNEUROSCI.0540-04.2004.

Berry, Stephen D. and Richard F. Thompson (June 1978). "Prediction of Learning Rate from the Hippocampal Electroencephalogram". In: *Science* 200.4347. Publisher: American Association for the Advancement of Science, pp. 1298–1300. DOI: 10.1126/science.663612.

Boccara, Charlotte N. et al. (Mar. 2019). "The entorhinal cognitive map is attracted to goals". en. In: *Science* 363.6434, pp. 1443–1447. ISSN: 0036-8075, 1095-9203. DOI: 10.1126/science.aav4837.

Bollmann, Lars et al. (May 2025). "Sleep stages antagonistically modulate reactivation drift". English. In: *Neuron* 113.9. Publisher: Elsevier, 1446–1459.e6. ISSN: 0896-6273. DOI: 10.1016/j.neuron.2025.02.025.

Bostock, Elizabeth, Robert U. Muller, and John L. Kubie (1991). "Experience-dependent modifications of hippocampal place cell firing". en. In: *Hippocampus* 1.2. _eprint: https://onlinelibrary.wiley.com/d pp. 193–205. ISSN: 1098-1063. DOI: 10.1002/hipo.450010207.

Brandon, Mark P. et al. (May 2014). "New and Distinct Hippocampal Place Codes Are Generated in a New Environment during Septal Inactivation". English. In: *Neuron* 82.4. Publisher: Elsevier, pp. 789–796. ISSN: 0896-6273. DOI: 10.1016/j.neuron.2014.04.013.

Bush, Daniel, Caswell Barry, and Neil Burgess (Mar. 2014). "What do grid cells contribute to place cell firing?" In: *Trends in Neurosciences* 37.3, pp. 136–145. ISSN: 0166-2236. DOI: 10.1016/j.tins.2013.12.003.

Butler, William N., Kiah Hardcastle, and Lisa M. Giocomo (Mar. 2019). "Remembered reward locations restructure entorhinal spatial maps". en. In: *Science* 363.6434, pp. 1447–1452. ISSN: 0036-8075, 1095-9203. DOI: 10.1126/science.aav5297.

Buzsaki, G et al. (May 1992). "High-frequency network oscillation in the hippocampus". en. In: *Science* 256.5059, pp. 1025–1027. ISSN: 0036-8075, 1095-9203. DOI: 10.1126/science.1589772.

Buzsáki, G. (Jan. 1989). "Two-stage model of memory trace formation: A role for "noisy" brain states". en. In: *Neuroscience* 31.3, pp. 551–570. ISSN: 03064522. DOI: 10.1016/0306-4522(89)90423-5.

— (1996). "The Hippocampo-Neocortical Dialogue". en. In: *Cerebral Cortex* 6.2, pp. 81–92. ISSN: 1047-3211, 1460-2199. DOI: 10.1093/cercor/6.2.81.

Buzsáki, György (Nov. 1986). "Hippocampal sharp waves: Their origin and significance". In: *Brain Research* 398.2, pp. 242–252. ISSN: 0006-8993. DOI: 10.1016/0006-8993(86)91483-6.

— (2015). "Hippocampal sharp wave-ripple: A cognitive biomarker for episodic memory and planning". en. In: *Hippocampus* 25.10. _eprint: https://onlinelibrary.wiley.com/doi/pdf/10.1002/hipo.2248 pp. 1073–1188. ISSN: 1098-1063. DOI: 10.1002/hipo.22488.

Buzsáki, György and Edvard I Moser (Feb. 2013). "Memory, navigation and theta rhythm in the hippocampal-entorhinal system". en. In: *Nature Neuroscience* 16.2, pp. 130–138. ISSN: 1097-6256, 1546-1726. DOI: 10.1038/nn.3304.

Cacucci, F. et al. (July 2007). "Experience-Dependent Increase in CA1 Place Cell Spatial Information, But Not Spatial Reproducibility, Is Dependent on the Autophosphorylation

of the -Isoform of the Calcium/Calmodulin-Dependent Protein Kinase II". en. In: *Journal of Neuroscience* 27.29, pp. 7854–7859. ISSN: 0270-6474, 1529-2401. DOI: 10.1523/JNEUROSCI.1704-07.2007.

Cambrainha, Gustavo G. et al. (Sept. 2025). "Criticality at Work: Scaling in the Mouse Cortex Enhances Performance". In: *PRX Life* 3.3. Publisher: American Physical Society, p. 033026. DOI: 10.1103/w49n-2vz8.

Canto, Cathrin B., Floris G. Wouterlood, and Menno P. Witter (2008). "What Does the Anatomical Organization of the Entorhinal Cortex Tell Us?" en. In: *Neural Plasticity* 2008.1. _eprint: https://onlinelibrary.wiley.com/doi/pdf/10.1155/2008/381243, p. 381243. ISSN: 1687-5443. DOI: 10.1155/2008/381243.

Carr, Margaret F., Shantanu P. Jadhav, and Loren M. Frank (Feb. 2011). "Hippocampal replay in the awake state: a potential substrate for memory consolidation and retrieval". en. In: *Nature Neuroscience* 14.2. Publisher: Nature Publishing Group, pp. 147–153. ISSN: 1546-1726. DOI: 10.1038/nn.2732.

Castelli, Manfredi et al. (Oct. 2025). "Hippocampal ripple diversity organizes neuronal reactivation dynamics in the offline brain". In: *Neuron*. ISSN: 0896-6273. DOI: 10.1016/j.neuron.2025.09.012.

Castro, Daniel M. et al. (May 2024). "In and Out of Criticality? State-Dependent Scaling in the Rat Visual Cortex". en. In: *PRX Life* 2.2, p. 023008. ISSN: 2835-8279. DOI: 10.1103/PRXLife.2.023008.

Cavanagh, Sean E et al. (Oct. 2016). "Autocorrelation structure at rest predicts value correlates of single neurons during reward-guided choice". In: *eLife* 5. Ed. by Michael J Frank. Publisher: eLife Sciences Publications, Ltd, e18937. ISSN: 2050-084X. DOI: 10.7554/eLife.18937.

Cavanagh, Sean E., Laurence T. Hunt, and Steven W. Kennerley (Dec. 2020). "A Diversity of Intrinsic Timescales Underlie Neural Computations". English. In: *Frontiers in Neural Circuits* 14. Publisher: Frontiers. ISSN: 1662-5110. DOI: 10.3389/fncir.2020.615626.

Cembrowski, Mark S. and Nelson Spruston (Apr. 2019). "Heterogeneity within classical cell types is the rule: lessons from hippocampal pyramidal neurons". en. In: *Nature Reviews Neuroscience* 20.4. Publisher: Nature Publishing Group, pp. 193–204. ISSN: 1471-0048. DOI: 10.1038/s41583-019-0125-5.

Chen, Cheng, Yuanxin Liao, and Guangdun Peng (Nov. 2022). "Connecting past and present: single-cell lineage tracing". en. In: *Protein & Cell* 13.11, pp. 790–807. ISSN: 1674-8018. DOI: 10.1007/s13238-022-00913-7.

Chialvo, Dante R. (Oct. 2010). "Emergent complex neural dynamics". en. In: *Nature Physics* 6.10, pp. 744–750. ISSN: 1745-2473, 1745-2481. DOI: 10.1038/nphys1803.

Chintaluri, Chaitanya and Tim P. Vogels (Nov. 2023). "Metabolically regulated spiking could serve neuronal energy homeostasis and protect from reactive oxygen species". EN. In: *Proceedings of the National Academy of Sciences* 120.48. Company: National Academy of Sciences Distributor: National Academy of Sciences Institution: National Academy of Sciences Label: National Academy of Sciences Publisher: Proceedings of the National Academy of Sciences, e2306525120. DOI: 10.1073/pnas.2306525120.

Chung, Jason E. et al. (Sept. 2017). "A Fully Automated Approach to Spike Sorting". en. In: *Neuron* 95.6, 1381–1394.e6. ISSN: 0896-6273. DOI: 10.1016/j.neuron.2017.08.030.

Cohen, Zach and Jan Drugowitsch (n.d.). "A unifying theory of receptive field heterogeneity predicts hippocampal spatial tuning". en. In: ().

Colgin, Laura Lee (Apr. 2016). "Rhythms of the hippocampal network". en. In: *Nature Reviews Neuroscience* 17.4, pp. 239–249. ISSN: 1471-003X, 1471-0048. DOI: 10.1038/nrn.2016.21.

Colgin, Laura Lee, Edvard I. Moser, and May-Britt Moser (Sept. 2008). "Understanding memory through hippocampal remapping". In: *Trends in Neurosciences* 31.9, pp. 469–477. ISSN: 0166-2236. DOI: 10.1016/j.tins.2008.06.008.

Cranmer, Kyle, Johann Brehmer, and Gilles Louppe (Dec. 2020). "The frontier of simulation-based inference". In: *Proceedings of the National Academy of Sciences* 117.48. Publisher: Proceedings of the National Academy of Sciences, pp. 30055–30062. DOI: 10.1073/pnas.1912789117.

Csicsvari, Jozsef et al. (Jan. 1999). "Oscillatory Coupling of Hippocampal Pyramidal Cells and Interneurons in the Behaving Rat". en. In: *Journal of Neuroscience* 19.1. Publisher: Society for Neuroscience Section: ARTICLE, pp. 274–287. ISSN: 0270-6474, 1529-2401. DOI: 10.1523/JNEUROSCI.19-01-00274.1999.

Csicsvari, tJozsef et al. (Aug. 1999). "Fast Network Oscillations in the Hippocampal CA1 Region of the Behaving Rat". en. In: *The Journal of Neuroscience* 19.16, RC20–RC20. ISSN: 0270-6474, 1529-2401. DOI: 10.1523/JNEUROSCI.19-16-j0001.1999.

Danielson, Nathan B. et al. (Aug. 2016). "Sublayer-Specific Coding Dynamics during Spatial Navigation and Learning in Hippocampal Area CA1". In: *Neuron* 91.3, pp. 652–665. ISSN: 0896-6273. DOI: 10.1016/j.neuron.2016.06.020.

Davidson, Thomas J., Fabian Kloosterman, and Matthew A. Wilson (Aug. 2009). "Hippocampal Replay of Extended Experience". English. In: *Neuron* 63.4. Publisher: Elsevier, pp. 497–507. ISSN: 0896-6273. DOI: 10.1016/j.neuron.2009.07.027.

Denève, Sophie and Christian K. Machens (Mar. 2016). "Efficient codes and balanced networks". en. In: *Nature Neuroscience* 19.3. Publisher: Nature Publishing Group, pp. 375–382. ISSN: 1546-1726. DOI: 10.1038/nn.4243.

Destexhe, Alain (Dec. 2009). "Self-sustained asynchronous irregular states and Up–Down states in thalamic, cortical and thalamocortical networks of nonlinear integrate-and-fire neurons". en. In: *Journal of Computational Neuroscience* 27.3, pp. 493–506. ISSN: 1573-6873. DOI: 10.1007/s10827-009-0164-4.

Developers, The joblib (2025). "joblib". en. In: (). DOI: 10.5281/zenodo.16964648.

Diekelmann, Susanne and Jan Born (Feb. 2010). "The memory function of sleep". en. In: *Nature Reviews Neuroscience* 11.2. Publisher: Nature Publishing Group, pp. 114–126. ISSN: 1471-0048. DOI: 10.1038/nrn2762.

Dimidschstein, Jordane et al. (Dec. 2016). "A viral strategy for targeting and manipulating interneurons across vertebrate species". en. In: *Nature Neuroscience* 19.12. Publisher: Nature Publishing Group, pp. 1743–1749. ISSN: 1546-1726. DOI: 10.1038/nn.4430.

Dommett, Eleanor et al. (Mar. 2005). "How Visual Stimuli Activate Dopaminergic Neurons at Short Latency". In: *Science* 307.5714. Publisher: American Association for the Advancement of Science, pp. 1476–1479. DOI: 10.1126/science.1107026.

Douglas, Rodney J., Christof Koch, et al. (Aug. 1995). "Recurrent Excitation in Neocortical Circuits". In: *Science* 269.5226. Publisher: American Association for the Advancement of Science, pp. 981–985. DOI: 10.1126/science.7638624.

Douglas, Rodney J. and Kevan A. C. Martin (July 2007). "Recurrent neuronal circuits in the neocortex". In: *Current Biology* 17.13, R496–R500. ISSN: 0960-9822. DOI: 10.1016/j.cub.2007.04.024.

Dupret, David et al. (Aug. 2010). "The reorganization and reactivation of hippocampal maps predict spatial memory performance". en. In: *Nature Neuroscience* 13.8, pp. 995–1002. ISSN: 1097-6256, 1546-1726. DOI: 10.1038/nn.2599.

Effenberger, Felix, Jürgen Jost, and Anna Levina (Sept. 2015). "Self-organization in Balanced State Networks by STDP and Homeostatic Plasticity". en. In: *PLOS Computational Biology* 11.9. Publisher: Public Library of Science, e1004420. ISSN: 1553-7358. DOI: 10.1371/journal.pcbi.1004420.

Ego-Stengel, Valérie and Matthew A. Wilson (2009). "Disruption of ripple-associated hippocampal activity during rest impairs spatial learning in the rat". en. In: *Hippocampus*, NA–NA. ISSN: 10509631, 10981063. DOI: 10.1002/hipo.20707.

Eichenbaum, Howard (Jan. 2013). "What H.M. Taught Us". In: *Journal of Cognitive Neuroscience* 25.1, pp. 14–21. ISSN: 0898-929X. DOI: 10.1162/jocn_a_00285.

— (Sept. 2017). "Prefrontal–hippocampal interactions in episodic memory". en. In: *Nature Reviews Neuroscience* 18.9. Publisher: Nature Publishing Group, pp. 547–558. ISSN: 1471-0048. DOI: 10.1038/nrn.2017.74.

Eurich, Christian W., J. Michael Herrmann, and Udo A. Ernst (Dec. 2002). "Finite-size effects of avalanche dynamics". In: *Physical Review E* 66.6. Publisher: American Physical Society, p. 066137. DOI: 10.1103/PhysRevE.66.066137.

Fenton, André A. et al. (Oct. 2008). "Unmasking the CA1 Ensemble Place Code by Exposures to Small and Large Environments: More Place Cells and Multiple, Irregularly Arranged, and Expanded Place Fields in the Larger Space". en. In: *Journal of Neuroscience* 28.44. Publisher: Society for Neuroscience Section: Articles, pp. 11250–11262. ISSN: 0270-6474, 1529-2401. DOI: 10.1523/JNEUROSCI.2862-08.2008.

Fernández-Ruiz, Antonio et al. (June 2019). "Long-duration hippocampal sharp wave ripples improve memory". In: *Science* 364.6445. Publisher: American Association for the Advancement of Science, pp. 1082–1086. DOI: 10.1126/science.aax0758.

Fontenele, Antonio J. et al. (May 2019). "Criticality between Cortical States". In: *Physical Review Letters* 122.20. Publisher: American Physical Society, p. 208101. DOI: 10.1103/PhysRevLett.122.208101.

Fosque, Leandro J. et al. (Mar. 2021). "Evidence for Quasicritical Brain Dynamics". In: *Physical Review Letters* 126.9. Publisher: American Physical Society, p. 098101. DOI: 10.1103/PhysRevLett.126.098101.

Foster, David J. and Matthew A. Wilson (2007). "Hippocampal theta sequences". en. In: *Hippocampus* 17.11. _eprint: https://onlinelibrary.wiley.com/doi/pdf/10.1002/hipo.20345, pp. 1093–1099. ISSN: 1098-1063. DOI: 10.1002/hipo.20345.

Frankland, Paul W. and Bruno Bontempi (Feb. 2005). "The organization of recent and remote memories". en. In: *Nature Reviews Neuroscience* 6.2. Publisher: Nature Publishing Group, pp. 119–130. ISSN: 1471-0048. DOI: 10.1038/nrn1607.

Freeman, Walter J. et al. (June 2003). "Spatial spectra of scalp EEG and EMG from awake humans". In: *Clinical Neurophysiology* 114.6, pp. 1053–1068. ISSN: 1388-2457. DOI: 10.1016/S1388-2457(03)00045-2.

Friedman, Nir et al. (May 2012). "Universal Critical Dynamics in High Resolution Neuronal Avalanche Data". In: *Physical Review Letters* 108.20. Publisher: American Physical Society, p. 208102. DOI: 10.1103/PhysRevLett.108.208102.

Gauthier, Jeffrey L. and David W. Tank (July 2018). "A Dedicated Population for Reward Coding in the Hippocampus". en. In: *Neuron* 99.1, 179–193.e7. ISSN: 0896-6273. DOI: 10.1016/j.neuron.2018.06.008.

Girardeau, Gabrielle, Karim Benchenane, et al. (Oct. 2009). "Selective suppression of hippocampal ripples impairs spatial memory". en. In: *Nature Neuroscience* 12.10, pp. 1222–1223. ISSN: 1097-6256, 1546-1726. DOI: 10.1038/nn.2384.

Girardeau, Gabrielle and Vítor Lopes-dos-Santos (Oct. 2021). "Brain neural patterns and the memory function of sleep". In: *Science* 374.6567. Publisher: American Association for the Advancement of Science, pp. 560–564. DOI: 10.1126/science.abi8370.

Gireesh, Elakkat D. and Dietmar Plenz (May 2008). "Neuronal avalanches organize as nested theta- and beta/gamma-oscillations during development of cortical layer 2/3". In: *Proceedings of the National Academy of Sciences* 105.21. Publisher: Proceedings of the National Academy of Sciences, pp. 7576–7581. DOI: 10.1073/pnas.0800537105.

Goutagny, Romain, Jesse Jackson, and Sylvain Williams (Dec. 2009). "Self-generated theta oscillations in the hippocampus". en. In: *Nature Neuroscience* 12.12. Publisher: Nature Publishing Group, pp. 1491–1493. ISSN: 1546-1726. DOI: 10.1038/nn.2440.

Green, John D. and Arnaldo A. Arduini (Nov. 1954). "Hippocampal electrical activity in arousal". In: *Journal of Neurophysiology* 17.6. Publisher: American Physiological Society, pp. 533–557. ISSN: 0022-3077. DOI: 10.1152/jn.1954.17.6.533.

Gridchyn, Igor et al. (Apr. 2020). "Assembly-Specific Disruption of Hippocampal Replay Leads to Selective Memory Deficit". en. In: *Neuron* 106.2, 291–300.e6. ISSN: 0896-6273. DOI: 10.1016/j.neuron.2020.01.021.

Grosmark, Andres D. and György Buzsáki (Mar. 2016). "Diversity in neural firing dynamics supports both rigid and learned hippocampal sequences". In: *Science* 351.6280. Publisher: American Association for the Advancement of Science, pp. 1440–1443. DOI: 10.1126/science.aad1935.

Gupta, Anoopum S et al. (July 2012). "Segmentation of spatial experience by hippocampal theta sequences". en. In: *Nature Neuroscience* 15.7, pp. 1032–1039. ISSN: 1097-6256, 1546-1726. DOI: 10.1038/nn.3138.

Habibollahi, Forough et al. (Aug. 2023). "Critical dynamics arise during structured information presentation within embodied in vitro neuronal networks". en. In: *Nature Communications* 14.1. Number: 1 Publisher: Nature Publishing Group, p. 5287. ISSN: 2041-1723. DOI: 10.1038/s41467-023-41020-3.

Hafting, Torkel et al. (Aug. 2005). "Microstructure of a spatial map in the entorhinal cortex". en. In: *Nature* 436.7052. Publisher: Nature Publishing Group, pp. 801–806. ISSN: 1476-4687. DOI: 10.1038/nature03721.

Hahn, Gerald, Thomas Petermann, et al. (Dec. 2010). "Neuronal Avalanches in Spontaneous Activity In Vivo". In: *Journal of Neurophysiology* 104.6. Publisher: American Physiological Society, pp. 3312–3322. ISSN: 0022-3077. DOI: 10.1152/jn.00953.2009.

Hahn, Gerald, Adrian Ponce-Alvarez, et al. (May 2017). "Spontaneous cortical activity is transiently poised close to criticality". en. In: *PLOS Computational Biology* 13.5. Publisher: Public Library of Science, e1005543. ISSN: 1553-7358. DOI: 10.1371/journal.pcbi.1005543.

Haldeman, Clayton and John M. Beggs (Feb. 2005). "Critical Branching Captures Activity in Living Neural Networks and Maximizes the Number of Metastable States". In: *Physical Review Letters* 94.5. Publisher: American Physical Society, p. 058101. DOI: 10.1103/PhysRevLett.94.058101.

Hargreaves, Eric L. et al. (June 2005). "Major Dissociation Between Medial and Lateral Entorhinal Input to Dorsal Hippocampus". In: *Science* 308.5729. Publisher: American Association for the Advancement of Science, pp. 1792–1794. DOI: 10.1126/science.1110449.

Harris, Charles R. et al. (Sept. 2020). "Array programming with NumPy". en. In: *Nature* 585.7825. Publisher: Nature Publishing Group, pp. 357–362. ISSN: 1476-4687. DOI: 10.1038/s41586-020-2649-2.

He, Biyu J. (Sept. 2011). "Scale-Free Properties of the Functional Magnetic Resonance Imaging Signal during Rest and Task". en. In: *Journal of Neuroscience* 31.39. Publisher: Society for Neuroscience Section: Articles, pp. 13786–13795. ISSN: 0270-6474, 1529-2401. DOI: 10.1523/JNEUROSCI.2111-11.2011.

Heiney, Kristine et al. (2021). "Criticality, Connectivity, and Neural Disorder: A Multifaceted Approach to Neural Computation". English. In: *Frontiers in Computational Neuroscience* 15. Publisher: Frontiers. ISSN: 1662-5188. DOI: 10.3389/fncom.2021.611183.

Hengen, Keith B. and Woodrow L. Shew (Aug. 2025). "Is criticality a unified setpoint of brain function?" In: *Neuron* 113.16, 2582–2598.e2. ISSN: 0896-6273. DOI: 10.1016/j.neuron.2025.05.020.

Hernández-Frausto, Melissa and Carmen Vivar (Sept. 2024). "Entorhinal cortex–hippocampal circuit connectivity in health and disease". English. In: *Frontiers in Human Neuroscience* 18. Publisher: Frontiers. ISSN: 1662-5161. DOI: 10.3389/fnhum.2024.1448791.

Hesse, Janina and Thilo Gross (Sept. 2014). "Self-organized criticality as a fundamental property of neural systems". In: *Frontiers in Systems Neuroscience* 8. ISSN: 1662-5137. DOI: 10.3389/fnsys.2014.00166.

Hill, A.J. (Nov. 1978). "First occurrence of hippocampal spatial firing in a new environment". en. In: *Experimental Neurology* 62.2, pp. 282–297. ISSN: 00144886. DOI: 10.1016/0014-4886(78)90058-4.

Hopfield, J J (Apr. 1982). "Neural networks and physical systems with emergent collective computational abilities." In: *Proceedings of the National Academy of Sciences* 79.8. Publisher: Proceedings of the National Academy of Sciences, pp. 2554–2558. DOI: 10.1073/pnas.79.8.2554.

Hunter, John D. (May 2007). "Matplotlib: A 2D Graphics Environment". In: *Computing in Science & Engineering* 9.3, pp. 90–95. ISSN: 1558-366X. DOI: 10.1109/MCSE.2007.55.

Inc, Plotly Technologies (2015). *Collaborative data science*. Place: Montreal, QC Publisher: Plotly Technologies Inc.

Jadhav, Shantanu P. et al. (June 2012). "Awake Hippocampal Sharp-Wave Ripples Support Spatial Memory". In: *Science* 336.6087. Publisher: American Association for the Advancement of Science, pp. 1454–1458. DOI: 10.1126/science.1217230.

Jones, Sabrina A et al. (Jan. 2023). "Scale-free behavioral dynamics directly linked with scale-free cortical dynamics". en. In: *eLife* 12, e79950. ISSN: 2050-084X. DOI: 10.7554/eLife.79950.

Joshi, Abhilasha et al. (May 2023). "Dynamic synchronization between hippocampal representations and stepping". en. In: *Nature* 617.7959. Publisher: Nature Publishing Group, pp. 125–131. ISSN: 1476-4687. DOI: 10.1038/s41586-023-05928-6.

Kadanoff, Leo P. (June 1966). "Scaling laws for ising models near ${T}_{c}$". In: *Physics Physique Fizika* 2.6. Publisher: American Physical Society, pp. 263–272. DOI: 10.1103/PhysicsPhysiqueFizika.2.263.

Kandel, Eric R., Yadin Dudai, and Mark R. Mayford (Mar. 2014). "The Molecular and Systems Biology of Memory". In: *Cell* 157.1, pp. 163–186. ISSN: 0092-8674. DOI: 10.1016/j.cell.2014.03.001.

Kinouchi, Osame and Mauro Copelli (May 2006). "Optimal dynamical range of excitable networks at criticality". en. In: *Nature Physics* 2.5. Publisher: Nature Publishing Group, pp. 348–351. ISSN: 1745-2481. DOI: 10.1038/nphys289.

Klausberger, Thomas, Peter J. Magill, et al. (Feb. 2003). "Brain-state- and cell-type-specific firing of hippocampal interneurons in vivo". en. In: *Nature* 421.6925. Publisher: Nature Publishing Group, pp. 844–848. ISSN: 1476-4687. DOI: 10.1038/nature01374.

Klausberger, Thomas and Peter Somogyi (July 2008). "Neuronal Diversity and Temporal Dynamics: The Unity of Hippocampal Circuit Operations". In: *Science* 321.5885. Publisher: American Association for the Advancement of Science, pp. 53–57. DOI: 10.1126/science.1149381.

Klinzing, Jens G., Niels Niethard, and Jan Born (Oct. 2019). "Mechanisms of systems memory consolidation during sleep". en. In: *Nature Neuroscience* 22.10. Publisher: Nature Publishing Group, pp. 1598–1610. ISSN: 1546-1726. DOI: 10.1038/s41593-019-0467-3.

Kovács, Krisztián A. et al. (Oct. 2016). "Optogenetically Blocking Sharp Wave Ripple Events in Sleep Does Not Interfere with the Formation of Stable Spatial Representation in the CA1 Area of the Hippocampus". en. In: *PLOS ONE* 11.10. Ed. by Vladyslav Vyazovskiy, e0164675. ISSN: 1932-6203. DOI: 10.1371/journal.pone.0164675.

Kubie, John L., Eliott R. J. Levy, and André A. Fenton (Aug. 2020). "Is hippocampal remapping the physiological basis for context?" en. In: *Hippocampus* 30.8, pp. 851–864. ISSN: 1050-9631, 1098-1063. DOI: 10.1002/hipo.23160.

Kurikawa, Tomoki (June 2025). *Slow and Fast Neurons Cooperate in Contextual Working Memory through Timescale Diversity*. en. arXiv:2506.07341 [q-bio]. DOI: 10.48550/arXiv.2506.07341.

Larremore, Daniel B. et al. (June 2012). "Statistical properties of avalanches in networks". In: *Physical Review E* 85.6. Publisher: American Physical Society, p. 066131. DOI: 10.1103/PhysRevE.85.066131.

Law, L. Matthew, David A. Bulkin, and David M. Smith (Dec. 2016). "Slow stabilization of concurrently acquired hippocampal context representations". en. In: *Hippocampus* 26.12, pp. 1560–1569. ISSN: 10509631. DOI: 10.1002/hipo.22656.

Lee, Albert K. and Matthew A. Wilson (Dec. 2002). "Memory of Sequential Experience in the Hippocampus during Slow Wave Sleep". In: *Neuron* 36.6, pp. 1183–1194. ISSN: 0896-6273. DOI: 10.1016/S0896-6273(02)01096-6.

Lepeu, Gregory et al. (Aug. 2024). "The critical dynamics of hippocampal seizures". en. In: *Nature Communications* 15.1. Publisher: Nature Publishing Group, p. 6945. ISSN: 2041-1723. DOI: 10.1038/s41467-024-50504-9.

Lever, Colin et al. (Mar. 2002). "Long-term plasticity in hippocampal place-cell representation of environmental geometry". en. In: *Nature* 416.6876, pp. 90–94. ISSN: 0028-0836, 1476-4687. DOI: 10.1038/416090a.

Levina, A., J. M. Herrmann, and T. Geisel (Dec. 2007). "Dynamical synapses causing self-organized criticality in neural networks". en. In: *Nature Physics* 3.12. Publisher: Nature Publishing Group, pp. 857–860. ISSN: 1745-2481. DOI: 10.1038/nphys758.

Levina, Anna, J. Michael Herrmann, and Theo Geisel (Mar. 2009). "Phase Transitions towards Criticality in a Neural System with Adaptive Interactions". In: *Physical Review Letters* 102.11. Publisher: American Physical Society, p. 118110. DOI: 10.1103/PhysRevLett.102.118110.

Li, Jingwen and Woodrow L. Shew (Sept. 2020). "Tuning network dynamics from criticality to an asynchronous state". en. In: *PLOS Computational Biology* 16.9. Ed. by Alireza Soltani, e1008268. ISSN: 1553-7358. DOI: 10.1371/journal.pcbi.1008268.

Liu, Shun, Fali Li, and Feng Wan (Aug. 2023). "Distance to criticality undergoes critical transition before epileptic seizure attacks". In: *Brain Research Bulletin* 200, p. 110684. ISSN: 0361-9230. DOI: 10.1016/j.brainresbull.2023.110684.

Lombardi, Fabrizio, Selver Pepić, et al. (Mar. 2023). "Statistical modeling of adaptive neural networks explains co-existence of avalanches and oscillations in resting human brain". en. In: *Nature Computational Science* 3.3. Publisher: Nature Publishing Group, pp. 254–263. ISSN: 2662-8457. DOI: 10.1038/s43588-023-00410-9.

Lombardi, Fabrizio, Oren Shriki, et al. (Oct. 2021). "Long-range temporal correlations in the broadband resting state activity of the human brain revealed by neuronal avalanches". In: *Neurocomputing* 461, pp. 657–666. ISSN: 0925-2312. DOI: 10.1016/j.neucom.2020.05.126.

Lombardi, Fabrizio, Jilin W.J.L. Wang, et al. (2020). "Power-law correlations and coupling of active and quiet states underlie a class of complex systems with self-organization at criticality". In: *EPJ Web of Conferences* 230. Ed. by E. Puppin, p. 00005. ISSN: 2100-014X. DOI: 10.1051/epjconf/202023000005.

Louie, Kenway and Matthew A. Wilson (Jan. 2001). "Temporally Structured Replay of Awake Hippocampal Ensemble Activity during Rapid Eye Movement Sleep". In: *Neuron* 29.1, pp. 145–156. ISSN: 0896-6273. DOI: 10.1016/S0896-6273(01)00186-6.

Lutz, Nicolas D., Maximilian Harkotte, and Jan Born (Aug. 2025). "Sleep's contribution to memory formation". In: *Physiological Reviews*. Publisher: American Physiological Society. ISSN: 0031-9333. DOI: 10.1152/physrev.00054.2024.

Ma, Zhengyu et al. (Nov. 2019). "Cortical Circuit Dynamics Are Homeostatically Tuned to Criticality *In Vivo*". In: *Neuron* 104.4, 655–664.e4. ISSN: 0896-6273. DOI: 10.1016/j.neuron.2019.08.031.

Mainali, Nischal, Rava Azeredo da Silveira, and Yoram Burak (Apr. 2025). "Universal statistics of hippocampal place fields across species and dimensionalities". In: *Neuron* 113.7, 1110–1120.e3. ISSN: 0896-6273. DOI: 10.1016/j.neuron.2025.01.017.

Malvache, Arnaud et al. (Sept. 2016). "Awake hippocampal reactivations project onto orthogonal neuronal assemblies". In: *Science* 353.6305. Publisher: American Association for the Advancement of Science, pp. 1280–1283. DOI: 10.1126/science.aaf3319.

Manual Clustering Practical Guide (by S. Lenzi and N. Steinmetz) - phy (2025).

Mariani, Benedetta et al. (Aug. 2021). "Neuronal Avalanches Across the Rat Somatosensory Barrel Cortex and the Effect of Single Whisker Stimulation". English. In: *Frontiers in Systems Neuroscience* 15. Publisher: Frontiers. ISSN: 1662-5137. DOI: 10.3389/fnsys.2021.709677.

Markus, Etan J. et al. (Aug. 1994). "Spatial information content and reliability of hippocampal CA1 neurons: Effects of visual input". en. In: *Hippocampus* 4.4, pp. 410–421. ISSN: 1050-9631, 1098-1063. DOI: 10.1002/hipo.450040404.

Marr (July 1971). "Simple memory: a theory for archicortex". en. In: *Philosophical Transactions of the Royal Society of London. B, Biological Sciences* 262.841, pp. 23–81. ISSN: 0080-4622, 2054-0280. DOI: 10.1098/rstb.1971.0078.

Marshall, Najja et al. (June 2016). "Analysis of Power Laws, Shape Collapses, and Neural Complexity: New Techniques and MATLAB Support via the NCC Toolbox". English. In: *Frontiers in Physiology* 7. Publisher: Frontiers. ISSN: 1664-042X. DOI: 10.3389/fphys.2016.00250.

Mazzoni, Alberto et al. (May 2007). "On the Dynamics of the Spontaneous Activity in Neuronal Networks". en. In: *PLOS ONE* 2.5. Publisher: Public Library of Science, e439. ISSN: 1932-6203. DOI: 10.1371/journal.pone.0000439.

McKinney, Wes (2010). "Data Structures for Statistical Computing in Python". In: *Proceedings of the 9th Python in Science Conference*. Ed. by Stéfan van der Walt and Jarrod Millman, pp. 56–61. DOI: 10.25080/Majora-92bf1922-00a.

McNaughton, Bruce L. et al. (Aug. 2006). "Path integration and the neural basis of the 'cognitive map'". en. In: *Nature Reviews Neuroscience* 7.8. Publisher: Nature Publishing Group, pp. 663–678. ISSN: 1471-0048. DOI: 10.1038/nrn1932.

Meisel, Christian et al. (Oct. 2013). "Fading Signatures of Critical Brain Dynamics during Sustained Wakefulness in Humans". en. In: *Journal of Neuroscience* 33.44. Publisher:

Society for Neuroscience Section: Articles, pp. 17363–17372. ISSN: 0270-6474, 1529-2401. DOI: 10.1523/JNEUROSCI.1516-13.2013.

Meshulam, Leenoy et al. (Dec. 2018). *Coarse–graining and hints of scaling in a population of 1000+ neurons*. en. arXiv:1812.11904 [physics]. DOI: 10.48550/arXiv.1812.11904.

— (Oct. 2019). "Coarse Graining, Fixed Points, and Scaling in a Large Population of Neurons". en. In: *Physical Review Letters* 123.17, p. 178103. ISSN: 0031-9007, 1079-7114. DOI: 10.1103/PhysRevLett.123.178103.

Mitchell, Anna S. et al. (Nov. 2014). "Advances in Understanding Mechanisms of Thalamic Relays in Cognition and Behavior". en. In: *Journal of Neuroscience* 34.46. Publisher: Society for Neuroscience Section: Symposium, pp. 15340–15346. ISSN: 0270-6474, 1529-2401. DOI: 10.1523/JNEUROSCI.3289-14.2014.

Monaco, Joseph D. and Larry F. Abbott (June 2011). "Modular Realignment of Entorhinal Grid Cell Activity as a Basis for Hippocampal Remapping". en. In: *Journal of Neuroscience* 31.25. Publisher: Society for Neuroscience Section: Articles, pp. 9414–9425. ISSN: 0270-6474, 1529-2401. DOI: 10.1523/JNEUROSCI.1433-11.2011.

Morales, Guillermo B., Serena di Santo, and Miguel A. Muñoz (Feb. 2023). "Quasiuniversal scaling in mouse-brain neuronal activity stems from edge-of-instability critical dynamics". In: *Proceedings of the National Academy of Sciences* 120.9. Publisher: Proceedings of the National Academy of Sciences, e2208998120. DOI: 10.1073/pnas.2208998120.

Moretti, Paolo and Miguel A. Muñoz (2013). *Griffiths phases and the stretching of criticality in brain networks | Nature Communications*.

Morrell, Mia C, Ilya Nemenman, and Audrey Sederberg (Mar. 2024). "Neural criticality from effective latent variables". In: *eLife* 12. Ed. by Peter Latham and Timothy E Behrens. Publisher: eLife Sciences Publications, Ltd, RP89337. ISSN: 2050-084X. DOI: 10.7554/eLife.89337.

Morrell, Mia C., Audrey J. Sederberg, and Ilya Nemenman (Mar. 2021). "Latent Dynamical Variables Produce Signatures of Spatiotemporal Criticality in Large Biological Systems". In: *Physical Review Letters* 126.11. Publisher: American Physical Society, p. 118302. DOI: 10.1103/PhysRevLett.126.118302.

Moser, Edvard I, May-Britt Moser, and Bruce L McNaughton (Nov. 2017). "Spatial representation in the hippocampal formation: a history". en. In: *Nature Neuroscience* 20.11, pp. 1448–1464. ISSN: 1097-6256, 1546-1726. DOI: 10.1038/nn.4653.

Moser, Edvard I. and May-Britt Moser (2008). "A metric for space". en. In: *Hippocampus* 18.12. _eprint: https://onlinelibrary.wiley.com/doi/pdf/10.1002/hipo.20483, pp. 1142–1156. ISSN: 1098-1063. DOI: 10.1002/hipo.20483.

Mueller, Adrienne et al. (Jan. 2020). "Dopamine Receptor Expression Among Local and Visual Cortex-Projecting Frontal Eye Field Neurons". In: *Cerebral Cortex* 30.1, pp. 148–164. ISSN: 1047-3211. DOI: 10.1093/cercor/bhz078.

Muller, R. U. and J. L. Kubie (July 1987). "The effects of changes in the environment on the spatial firing of hippocampal complex-spike cells". en. In: *Journal of Neuroscience* 7.7. Publisher: Society for Neuroscience Section: Articles, pp. 1951–1968. ISSN: 0270-6474, 1529-2401. DOI: 10.1523/JNEUROSCI.07-07-01951.1987.

Muller, Ru, Jl Kubie, and Jb Ranck (July 1987). "Spatial firing patterns of hippocampal complex-spike cells in a fixed environment". en. In: *The Journal of Neuroscience* 7.7, pp. 1935–1950. ISSN: 0270-6474, 1529-2401. DOI: 10.1523/JNEUROSCI.07-07-01935.1987.

Müller, Paul Manuel et al. (Apr. 2025). "Critical dynamics predicts cognitive performance and provides a common framework for heterogeneous mechanisms impacting cognition". In: *Proceedings of the National Academy of Sciences* 122.14. Publisher: Proceedings of the National Academy of Sciences, e2417117122. DOI: 10.1073/pnas.2417117122.

Munn, Brandon R. et al. (Dec. 2024). "Multiscale organization of neuronal activity unifies scale-dependent theories of brain function". English. In: *Cell* 187.25. Publisher: Elsevier, 7303–7313.e15. ISSN: 0092-8674, 1097-4172. DOI: 10.1016/j.cell.2024.10.004.

Muñoz, Miguel A. (2018). "*Colloquium*: Criticality and dynamical scaling in living systems". In: *Reviews of Modern Physics* 90.3. DOI: 10.1103/RevModPhys.90.031001.

Nardin, Michele et al. (Sept. 2023). "Theta oscillations as a substrate for medial prefrontal-hippocampal assembly interactions". English. In: *Cell Reports* 42.9. Publisher: Elsevier. ISSN: 2211-1247. DOI: 10.1016/j.celrep.2023.113015.

Nascimento, Kaio F. R. et al. (June 2025). *The phenomenological renormalization group in neuronal models near criticality*. en. arXiv:2506.14053 [cond-mat]. DOI: 10.48550/arXiv.2506.14053.

Nicoletti, Giorgio, Samir Suweis, and Amos Maritan (May 8, 2020). "Scaling and criticality in a phenomenological renormalization group". In: *Physical Review Research* 2.2. Publisher: American Physical Society, p. 023144. DOI: 10.1103/PhysRevResearch.2.023144.

Nonnenmacher, Marcel et al. (Oct. 2017). "Signatures of criticality arise from random subsampling in simple population models". en. In: *PLOS Computational Biology* 13.10. Ed. by Peter E. Latham, e1005718. ISSN: 1553-7358. DOI: 10.1371/journal.pcbi.1005718.

Noudoost, Behrad and Tirin Moore (June 2011). "Control of visual cortical signals by prefrontal dopamine". en. In: *Nature* 474.7351. Publisher: Nature Publishing Group, pp. 372–375. ISSN: 1476-4687. DOI: 10.1038/nature09995.

O'Keefe, J. and J. Dostrovsky (Nov. 1971). "The hippocampus as a spatial map. Preliminary evidence from unit activity in the freely-moving rat". en. In: *Brain Research* 34.1, pp. 171–175. ISSN: 00068993. DOI: 10.1016/0006-8993(71)90358-1.

O'Keefe, John and Neil Burgess (May 1996). "Geometric determinants of the place fields of hippocampal neurons". en. In: *Nature* 381.6581. Publisher: Nature Publishing Group, pp. 425–428. ISSN: 1476-4687. DOI: 10.1038/381425a0.

O'Keefe, John and Lynn Nadel (1978). *The hippocampus as a cognitive map*. Oxford : New York: Clarendon Press ; Oxford University Press. ISBN: 978-0-19-857206-0.

O'Byrne, Jordan and Karim Jerbi (Nov. 2022). "How critical is brain criticality?" English. In: *Trends in Neurosciences* 45.11. Publisher: Elsevier, pp. 820–837. ISSN: 0166-2236, 1878-108X. DOI: 10.1016/j.tins.2022.08.007.

O'Neill, J. et al. (Jan. 2017). "Superficial layers of the medial entorhinal cortex replay independently of the hippocampus". In: *Science* 355.6321. Publisher: American Association for the Advancement of Science, pp. 184–188. DOI: 10.1126/science.aag2787.

O'Neill, Joseph et al. (May 2010). "Play it again: reactivation of waking experience and memory". en. In: *Trends in Neurosciences* 33.5, pp. 220–229. ISSN: 0166-2236. DOI: 10.1016/j.tins.2010.01.006.

Osanai, Hisayuki, Indrajith R. Nair, and Takashi Kitamura (2023). "Dissecting cell-type-specific pathways in medial entorhinal cortical-hippocampal network for episodic memory". en. In: *Journal of Neurochemistry* 166.2. _eprint: https://onlinelibrary.wiley.com/doi/pdf/10.1111/jnc.15850, pp. 172–188. ISSN: 1471-4159. DOI: 10.1111/jnc.15850.

Paczuski, Maya, Sergei Maslov, and Per Bak (Jan. 1996). "Avalanche dynamics in evolution, growth, and depinning models". en. In: *Physical Review E* 53.1, pp. 414–443. ISSN: 1063-651X, 1095-3787. DOI: 10.1103/PhysRevE.53.414.

Panzeri, Stefano et al. (Sept. 2022). "The structures and functions of correlations in neural population codes". en. In: *Nature Reviews Neuroscience* 23.9. Publisher: Nature Publishing Group, pp. 551–567. ISSN: 1471-0048. DOI: 10.1038/s41583-022-00606-4.

Pasquale, V. et al. (June 2008). "Self-organization and neuronal avalanches in networks of dissociated cortical neurons". In: *Neuroscience* 153.4, pp. 1354–1369. ISSN: 0306-4522. DOI: 10.1016/j.neuroscience.2008.03.050.

Pedregosa, Fabian et al. (n.d.). "Scikit-learn: Machine Learning in Python". en. In: *MACHINE LEARNING IN PYTHON* ().

Peel, Leto, Tiago P. Peixoto, and Manlio De Domenico (Nov. 2022). "Statistical inference links data and theory in network science". en. In: *Nature Communications* 13.1. Publisher: Nature Publishing Group, p. 6794. ISSN: 2041-1723. DOI: 10.1038/s41467-022-34267-9.

Pelkey, Kenneth A. et al. (Oct. 2017). "Hippocampal GABAergic Inhibitory Interneurons". In: *Physiological Reviews* 97.4. Publisher: American Physiological Society, pp. 1619–1747. ISSN: 0031-9333. DOI: 10.1152/physrev.00007.2017.

Perez-Nieves, Nicolas et al. (Oct. 2021). "Neural heterogeneity promotes robust learning". en. In: *Nature Communications* 12.1. Publisher: Nature Publishing Group, p. 5791. ISSN: 2041-1723. DOI: 10.1038/s41467-021-26022-3.

Peron, Simon et al. (Mar. 2020). "Recurrent interactions in local cortical circuits". en. In: *Nature* 579.7798. Publisher: Nature Publishing Group, pp. 256–259. ISSN: 1476-4687. DOI: 10.1038/s41586-020-2062-x.

Petermann, Thomas et al. (Sept. 2009). "Spontaneous cortical activity in awake monkeys composed of neuronal avalanches". In: *Proceedings of the National Academy of Sciences* 106.37. Publisher: Proceedings of the National Academy of Sciences, pp. 15921–15926. DOI: 10.1073/pnas.0904089106.

Plenz, Dietmar et al. (July 2021). "Self-Organized Criticality in the Brain". English. In: *Frontiers in Physics* 9. Publisher: Frontiers. ISSN: 2296-424X. DOI: 10.3389/fphy.2021.639389.

Poil, Simon-Shlomo et al. (July 2012). "Critical-State Dynamics of Avalanches and Oscillations Jointly Emerge from Balanced Excitation/Inhibition in Neuronal Networks". en. In: *Journal of Neuroscience* 32.29. Publisher: Society for Neuroscience Section: Articles, pp. 9817–9823. ISSN: 0270-6474, 1529-2401. DOI: 10.1523/JNEUROSCI.5990-11.2012.

Ponce-Alvarez, Adrián, Morten L. Kringelbach, and Gustavo Deco (June 2023). "Critical scaling of whole-brain resting-state dynamics". en. In: *Communications Biology* 6.1. Number: 1 Publisher: Nature Publishing Group, pp. 1–11. ISSN: 2399-3642. DOI: 10.1038/s42003-023-05001-y.

Priesemann, Viola and Oren Shriki (May 2018). "Can a time varying external drive give rise to apparent criticality in neural systems?" en. In: *PLOS Computational Biology* 14.5. Publisher: Public Library of Science, e1006081. ISSN: 1553-7358. DOI: 10.1371/journal.pcbi.1006081.

Priesemann, Viola, Michael Wibral, et al. (June 2014). "Spike avalanches in vivo suggest a driven, slightly subcritical brain state". English. In: *Frontiers in Systems Neuroscience* 8. Publisher: Frontiers. ISSN: 1662-5137. DOI: 10.3389/fnsys.2014.00108.

Puentes-Mestril, Carlos and Sara J. Aton (Sept. 2017). "Linking Network Activity to Synaptic Plasticity during Sleep: Hypotheses and Recent Data". English. In: *Frontiers in Neural Circuits* 11. Publisher: Frontiers. ISSN: 1662-5110. DOI: 10.3389/fncir.2017.00061.

Quirk, G. J., R. U. Muller, and J. L. Kubie (June 1990). "The firing of hippocampal place cells in the dark depends on the rat's recent experience". en. In: *Journal of Neuroscience* 10.6. Publisher: Society for Neuroscience Section: Articles, pp. 2008–2017. ISSN: 0270-6474, 1529-2401. DOI: 10.1523/JNEUROSCI.10-06-02008.1990.

Ramirez-Villegas, Juan F., Michel Besserve, et al. (Jan. 2021). "Coupling of hippocampal theta and ripples with pontogeniculooccipital waves". en. In: *Nature* 589.7840. Publisher:

Nature Publishing Group, pp. 96–102. ISSN: 1476-4687. DOI: 10.1038/s41586-020-2914-4.

Ramirez-Villegas, Juan F., Nikos K. Logothetis, and Michel Besserve (Nov. 2015). "Diversity of sharp-wave–ripple LFP signatures reveals differentiated brain-wide dynamical events". In: *Proceedings of the National Academy of Sciences* 112.46. Publisher: Proceedings of the National Academy of Sciences, E6379–E6387. DOI: 10.1073/pnas.1518257112.

Rapp, Peter R. et al. (Nov. 2002). "Neuron Number in the Parahippocampal Region is Preserved in Aged Rats with Spatial Learning Deficits". In: *Cerebral Cortex* 12.11, pp. 1171–1179. ISSN: 1047-3211. DOI: 10.1093/cercor/12.11.1171.

Rasch, Björn and Jan Born (Apr. 2013). "About Sleep's Role in Memory". In: *Physiological Reviews* 93.2. Publisher: American Physiological Society, pp. 681–766. ISSN: 0031-9333. DOI: 10.1152/physrev.00032.2012.

Ribeiro, Tiago L. et al. (Nov. 2010). "Spike Avalanches Exhibit Universal Dynamics across the Sleep-Wake Cycle". en. In: *PLOS ONE* 5.11. Publisher: Public Library of Science, e14129. ISSN: 1932-6203. DOI: 10.1371/journal.pone.0014129.

Rich, P. Dylan, Hua-Peng Liaw, and Albert K. Lee (Aug. 2014). "Large environments reveal the statistical structure governing hippocampal representations". In: *Science* 345.6198. Publisher: American Association for the Advancement of Science, pp. 814–817. DOI: 10.1126/science.1255635.

Robinson, Heath L. et al. (Sept. 2025). *Large sharp-wave ripples promote hippocampo-cortical memory reactivation and consolidation*. en. ISSN: 2692-8205 Pages: 2025.06.27.662061 Section: New Results. DOI: 10.1101/2025.06.27.662061.

Roumis, Demetris K and Loren M Frank (Dec. 2015). "Hippocampal sharp-wave ripples in waking and sleeping states". In: *Current Opinion in Neurobiology*. Circuit plasticity and memory 35, pp. 6–12. ISSN: 0959-4388. DOI: 10.1016/j.conb.2015.05.001.

Roux, Lisa et al. (June 2017). "Sharp wave ripples during learning stabilize the hippocampal spatial map". en. In: *Nature Neuroscience* 20.6, pp. 845–853. ISSN: 1097-6256, 1546-1726. DOI: 10.1038/nn.4543.

Safavi, Shervin et al. (Oct. 2024). "Signatures of criticality in efficient coding networks". In: *Proceedings of the National Academy of Sciences* 121.41. Publisher: Proceedings of the National Academy of Sciences, e2302730121. DOI: 10.1073/pnas.2302730121.

Sargolini, Francesca et al. (May 2006). "Conjunctive Representation of Position, Direction, and Velocity in Entorhinal Cortex". In: *Science* 312.5774. Publisher: American Association for the Advancement of Science, pp. 758–762. DOI: 10.1126/science.1125572.

Savelli, Francesco, D. Yoganarasimha, and James J. Knierim (2008). "Influence of boundary removal on the spatial representations of the medial entorhinal cortex". en. In: *Hippocampus* 18.12. _eprint: https://onlinelibrary.wiley.com/doi/pdf/10.1002/hipo.20511, pp. 1270–1282. ISSN: 1098-1063. DOI: 10.1002/hipo.20511.

Schneidman, Elad et al. (2006). "Weak pairwise correlations imply strongly correlated network states in a neural population". In: *Nature* 440.7087. Publisher: Nature Publishing Group UK London, pp. 1007–1012.

Scoville, W. B. and B. Milner (Feb. 1957). "Loss of recent memory after bilateral hippocampal lesions". en. In: *Journal of Neurology, Neurosurgery & Psychiatry* 20.1, pp. 11–21. ISSN: 0022-3050. DOI: 10.1136/jnnp.20.1.11.

Seabold, Skipper and Josef Perktold (2010). "statsmodels: Econometric and statistical modeling with python". In: *9th Python in Science Conference*.

Sebastian, Enrique R. et al. (Dec. 2023). "Topological analysis of sharp-wave ripple waveforms reveals input mechanisms behind feature variations". en. In: *Nature Neuroscience* 26.12.

Publisher: Nature Publishing Group, pp. 2171–2181. ISSN: 1546-1726. DOI: 10.1038/s41593-023-01471-9.

Sethna, James P., Karin A. Dahmen, and Christopher R. Myers (Mar. 2001). "Crackling noise". en. In: *Nature* 410.6825. Publisher: Nature Publishing Group, pp. 242–250. ISSN: 1476-4687. DOI: 10.1038/35065675.

Sherman, S. Murray (Sept. 2006). "Thalamus". en. In: *Scholarpedia* 1.9, p. 1583. ISSN: 1941-6016. DOI: 10.4249/scholarpedia.1583.

Shew, Woodrow L. and Dietmar Plenz (Feb. 2013). "The Functional Benefits of Criticality in the Cortex". en. In: *The Neuroscientist* 19.1. Publisher: SAGE Publications Inc STM, pp. 88–100. ISSN: 1073-8584. DOI: 10.1177/1073858412445487.

Shew, Woodrow L., Hongdian Yang, Thomas Petermann, et al. (Dec. 2009). "Neuronal Avalanches Imply Maximum Dynamic Range in Cortical Networks at Criticality". en. In: *Journal of Neuroscience* 29.49. Publisher: Society for Neuroscience Section: Brief Communications, pp. 15595–15600. ISSN: 0270-6474, 1529-2401. DOI: 10.1523/JNEUROSCI.3864-09.2009.

Shew, Woodrow L., Hongdian Yang, Shan Yu, et al. (2011). "Information capacity and transmission are maximized in balanced cortical networks with neuronal avalanches". English. In: *Journal of Neuroscience* 31.1, pp. 55–63. ISSN: 1529-2401. DOI: 10.1523/JNEUROSCI.4637-10.2011.

Shin, Hyeyoung et al. (Sept. 2025). "Recurrent pattern completion drives the neocortical representation of sensory inference". en. In: *Nature Neuroscience*. Publisher: Nature Publishing Group, pp. 1–11. ISSN: 1546-1726. DOI: 10.1038/s41593-025-02055-5.

Siapas, Athanassios G., Evgueniy V. Lubenov, and Matthew A. Wilson (Apr. 2005). "Prefrontal Phase Locking to Hippocampal Theta Oscillations". English. In: *Neuron* 46.1. Publisher: Elsevier, pp. 141–151. ISSN: 0896-6273. DOI: 10.1016/j.neuron.2005.02.028.

Skaggs, William E, Bruce L McNaughton, and Katalin M Gothard (1993). "An Information-Theoretic Approach to Deciphering the Hippocampal Code". en. In: p. 9.

Skaggs, William E., Bruce L. McNaughton, Katalin M. Gothard, et al. (Nov. 1992). "An information-theoretic approach to deciphering the hippocampal code". In: *Proceedings of the 5th International Conference on Neural Information Processing Systems*. NIPS'92. San Francisco, CA, USA: Morgan Kaufmann Publishers Inc., pp. 1030–1037. ISBN: 978-1-55860-274-8.

Skaggs, William E., Bruce L. McNaughton, Matthew A. Wilson, et al. (1996). "Theta phase precession in hippocampal neuronal populations and the compression of temporal sequences". en. In: *Hippocampus* 6.2. _eprint: https://onlinelibrary.wiley.com/doi/pdf/10.1002/%28SICI%291098-1063%281996%296%3A2%3C149%3A%3AAID-HIPO6%3E3.0.CO%3B2-K, pp. 149–172. ISSN: 1098-1063. DOI: https://doi.org/10.1002/(SICI)1098-1063(1996)6:2<149::AID-HIPO6>3.0.CO;2-K.

Solovey, Guillermo et al. (July 2012). "Self-Regulated Dynamical Criticality in Human ECoG". English. In: *Frontiers in Integrative Neuroscience* 6. Publisher: Frontiers. ISSN: 1662-5145. DOI: 10.3389/fnint.2012.00044.

Solstad, Trygve, Charlotte N. Boccara, et al. (Dec. 2008). "Representation of Geometric Borders in the Entorhinal Cortex". In: *Science* 322.5909. Publisher: American Association for the Advancement of Science, pp. 1865–1868. DOI: 10.1126/science.1166466.

Solstad, Trygve, Edvard I. Moser, and Gaute T. Einevoll (2006). "From grid cells to place cells: A mathematical model". en. In: *Hippocampus* 16.12. _eprint: https://onlinelibrary.wiley.com/doi/pdf/10.1002 pp. 1026–1031. ISSN: 1098-1063. DOI: 10.1002/hipo.20244.

Soltesz, Ivan and Attila Losonczy (Apr. 2018). "CA1 pyramidal cell diversity enabling parallel information processing in the hippocampus". en. In: *Nature Neuroscience* 21.4. Publisher:

Nature Publishing Group, pp. 484–493. ISSN: 1546-1726. DOI: 10.1038/s41593-018-0118-0.

Souza, Bryan C et al. (Sept. 2017). "On information metrics for spatial coding". en. In: p. 7.

Squire, Larry R and Pablo Alvarez (Apr. 1995). "Retrograde amnesia and memory consolidation: a neurobiological perspective". In: *Current Opinion in Neurobiology* 5.2, pp. 169–177. ISSN: 0959-4388. DOI: 10.1016/0959-4388(95)80023-9.

Squire, Larry R. et al. (Aug. 2015). "Memory Consolidation". en. In: *Cold Spring Harbor Perspectives in Biology* 7.8. Company: Cold Spring Harbor Laboratory Press Distributor: Cold Spring Harbor Laboratory Press Institution: Cold Spring Harbor Laboratory Press Label: Cold Spring Harbor Laboratory Press Publisher: Cold Spring Harbor Lab, a021766. ISSN: , 1943-0264. DOI: 10.1101/cshperspect.a021766.

Srivastava, Pragya et al. (Sept. 2022). "The expanding horizons of network neuroscience: From description to prediction and control". In: *NeuroImage* 258, p. 119250. ISSN: 1053-8119. DOI: 10.1016/j.neuroimage.2022.119250.

Stalter, Maximilian, Stephanie Westendorff, and Andreas Nieder (Jan. 2020). "Dopamine Gates Visual Signals in Monkey Prefrontal Cortex Neurons". English. In: *Cell Reports* 30.1. Publisher: Elsevier, 164–172.e4. ISSN: 2211-1247. DOI: 10.1016/j.celrep.2019.11.082.

Stewart, Craig V. and Dietmar Plenz (Aug. 2006). "Inverted-U Profile of Dopamine–NMDA-Mediated Spontaneous Avalanche Recurrence in Superficial Layers of Rat Prefrontal Cortex". en. In: *Journal of Neuroscience* 26.31. Publisher: Society for Neuroscience Section: Articles, pp. 8148–8159. ISSN: 0270-6474, 1529-2401. DOI: 10.1523/JNEUROSCI.0723-06.2006.

— (Apr. 2008). "Homeostasis of neuronal avalanches during postnatal cortex development *in vitro*". In: *Journal of Neuroscience Methods*. Methods for Computational Neuroscience 169.2, pp. 405–416. ISSN: 0165-0270. DOI: 10.1016/j.jneumeth.2007.10.021.

Stickgold, Robert (Oct. 2005). "Sleep-dependent memory consolidation". en. In: *Nature* 437.7063. Publisher: Nature Publishing Group, pp. 1272–1278. ISSN: 1476-4687. DOI: 10.1038/nature04286.

Tang, Wenbo et al. (Aug. 2025). *Goal-directed hippocampal theta sweeps during memory-guided navigation*. en. ISSN: 2692-8205 Pages: 2025.08.26.672489 Section: New Results. DOI: 10.1101/2025.08.26.672489.

Taube, J. S., R. U. Muller, and J. B. Ranck (Feb. 1990). "Head-direction cells recorded from the postsubiculum in freely moving rats. II. Effects of environmental manipulations". en. In: *Journal of Neuroscience* 10.2. Publisher: Society for Neuroscience Section: Articles, pp. 436–447. ISSN: 0270-6474, 1529-2401. DOI: 10.1523/JNEUROSCI.10-02-00436.1990.

Taxidis, Jiannis et al. (Aug. 2015). "Local Field Potentials Encode Place Cell Ensemble Activation during Hippocampal Sharp Wave Ripples". English. In: *Neuron* 87.3. Publisher: Elsevier, pp. 590–604. ISSN: 0896-6273. DOI: 10.1016/j.neuron.2015.07.014.

team, The pandas development (Feb. 2020). *pandas-dev/pandas: Pandas*. DOI: 10.5281/zenodo.3509134.

team, The plotnine development (n.d.). *plotnine: A grammar of graphics for Python*. DOI: https://doi.org/10.5281/zenodo.1325308.

The Theory of Branching Processes (2025). en.

Tian, Yang et al. (Oct. 2022). "Theoretical foundations of studying criticality in the brain". en. In: *Network Neuroscience* 6.4, pp. 1148–1185. ISSN: 2472-1751. DOI: 10.1162/netn_a_00269.

Tkačik, Gašper, Olivier Marre, et al. (Jan. 2014). "Searching for Collective Behavior in a Large Network of Sensory Neurons". en. In: *PLOS Computational Biology* 10.1. Publisher: Public Library of Science, e1003408. ISSN: 1553-7358. DOI: 10.1371/journal.pcbi.1003408.

Tkačik, Gašper, Thierry Mora, et al. (Sept. 2015). "Thermodynamics and signatures of criticality in a network of neurons". In: *Proceedings of the National Academy of Sciences* 112.37. Publisher: Proceedings of the National Academy of Sciences, pp. 11508–11513. DOI: 10.1073/pnas.1514188112.

Topolnik, Lisa and Suhel Tamboli (Aug. 2022). "The role of inhibitory circuits in hippocampal memory processing". en. In: *Nature Reviews Neuroscience* 23.8. Publisher: Nature Publishing Group, pp. 476–492. ISSN: 1471-0048. DOI: 10.1038/s41583-022-00599-0.

Touboul, Jonathan and Alain Destexhe (Feb. 2010). "Can Power-Law Scaling and Neuronal Avalanches Arise from Stochastic Dynamics?" en. In: *PLOS ONE* 5.2. Publisher: Public Library of Science, e8982. ISSN: 1932-6203. DOI: 10.1371/journal.pone.0008982.

— (Jan. 2017). "Power-law statistics and universal scaling in the absence of criticality". In: *Physical Review E* 95.1. Publisher: American Physical Society, p. 012413. DOI: 10.1103/PhysRevE.95.012413.

Tsao, Albert, May-Britt Moser, and Edvard I. Moser (Mar. 2013). "Traces of Experience in the Lateral Entorhinal Cortex". en. In: *Current Biology* 23.5, pp. 399–405. ISSN: 09609822. DOI: 10.1016/j.cub.2013.01.036.

Van Cauter, Tiffany et al. (Feb. 2013). "Distinct Roles of Medial and Lateral Entorhinal Cortex in Spatial Cognition". In: *Cerebral Cortex* 23.2, pp. 451–459. ISSN: 1047-3211. DOI: 10.1093/cercor/bhs033.

Van Rossum, Guido and Fred L. Drake (Feb. 2009). *Python 3 Reference Manual*. Scotts Valley, CA: CreateSpace. ISBN: 978-1-4414-1269-0.

Vandecasteele, Marie et al. (Sept. 2014). "Optogenetic activation of septal cholinergic neurons suppresses sharp wave ripples and enhances theta oscillations in the hippocampus". In: *Proceedings of the National Academy of Sciences* 111.37. Publisher: Proceedings of the National Academy of Sciences, pp. 13535–13540. DOI: 10.1073/pnas.1411233111.

Ven, Gido M. van de et al. (Dec. 2016). "Hippocampal Offline Reactivation Consolidates Recently Formed Cell Assembly Patterns during Sharp Wave-Ripples". In: *Neuron* 92.5, pp. 968–974. ISSN: 0896-6273. DOI: 10.1016/j.neuron.2016.10.020.

Virtanen, Pauli et al. (Mar. 2020). "SciPy 1.0: fundamental algorithms for scientific computing in Python". en. In: *Nature Methods* 17.3. Publisher: Nature Publishing Group, pp. 261–272. ISSN: 1548-7105. DOI: 10.1038/s41592-019-0686-2.

Vollan, Abraham Z. et al. (Mar. 2025). "Left–right-alternating theta sweeps in entorhinal–hippocampal maps of space". en. In: *Nature* 639.8056. Publisher: Nature Publishing Group, pp. 995–1005. ISSN: 1476-4687. DOI: 10.1038/s41586-024-08527-1.

Waskom, Michael et al. (Nov. 2014). *seaborn: v0.5.0 (November 2014)*. DOI: 10.5281/zenodo.12710.

Wasmuht, D. F. et al. (Aug. 2018). "Intrinsic neuronal dynamics predict distinct functional roles during working memory". en. In: *Nature Communications* 9.1. Publisher: Nature Publishing Group, p. 3499. ISSN: 2041-1723. DOI: 10.1038/s41467-018-05961-4.

Wikenheiser, Andrew M. and A. David Redish (Feb. 2015). "Hippocampal theta sequences reflect current goals". en. In: *Nature Neuroscience* 18.2. Publisher: Nature Publishing Group, pp. 289–294. ISSN: 1546-1726. DOI: 10.1038/nn.3909.

Williams-García, Rashid V. et al. (Dec. 2014). "Quasicritical brain dynamics on a nonequilibrium Widom line". In: *Physical Review E* 90.6. Publisher: American Physical Society, p. 062714. DOI: 10.1103/PhysRevE.90.062714.

Wilson, Kenneth G. (Oct. 1975). "The renormalization group: Critical phenomena and the Kondo problem". In: *Reviews of Modern Physics* 47.4. Publisher: American Physical Society, pp. 773–840. DOI: 10.1103/RevModPhys.47.773.

Wilson, M. and B. McNaughton (July 1994). "Reactivation of hippocampal ensemble memories during sleep". en. In: *Science* 265.5172, pp. 676–679. ISSN: 0036-8075, 1095-9203. DOI: 10.1126/science.8036517.

Wilting, J and V Priesemann (Oct. 2019). "25 years of criticality in neuroscience — established results, open controversies, novel concepts". en. In: *Current Opinion in Neurobiology* 58, pp. 105–111. ISSN: 09594388. DOI: 10.1016/j.conb.2019.08.002.

Wilting, Jens et al. (Nov. 2018). "Operating in a Reverberating Regime Enables Rapid Tuning of Network States to Task Requirements". In: *Frontiers in Systems Neuroscience* 12, p. 55. ISSN: 1662-5137. DOI: 10.3389/fnsys.2018.00055.

Winson, Jonathan (July 1978). "Loss of Hippocampal Theta Rhythm Results in Spatial Memory Deficit in the Rat". In: *Science* 201.4351. Publisher: American Association for the Advancement of Science, pp. 160–163. DOI: 10.1126/science.663646.

Witter, Menno P. et al. (2000). "Anatomical Organization of the Parahippocampal-Hippocampal Network". en. In: *Annals of the New York Academy of Sciences* 911.1. _eprint: https://nyaspubs.onlinelibrary 6632.2000.tb06716.x, pp. 1–24. ISSN: 1749-6632. DOI: 10.1111/j.1749-6632.2000.tb06716.x.

Xu, Yifan et al. (Feb. 2024). "Sleep restores an optimal computational regime in cortical networks". en. In: *Nature Neuroscience* 27.2. Publisher: Nature Publishing Group, pp. 328–338. ISSN: 1546-1726. DOI: 10.1038/s41593-023-01536-9.

Yao, Zizhen et al. (June 2021). "A taxonomy of transcriptomic cell types across the isocortex and hippocampal formation". In: *Cell* 184.12, 3222–3241.e26. ISSN: 0092-8674. DOI: 10.1016/j.cell.2021.04.021.

Yartsev, Michael M. and Nachum Ulanovsky (Apr. 2013). "Representation of Three-Dimensional Space in the Hippocampus of Flying Bats". In: *Science* 340.6130. Publisher: American Association for the Advancement of Science, pp. 367–372. DOI: 10.1126/science.1235338.

Yu, Shan et al. (Nov. 2011). "Higher-Order Interactions Characterized in Cortical Activity". en. In: *Journal of Neuroscience* 31.48. Publisher: Society for Neuroscience Section: Articles, pp. 17514–17526. ISSN: 0270-6474, 1529-2401. DOI: 10.1523/JNEUROSCI.3127-11.2011.

Zapperi, Stefano, Kent Bækgaard Lauritsen, and H. Eugene Stanley (Nov. 1995). "Self-Organized Branching Processes: Mean-Field Theory for Avalanches". In: *Physical Review Letters* 75.22. Publisher: American Physical Society, pp. 4071–4074. DOI: 10.1103/PhysRevLett.75.4071.

Zhang, Sheng-Jia et al. (Apr. 2013). "Optogenetic Dissection of Entorhinal-Hippocampal Functional Connectivity". In: *Science* 340.6128. Publisher: American Association for the Advancement of Science, p. 1232627. DOI: 10.1126/science.1232627.

Zheng, Yicong et al. (Nov. 2024). *Recurrent Inhibitory Dynamics in the Entorhinal Cortex Support Pattern Separation*. en. DOI: 10.1101/2024.11.14.623535.

Zierenberg, Johannes, Jens Wilting, and Viola Priesemann (July 2018). "Homeostatic Plasticity and External Input Shape Neural Network Dynamics". In: *Physical Review X* 8.3. Publisher: American Physical Society, p. 031018. DOI: 10.1103/PhysRevX.8.031018.

Zimmern, Vincent (Aug. 2020). "Why Brain Criticality Is Clinically Relevant: A Scoping Review". English. In: *Frontiers in Neural Circuits* 14. Publisher: Frontiers. ISSN: 1662-5110. DOI: 10.3389/fncir.2020.00054.

Zong, Hui et al. (May 2005). "Mosaic Analysis with Double Markers in Mice". English. In: *Cell* 121.3. Publisher: Elsevier, pp. 479–492. ISSN: 0092-8674, 1097-4172. DOI: 10.1016/j.cell.2005.02.012.

Zutshi, Ipshita et al. (Sept. 2018). "Recurrent circuits within medial entorhinal cortex superficial layers support grid cell firing". en. In: *Nature Communications* 9.1. Publisher: Nature Publishing Group, p. 3701. ISSN: 2041-1723. DOI: 10.1038/s41467-018-06104-5.